

BLEJSKE DELAVNICE IZ FIZIKE
BLED WORKSHOPS IN PHYSICS

LETNIK 7, ŠT. 1
VOL. 7, NO. 1

ISSN 1580-4992

Proceedings of the Mini-Workshop
Progress in Quark Models

Bled, Slovenia, July 10–17, 2006

Edited by

Bojan Golli
Mitja Rosina
Simon Širca

University of Ljubljana and Jožef Stefan Institute

DMFA – ZALOŽNIŠTVO
LJUBLJANA, NOVEMBER 2006

The Mini-Workshop *Progress in Quark Models*

was organized by

Jožef Stefan Institute, Ljubljana

Department of Physics, Faculty of Mathematics and Physics, University of Ljubljana

and sponsored by

Slovenian Research Agency

Department of Physics, Faculty of Mathematics and Physics, University of Ljubljana

Society of Mathematicians, Physicists and Astronomers of Slovenia

Organizing Committee

Mitja Rosina

Bojan Golli

Simon Širca

List of participants

Pedro Alberto, Coimbra, pedro@teor.fis.uc.pt

Marko Bračko, Ljubljana, marko.bracko@ijs.si

Bojan Golli, Ljubljana, bojan.golli@ijs.si

Mariana Kirchbach, San Luis Potosi, Mexico, mariana@ifisica.uaslp.mx

Dubravko Klabučar, Zagreb, klabucar@phy.hr

William Klink, Iowa, william-klink@uiowa.edu

Vladimir Kukuljin, Moscow, kukulin@nucl-th.sinp.msu.ru

Norma Mankoč Borštnik, Ljubljana, Norma.Mankoc@ijs.si

Thomas Melde, Graz, thomas.melde@uni-graz.at

Willibald Plessas, Graz, plessas@bkfug.kfunigraz.ac.at

Milan Potokar, Ljubljana, Milan.Potokar@ijs.si

Mitja Rosina, Ljubljana, mitja.rosina@ijs.si

Elena Santopinto, Genova, santopinto@ge.infn.it

Bianka Sengl, Graz, bianka.sengl@uni-graz.at

Ica Stancu, Liege, fstancu@ulg.ac.be

Simon Širca, Ljubljana, simon.sirca@fmf.uni-lj.si

Robert Wagenbrunn, Graz, robert.wagenbrunn@uni-graz.at

Electronic edition

<http://www-fl.ijs.si/BledPub/>

Contents

Preface	V
Pseudospin and spin symmetries in the relativistic harmonic oscillator <i>P. Alberto, A. Castro, M. Malheiro, R. Lisboa</i>	1
Angular momentum dependent quark potential of QCD traits and dynamical $O(4)$ symmetry <i>C. B. Compean and M. Kirchbach</i>	7
Separable Dyson-Schwinger model at finite T <i>D. Blaschke, D. Horvatić, D. Klabučar, A. E. Radzhabov</i>	20
Bosonic contractions <i>William H. Klink</i>	27
Electromagnetic currents in deuteron and NN-system induced by intermediate dibaryon <i>V. I. Kukulin, I. T. Obukhovskiy and V. N. Pomerantsev</i>	33
Hadronic decays and baryon structure <i>T. Melde, W. Plessas, and B. Sengl</i>	42
Baryons in relativistic constituent quark models <i>W. Plessas</i>	47
The hypercentral CQM and the electromagnetic form factors <i>E. Santopinto</i>	49
Relativistic calculation of hadronic baryon decays <i>B. Sengl, T. Melde and W. Plessas</i>	56
Baryon resonances in large N_c QCD <i>N. Matagne and Fl. Stancu</i>	61

Mesons and diquarks in Coulomb-gauge QCD

R. F. Wagenbrunn 67

New resonances and spectroscopy at Belle

M. Bračko..... 74

Excitation of the Roper resonance

B. Golli and S. Širca 82

The two-level Nambu–Jona-Lasinio model

Mitja Rosina and Borut Tone Oblak 92

Recent measurements of nucleon electro-magnetic and spin structure at MIT-Bates, MAMI, and JLab

S. Širca 101

Preface

Here they are, the Proceedings of the Mini-Workshop Bled 2006, documenting our *Progress in Quark Models*, and reminding us of open problems and unanswered questions. We were all feeling happy that we could not only present our own work, but also ask many questions in order to really understand other participants' results.

Quark models have played an important role in understanding baryonic and mesonic spectra and processes at not too high energies. The agreement with phenomenology is in some cases surprisingly good and in some cases not yet satisfactory. There has been progress in more quantitative descriptions, in implementing relativity and in better understanding of the effective quark-quark interactions. All this makes predictions of new exotic (multi-quark) states more reliable in order to guide experimentalists, but they are still controversial and wait for experimental confirmation.

Electromagnetic form-factors, hadronic decay widths and features of new resonances remained our main topics and benchmarks, as well as some naughty "old" resonances such as the Roper and the σ -meson.

For further progress, we should no longer over-specialize only in our few-body techniques, and a need for interdisciplinarity with Lattice QCD has been expressed. Therefore, the topic for the Bled 2007 workshop might be "*What the quark modellers can learn from Lattice QCD experts and what Lattice QCD practitioners can learn from quark-model wavefunctions.*"

Ljubljana, November 2006

M. Rosina
B. Golli
S. Širca

Workshops organized at Bled

- ▷ *What Comes beyond the Standard Model* (June 29–July 9, 1998)
Bled Workshops in Physics **0** (1999) No. 1
- ▷ *Hadrons as Solitons* (July 6–17, 1999)
- ▷ *What Comes beyond the Standard Model* (July 22–31, 1999)
- ▷ *Few-Quark Problems* (July 8–15, 2000)
Bled Workshops in Physics **1** (2000) No. 1
- ▷ *What Comes beyond the Standard Model* (July 17–31, 2000)
- ▷ *Statistical Mechanics of Complex Systems* (August 27–September 2, 2000)
- ▷ *Selected Few-Body Problems in Hadronic and Atomic Physics* (July 7–14, 2001)
Bled Workshops in Physics **2** (2001) No. 1
- ▷ *What Comes beyond the Standard Model* (July 17–27, 2001)
Bled Workshops in Physics **2** (2001) No. 2
- ▷ *Studies of Elementary Steps of Radical Reactions in Atmospheric Chemistry*
- ▷ *Quarks and Hadrons* (July 6–13, 2002)
Bled Workshops in Physics **3** (2002) No. 3
- ▷ *What Comes beyond the Standard Model* (July 15–25, 2002)
Bled Workshops in Physics **3** (2002) No. 4
- ▷ *Effective Quark-Quark Interaction* (July 7–14, 2003)
Bled Workshops in Physics **4** (2003) No. 1
- ▷ *What Comes beyond the Standard Model* (July 17–27, 2003)
Bled Workshops in Physics **4** (2003) No. 2-3
- ▷ *Quark Dynamics* (July 12–19, 2004)
Bled Workshops in Physics **5** (2004) No. 1
- ▷ *What Comes beyond the Standard Model* (July 19–29, 2004)
- ▷ *Exciting Hadrons* (July 11–18, 2005)
Bled Workshops in Physics **6** (2005) No. 1
- ▷ *What Comes beyond the Standard Model* (July 18–28, 2005)
- ▷ *Progress in Quark Models* (July 10–17, 2006)
Bled Workshops in Physics **7** (2006) No. 1
- ▷ *What Comes beyond the Standard Model* (September 16–29, 2006)

Also published in this series

- ▷ Book of Abstracts, *XVIII European Conference on Few-Body Problems in Physics*, Bled, Slovenia, September 8–14, 2002, Edited by Rajmund Krivec, Bojan Golli, Mitja Rosina, and Simon Širca
Bled Workshops in Physics **3** (2002) No. 1–2



Pseudospin and spin symmetries in the relativistic harmonic oscillator*

P. Alberto^a, A. Castro^b, M. Malheiro^{c,d}, R. Lisboa^d

^aDepartamento de Física and Centro de Física Computacional da Universidade de Coimbra

^bDepartamento de Física e Química, Universidade Estadual Paulista, 12516-410 Guaratinguetá, SP, Brazil

^cInstituto Tecnológico de Aeronáutica, CTA, 12228-900, São José dos Campos, SP, Brazil

^dInstituto de Física, Universidade Federal Fluminense, Niterói, Brazil

Abstract. We compute the analytical solutions of the generalized relativistic harmonic oscillator in 1+1 dimensions, including a linear pseudoscalar potential and quadratic scalar and vector potentials which have equal or opposite signs. These are the conditions in which pseudospin or spin symmetries can be realized. We consider positive and negative quadratic potentials and present their bound-state solutions for fermions and antifermions. We relate the spin-type and pseudospin-type spectra through charge conjugation and γ^5 chiral transformations. Finally, we establish a relation of the solutions found with single-particle states of nuclei described by relativistic mean-field theories with tensor interactions and discuss the conditions in which one may have both nucleon and antinucleon bound states.

1 Spin and pseudospin symmetries

The concept of pseudospin was introduced over 30 years ago [1] to explain the quasi-degeneracy in some nuclei between single-nucleon states with quantum numbers $(n, \ell, j = \ell + 1/2)$ and $(n - 1, \ell + 2, j = \ell + 3/2)$ where $n, \ell,$ and j are the radial, the orbital, and the total angular momentum quantum numbers, respectively. These levels have the same “pseudo” orbital angular momentum quantum number, $\tilde{\ell} = \ell + 1,$ and “pseudo” spin quantum number, $\tilde{s} = 1/2.$ For example, for $[ns_{1/2}, (n - 1)d_{3/2}]$ one has $\tilde{\ell} = 1,$ for $[np_{3/2}, (n - 1)f_{5/2}]$ one has $\tilde{\ell} = 2,$ etc. Pseudospin symmetry is exact when doublets with $j = \tilde{\ell} \pm \tilde{s}$ are degenerate.

More recently, the subject was revived when Ginocchio [2] revealed the relativistic character of the symmetry. He noted that the pseudo-orbital angular momentum is just the orbital angular momentum of the lower component of the Dirac spinor. Pseudospin symmetry is an exact symmetry for the Dirac Hamiltonian with an attractive scalar potential, $S,$ and a repulsive vector potential $V,$ when these potentials are equal in magnitude: $S + V = 0.$ Since in relativistic

* Talk delivered by P. Alberto

mean-field models of nuclei the nuclear saturation mechanism is explained by the cancelation between a large scalar and a large vector field [3], this symmetry can account for the degeneracy described above.

It turns out that this symmetry is nothing but a $SU(2)$ symmetry of the Dirac Hamiltonian [4]. In fact, the Dirac equation with scalar and vector potentials

$$H = \boldsymbol{\alpha} \cdot \mathbf{p} + \beta(m + S) + V = \boldsymbol{\alpha} \cdot \mathbf{p} + \beta m + \Sigma P_+ + \Delta P_- .$$

where $P_{\pm} = (I \pm \beta)/2$, $\Sigma = V + S$ and $\Delta = V - S$, has an additional $SU(2)$ symmetry when $V = \pm S$. When $V = -S$ or $\Sigma = 0$ (pseudospin symmetry), the generators are

$$\tilde{S}_i = s_i P_+ + \frac{\boldsymbol{\alpha} \cdot \mathbf{p} s_i \boldsymbol{\alpha} \cdot \mathbf{p}}{p^2} P_- = \begin{pmatrix} s_i & 0 \\ 0 & \tilde{s}_i \end{pmatrix} \quad (1)$$

whereas when $V = S$ or $\Delta = 0$ (spin symmetry), they are

$$S_i = \frac{\boldsymbol{\alpha} \cdot \mathbf{p} s_i \boldsymbol{\alpha} \cdot \mathbf{p}}{p^2} P_+ + s_i P_- = \begin{pmatrix} \tilde{s}_i & 0 \\ 0 & s_i \end{pmatrix} = \gamma^5 \tilde{S}_i \gamma^5 \quad (2)$$

In the equations above $\tilde{s}_i = U_p s_i U_p$, $s_i = \sigma_i/2$, where $U_p = \boldsymbol{\sigma} \cdot \mathbf{p}/p$ is the helicity operator. Spin symmetry could explain the small spin-orbit splitting of certain mesons with a heavy and a light quark [5].

If the potentials are radial, there is another $SU(2)$ rotational symmetry whose generators are [5]

$$\begin{aligned} \mathcal{L} &= L P_+ + \frac{1}{p^2} \boldsymbol{\alpha} \cdot \mathbf{p} L \boldsymbol{\alpha} \cdot \mathbf{p} P_- = \begin{pmatrix} \mathbf{L} & 0 \\ 0 & U_p \mathbf{L} U_p \end{pmatrix} \quad (\text{spin}) \\ \tilde{\mathcal{L}} &= \frac{1}{p^2} \boldsymbol{\alpha} \cdot \mathbf{p} L \boldsymbol{\alpha} \cdot \mathbf{p} P_+ + L P_- = \begin{pmatrix} U_p \mathbf{L} U_p & 0 \\ 0 & \mathbf{L} \end{pmatrix} \quad (\text{pseudospin}). \end{aligned}$$

2 Dirac equation in 1+1 dimensions

The time-independent Dirac equation in 1+1 dimensions for the most general combination of potentials with different Lorentz structures reads

$$H \tilde{\psi} = E \tilde{\psi} \quad (3)$$

where

$$H = c \boldsymbol{\alpha} p + \beta m c^2 + I V_t(x) + \boldsymbol{\alpha} V_{sp}(x) + \beta V_s(x) - i \beta \gamma^5 V_p(x) . \quad (4)$$

The potential $V_{sp}(x)$ can be absorbed into the wave function and the Hamiltonian can be rewritten in terms of the potentials Σ and Δ , yielding

$$H = c \boldsymbol{\alpha} p + \beta m c^2 + \frac{I + \beta}{2} \Sigma + \frac{I - \beta}{2} \Delta - i \beta \gamma^5 V_p . \quad (5)$$

Under charge conjugation and chiral γ^5 transformations, this Hamiltonian transforms into

$$H_c = c \boldsymbol{\alpha} p + \beta m c^2 - \frac{I + \beta}{2} \Delta - \frac{I - \beta}{2} \Sigma + i \beta \gamma^5 V_p , \quad (6)$$

$$H_\chi = c \boldsymbol{\alpha} p - \beta m c^2 + \frac{I + \beta}{2} \Delta + \frac{I - \beta}{2} \Sigma + i \beta \gamma^5 V_p . \quad (7)$$

This means that, under charge conjugation, $\Delta \rightarrow -\Sigma$, $\Sigma \rightarrow -\Delta$, and $V_p \rightarrow -V_p$, while for chiral transformations, $\Sigma \leftrightarrow \Delta$ and $V_p \rightarrow -V_p$. The same happens in 3+1 dimensions, where the pseudoscalar V_p potential corresponds now to a tensor potential. Notice that the chiral transformation, while changing the mass sign, does not change the eigenvalues, since it basically exchanges lines and columns of the Dirac matrix equation.

Defining $\psi_{\pm} = P_{\pm}\psi$ for the upper and lower components, the coupled first-order equations of motion are

$$-i\hbar c\psi'_- + mc^2\psi_+ + \Sigma\psi_+ - iV_p\psi_- = E\psi_+ \quad (8)$$

$$-i\hbar c\psi'_+ - mc^2\psi_- + \Delta\psi_- + iV_p\psi_+ = E\psi_- , \quad (9)$$

and the respective second-order ones are

$$\begin{aligned} -\hbar^2 c^2 \psi''_+ + \hbar c \Delta' \frac{V_p \psi_+ - \hbar c \psi'_+}{E + mc^2 - \Delta} \\ + [V_p^2 + \hbar c V'_p - (E - mc^2 - \Sigma)(E + mc^2 - \Delta)] \psi_+ = 0 \end{aligned} \quad (10)$$

$$\begin{aligned} -\hbar^2 c^2 \psi''_- - \hbar c \Sigma' \frac{V_p \psi_- + \hbar c \psi'_-}{E - mc^2 - \Sigma} \\ - [V_p^2 - \hbar c V'_p - (E - mc^2 - \Sigma)(E + mc^2 - \Delta)] \psi_- = 0 . \end{aligned} \quad (11)$$

In the non-relativistic limit ($\mathcal{E} = E - mc^2 \ll mc^2$ and $|\Sigma(x)| \ll mc^2$), when $\Delta = 0$, we have

$$-\frac{\hbar^2}{2m} \psi''_+ + \left(\frac{\hbar}{2mc} V'_p + \frac{V_p^2}{2mc^2} + \Sigma \right) \psi_+ = \mathcal{E} \psi_+ . \quad (12)$$

Σ plays the role of a binding potential in the nonrelativistic limit and V_p gives rise to effective binding potentials proportional to V'_p and V_p^2 . This means that even a pseudoscalar potential unbounded from below could be a confining potential. For the case $\Sigma = 0$ and if $|\Delta|/(mc^2)$ is very small in the classically accessible region, Eq. (11) becomes

$$-\frac{\hbar^2}{2m} \psi''_+ + \left(\frac{\hbar}{2mc} V'_p + \frac{V_p^2}{2mc^2} \right) \psi_+ = \mathcal{E} \psi_+ . \quad (13)$$

If $\Delta/(mc^2) \sim V_p/(mc^2) \ll 1$, $1/(2m) V'_p \ll V_p$, V_p gets suppressed and there is no binding potential! As far as bound states are concerned, $\Sigma = 0$ is an **intrinsic relativistic problem**.

3 The relativistic harmonic oscillator

The relativistic harmonic oscillator has at most quadratic potentials in the 2nd-order equations for ψ_+ or ψ_- . We consider

$$\Sigma = \frac{1}{2} k_1 x^2, \quad \Delta = 0, \quad V_p = k_2 x \quad (14)$$

The linear pseudo-scalar potential (tensor potential in 3+1 dimensions) is the potential for the *Dirac oscillator* [6]. We solve the relativistic harmonic oscillator for *all* signs of k_1 and k_2 so that we find bound states for *both* particles and anti-particles. For these potentials, the equation (10) reads

$$-\frac{\hbar^2}{2m}\psi_+'' + \frac{1}{2}Kx^2\psi_+ = \tilde{E}\psi_+ \quad (15)$$

where

$$K = \frac{1}{mc^2} \left(\frac{E + mc^2}{2} k_1 + k_2^2 \right) \quad (16)$$

$$\tilde{E} = \frac{E^2 - m^2c^4}{2mc^2} - \frac{\hbar k_2}{2mc}. \quad (17)$$

The bound solutions ($K > 0$) are

$$\psi_+ = N_n H_n(\lambda x) e^{-\lambda^2 x^2/2} \quad (18)$$

where $n = 0, 1, 2, \dots$, N_n is a normalization constant, $H_n(\lambda x)$ is a n -th degree Hermite polynomial $\lambda = (mK/(\hbar^2))^{1/4}$. The eigenvalues are such that

$$E^2 - m^2c^4 = (2n + 1) \hbar c \sqrt{\frac{E + mc^2}{2} k_1 + k_2^2} + \hbar c k_2. \quad (19)$$

In 3+1 dimensions the corresponding eigenvalue equation is

$$E^2 - m^2c^4 = (4n + 2l + 3) \hbar c \sqrt{\frac{E + mc^2}{2} k_1 + k_2^2} + (2\kappa - 1) \hbar c k_2, \quad (20)$$

where κ is the spin-orbit quantum number and l is the orbital angular momentum of the upper component. This means that the spectra of 1+1 relativistic harmonic oscillator solutions have the same qualitative behaviour as the spectra of the 3+1 relativistic harmonic oscillator.

4 Solutions and discussion

In the following plots, we use scaled quantities, $e = E/(mc^2)$, $\kappa_1 = \hbar^2 k_1/(m^3 c^4)$ and $\kappa_2 = \hbar k_2/(m^2 c^3)$. Unless otherwise specified, all plots are for $\Delta = 0$.

The value κ_2^* is a zero of a certain function of κ_2 whose sign determines the number of solutions for a fixed κ_1 and n [7]. When $0 \leq \kappa_2 \leq \kappa_2^*$ one can have just one particle bound solution. If $\kappa_2 < 0$, $\kappa_2 > \kappa_2^*$ one has both particle **and** anti-particle bound solutions.

One may notice that the spectrum in Fig. 3(b) can be obtained from Fig. 2(a) by a charge conjugation transformation, for which $k_2 \rightarrow -k_2$ and $E \rightarrow -E$. Also, from Figs. 4(a) and 4(b), we can see that, for massless fermions, the spectra for $\Delta = 0$ and $\Sigma = 0$ is the same except for the reversed sign of κ_2 , which is to be expected since these are related by the chiral γ^5 transformation.

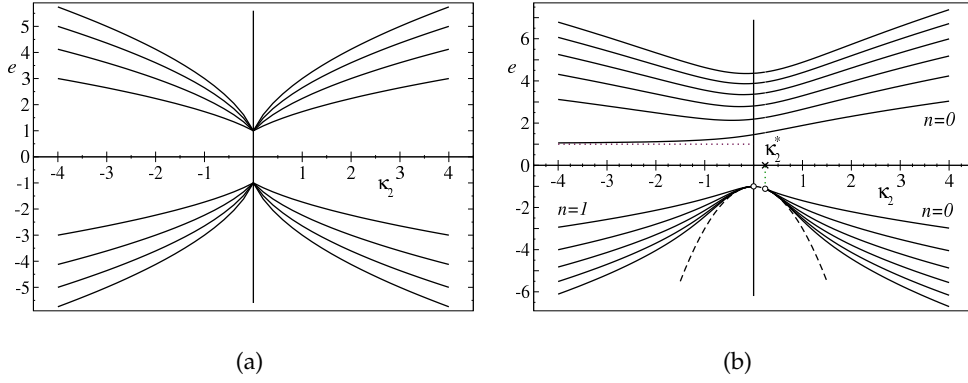


Fig. 1. (a) First four levels as a function of κ_2 when $\kappa_1 = 0$ (b) First six levels as a function of κ_2 when $\kappa_1 = 1$.

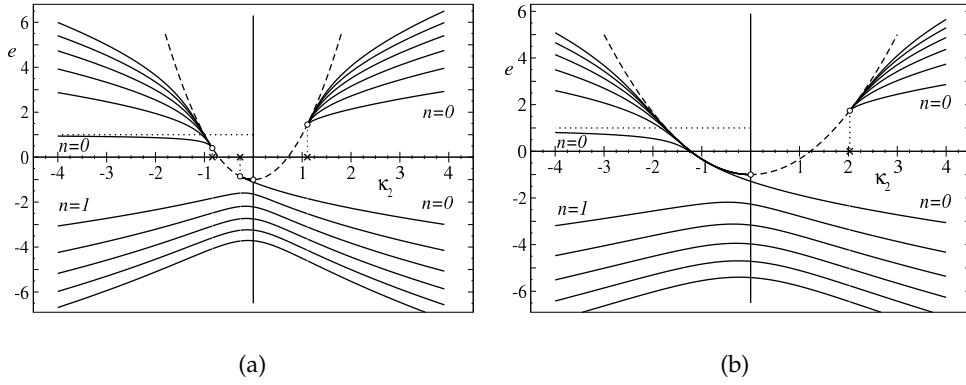


Fig. 2. (a) First six levels as a function of κ_2 when $\kappa_1 = -1 > \kappa_1^c = -64/27$ (b) First six levels as a function of κ_2 when $\kappa_1 = -3 < \kappa_1^c = -64/27$.

The existence of both positive- and negative-energy solutions in a system with $\Sigma = 0$ can be relevant for nuclei. In the 3+1 Dirac equation of relativistic nuclear mean-field theories there is a connection between the (isoscalar) vector and tensor potential. In our case one would have $\kappa_2 = \frac{f_v}{4} \kappa_1$ [8]. Since the constant f_v has an upper value in nuclei, the same should happen for harmonic oscillator mean-field potentials, so this relation sets a maximum for κ_2 in nuclei. As was seen above, this is relevant to know whether there can be simultaneously nucleon and antinucleon bound states in nuclei. This would depend very much on the strength of the Δ potential, which is given by k_1 .

References

1. K. T. Hecht and A. Adler, Nucl. Phys. **A137**, 129 (1969); A. Arima, M. Harvey, and K. Shimizu, Phys. Lett. **B30**, 517 (1969).

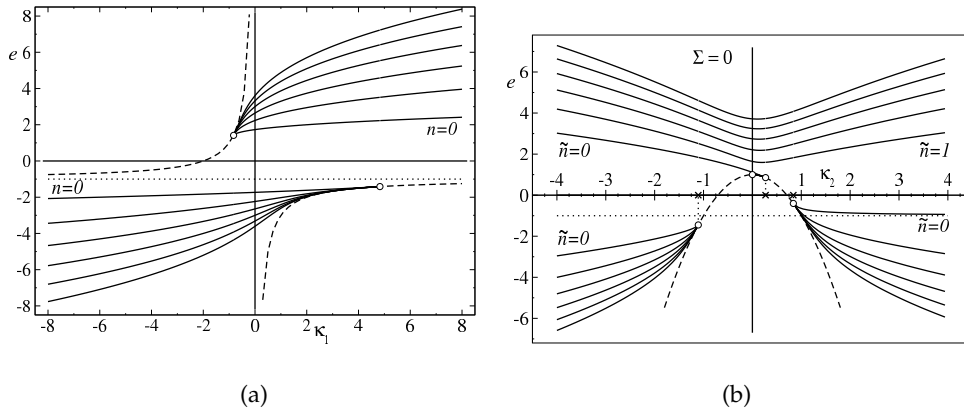


Fig. 3. (a) First six levels as a function of κ_1 when $\kappa_2 = 1 > \kappa_2^c = -1$ (b) First six levels as a function of κ_2 when $\kappa_1 = 1$ and $\Sigma = 0$.

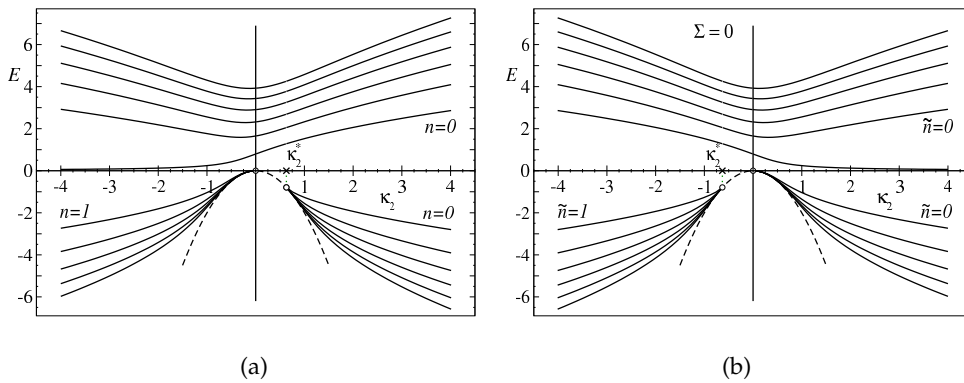


Fig. 4. (a) First six levels when $m = 0$ and $\Delta = 0$ (b) First six levels when $m = 0$ and $\Sigma = 0$. In both cases $\kappa = 1$.

2. J. N. Ginocchio, *Phys. Rev. Lett.* **78**, 436 (1997).
3. B. D. Serot and J. D. Walecka, *The Relativistic Nuclear Many - Body Problem in Advances in Nuclear Physics*, edited by J. W. Negele and E. Vogt, Vol. **16** (Plenum, New York, 1986).
4. J. S. Bell and H. Rugg, *Nucl. Phys.* **B98**, 151 (1975)
5. J. N. Ginocchio, *Phys. Rep.* **414** 165 (2005).
6. D. Itô, K. Mori, and E. Carriere, *Nuovo Cimento A* **51**, 1119 (1967); M. Moshinsky and A. Szczepaniak, *J. Phys. A* **22**, L817 (1989); V. I. Kukulin, G. Loyola, and M. Moshinsky, *Phys. Lett. A* **158**, 19 (1991).
7. A. S. de Castro, P. Alberto, R. Lisboa and M. Malheiro, *Phys. Rev. C* **73**, 054309 (2006).
8. P. Alberto, R. Lisboa, M. Malheiro, and A. S. de Castro, *Phys. Rev. C* **71**, 034313 (2005).



Angular momentum dependent quark potential of QCD traits and dynamical $O(4)$ symmetry*

C. B. Compean and M. Kirchbach

Instituto de Física, Universidad Autónoma de San Luis Potosí, Av. Manuel Nava 6, San Luis Potosí, S.L.P. 78290, México

Abstract. A common quark potential that captures the essential traits of the QCD quark-gluon dynamics is expected to (i) interpolate between a Coulomb-like potential (associated with one-gluon exchange) and the infinite wall potential (associated with trapped but asymptotically free quarks), (ii) reproduce in the intermediary region the linear confinement potential (associated with multi-gluon self-interactions) as established by lattice QCD calculations of hadron properties. We first show that the exactly soluble trigonometric Rosen-Morse potential possesses all these properties. Next we observe that this potential, once interpreted as angular momentum dependent, acquires a dynamical $O(4)$ symmetry and reproduces exactly quantum numbers and level splittings of the non-strange baryon spectra in the $SU(2)_I \otimes O(4)$ classification scheme according to which baryons cling on to multi-spin parity clusters of the type $(\frac{K}{2}, \frac{K}{2}) \otimes [(\frac{1}{2}, 0) \oplus (0, \frac{1}{2})]$, whose relativistic image is $\psi_{\mu_1 \dots \mu_K}$. Finally, we bring exact energies and wave functions of the levels within the above potential and thus put it on equal algebraic footing with such common potentials of wide spread as are the harmonic-oscillator- and the Coulomb potentials.

1 Introduction

The non-strange baryon spectra below ~ 2500 MeV reveal, isospin by isospin, as a striking phenomenon mass degenerate series of K pairs of resonances of opposite spatial parities and spins ranging from $\frac{1}{2}^\pm$ to $(K - \frac{1}{2})^\pm$ which terminate by a highest spin- $(K + \frac{1}{2})$ resonance that remains unpaired [1]. Such series (displayed in Fig. 1) perfectly fit into $SU(2)_I \otimes O(4)$ representations of the type $(\frac{K}{2}, \frac{K}{2}) \otimes [(\frac{1}{2}, 0) \oplus (0, \frac{1}{2})]$, an observation due again to [1]. The appeal of the above classification is twofold. On the one side, up to the $\Delta(1600)$ state which is likely to be a hybrid, no other resonances drop out of the proposed scheme. Also the prediction of less “missing” resonances relative to others schemes falls under this issue. On the other side, due to the local $O(4) \sim O(1, 3)$ isomorphism, the non-relativistic $O(4)$ multiplets have as an exact relativistic image the covariant high-spin degrees of freedom given by the totally symmetric rank- K Lorentz tensors with Dirac spinor components, $\psi_{\mu_1 \dots \mu_K}$ known as spin- $(K + \frac{1}{2})$ Rarita-Schwinger fields [2]. In this fashion, one can view the series of mass degenerate resonances of alternating parities and spins rising from $\frac{1}{2}^\pm$ to $(K + \frac{1}{2})^P$ as rest

* Talk delivered by M. Kirchbach

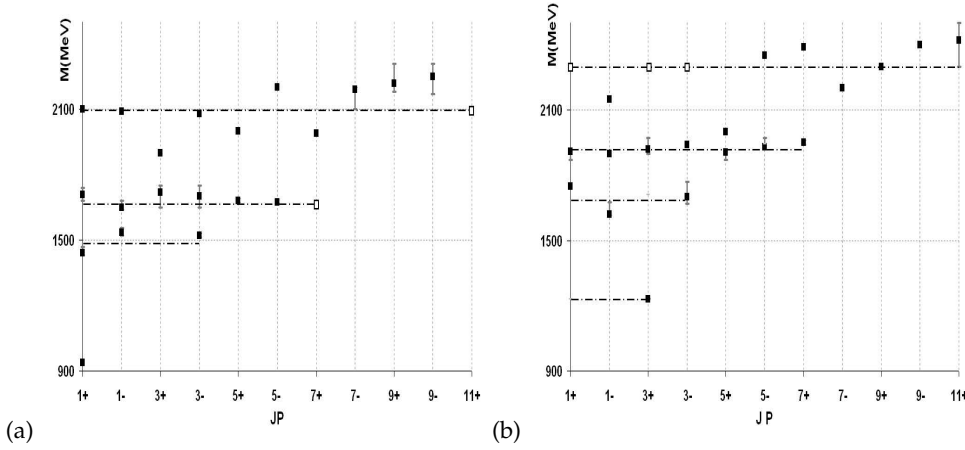


Fig. 1. Experimentally observed baryon resonances (l.h.s.) N and (r.h.s.) Δ . The dash-point lines represent the series mass average. Notice that the resonances with masses above 2000 MeV are of significantly lower confidence but those with masses below 2000 MeV where the degeneracy is very well pronounced. Empty squares denote predicted (“missing”) states. Typical, the **systematical lack of a parity partner to the first highest spins** D_{13} , F_{17} , and $H_{1,11}$ (the last two being among the “missing” N states).

frame $\psi_{\mu_1 \dots \mu_K}$ of mass m and look for possibilities to generate such multiplets as bound states within an appropriate quark potential. Although the degeneracy of the non-strange baryons follows same patterns as the states of an electron with spin in the Hydrogen atom, the level splittings are quite different. The mass formula that fits the N(Δ) spectrum has been encountered in Ref. [3] as

$$M_{(\sigma;1)} - M_{(1;1)} = -f_I \frac{1}{\sigma^2} + g_I \frac{\sigma^2 - 1}{4}, \quad \sigma = K + 1, \quad I = N, \Delta, \quad (1)$$

$$f_N = f_\Delta = 600 \text{ MeV}, \quad g_N = 70 \text{ MeV}, \quad g_\Delta = 40 \text{ MeV}, \quad (2)$$

and contains besides the Balmer-like term, ($\sim -1/\sigma^2$), also its inverse. In effect, the baryon mass splittings increase with σ . The degeneracy patterns and the mass formula have found explanation in Ref. [4] within a version of the interacting boson model (IBM) for baryons. To be specific, to the extent QCD prescribes baryons to be constituted of three quarks in a color singlet state, one can exploit for the description of baryonic systems algebraic models developed for the purposes of triatomic molecules, a path pursued by Refs. [5]. An interesting dynamical limit of the three quark system is the one where two of the quarks are “squeezed” to one independent entity, a di-quark (qq), while the third quark (q) remains spectator. In this limit, which corresponds to $U(7) \rightarrow U(3) \times U(4)$, one can exploit the following chain of reducing $U(4)$ down to $O(2)$

$$U(4) \supset O(4) \supset O(3) \supset O(2), \quad (3)$$

$$\begin{array}{cccc} N & K & l & m \\ K = N, N - 2, \dots, 1(0), & l = K, K - 1, \dots, 0, & |m| < l, & \end{array} \quad (4)$$

in order to describe the rotational and vibrational (rovibron) modes of the (qq)–q dumbbell. In so doing, one reproduces the quantum numbers describing the degeneracies in the light quark baryon spectra by means of the following Hamiltonian:

$$\mathcal{H} - \mathcal{H}_0 = -f_1(4\mathcal{C}_2(\text{so}(4)) + 1)^{-1} + g_1\mathcal{C}_2(\text{so}(4)), \quad (5)$$

$$\mathcal{C}_2(\text{so}(4)) \left(\frac{K}{2}, \frac{K}{2} \right) = \frac{(K+1)^2 - 1}{4} \left(\frac{K}{2}, \frac{K}{2} \right). \quad (6)$$

with $\mathcal{C}_2(\text{so}(4))$ being the second $\text{so}(4)$ Casimir operator. In the second row of Eq. (3) we indicate the quantum numbers associated with the respective group of the chain. Here, N stands for the principle quantum number of the four dimensional harmonic oscillator associated with $U(4)$, K refers to the $O(4)$ four dimensional angular momentum, while l , and m are in turn ordinary three- and two angular momenta. In Ref. [4] the interested reader can find all the details of the algebraic description of the nucleon and Δ resonances within the rovibron limit.

Yet, as a principle challenge still remains finding a suitable quark potential that leads to the above scenario. In the present work we make the case that the exactly soluble trigonometric Rosen-Morse potential is precisely the potential we are looking for.

The paper is organized as follows. In the next section we analyze the shape of the trigonometric Rosen-Morse potential. In section III we present the exact real orthogonal polynomial solutions of the corresponding Schrödinger equation. The paper ends with a brief concluding section.

2 The shape of the trigonometric Rosen-Morse potential

We adopt the following form of the trigonometric Rosen-Morse potential [6],[7]

$$v(z) = -2b \cot z + a(a+1) \csc^2 z, \quad a > -1/2, \quad (7)$$

displayed in Fig. 2. Here,

$$z = \frac{r}{d}, \quad v(z) = V(z)/(\hbar^2/2md^2), \quad \epsilon_n = E_n/(\hbar^2/2md^2), \quad (8)$$

the one-dimensional variable is $r = |r|$, d is a properly chosen length scale, $V(r)$ is the potential in ordinary coordinate space, and E_n is the energy of the levels. Our point here is that $v(z)$ interpolates between a Coulomb-like and an infinite-wall potential going through an intermediary region of linear, and quadratic (harmonic-oscillator) dependences in z . To see this (besides inspection of Fig. 2) it is quite instructive to expand the potential in a Taylor series which for appropriately small z , takes the form of a Coulomb-like potential with a centrifugal-barrier like term (if a were to be a positive integer) provided by the $\csc^2 z$ part,

$$v(z) \approx -\frac{2b}{z} + \frac{a(a+1)}{z^2}. \quad (9)$$

In an intermediary range where inverse powers of z may be neglected, one finds the linear plus a harmonic-oscillator potentials

$$v(z) \approx \frac{2b}{3}z + \frac{a(a+1)}{15}z^2. \quad (10)$$

Finally, as long as $\cot z \xrightarrow{z \rightarrow \pi} \infty$ and $\csc^2 z \xrightarrow{z \rightarrow \pi} \infty$, the potential obviously evolves to an infinite wall. The above shape captures surprisingly well the essentials of

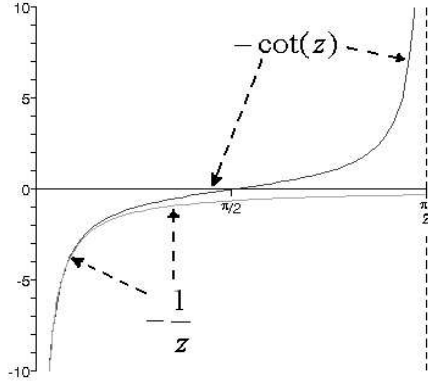


Fig. 2. The proximity of the $(\sim \cot z)$ - to the $(\sim \frac{1}{z})$ potential.

the QCD quark-gluon dynamics where the one gluon exchange gives rise to an effective Coulomb-like potential, while the self-gluon interactions produce a linear confinement potential as established by lattice calculations of hadron properties. Finally, the infinite wall piece of the trigonometric Rosen-Morse potential provides the regime suited for trapped but asymptotically free quarks. By the above considerations one is tempted to conclude that the potential under consideration may be a good candidate for a common quark potential of QCD traits.

In the next section we present the exact solutions of the Schrödinger equation with the trigonometric Rosen-Morse potential.

3 Energies and wave functions of the levels within the trigonometric Rosen-Morse potential

The three-dimensional Schrödinger equation with the trigonometric Rosen-Morse potential (tRMP) reads:

$$\nabla^2 \psi(\mathbf{z}) + \left(2b \cot z - \frac{a(a+1)}{\sin^2 z} + \epsilon \right) \psi(\mathbf{z}) = 0, \quad (11)$$

and is solved in polar coordinates in the standard way by separation of variables. In effect, the wave function factorizes according to

$$\psi(z) = \frac{R(z)}{z} Y_l^\mu(\theta, \phi), \quad l = 0, 1, 2, \dots, \quad |\mu| < l, \quad (12)$$

where $Y_l^\mu(\theta, \phi)$ stand for the standard spherical harmonics, and $R(z)$ satisfies the one-dimensional equation

$$\frac{d^2}{dz^2} R(z) + \left(2b \cot z - \frac{a(a+1)}{\sin^2 z} + \epsilon \right) R(z) = 0. \quad (13)$$

This equation (up to inessential notational differences) has been solved in our previous work [8]. There, we exploited the following factorization ansatz

$$R(z) = e^{-\alpha z/2} (1 + \cot^2 z)^{\frac{-(1-\beta)}{2}} C^{(\beta, \alpha)}(\cot z), \quad (14)$$

with α and β being constant parameters. Upon introducing the new variable $x = \cot z$, substituting the above factorization ansatz into Eq. (14), and a subsequent division by $(1+x^2)^{(1-\beta)/2}$ one finds

$$\begin{aligned} (1+x^2) \frac{d^2 C^{(\beta, \alpha)}(x)}{dx^2} + 2 \left(\frac{\alpha}{2} + \beta x \right) \frac{d C^{(\beta, \alpha)}(x)}{dx} + \left((-\beta(1-\beta) - a(a+1)) \right. \\ \left. + \frac{(-\alpha(1-\beta) + 2b)x + \left(\left(\frac{\alpha}{2} \right)^2 - (1-\beta)^2 + \epsilon_m \right)}{1+x^2} \right) C^{(\beta, \alpha)}(x) = 0. \end{aligned} \quad (15)$$

This equation is suited for comparison with

$$(1+x^2) \frac{d^2 \mathcal{R}_m^{(\beta, \alpha)}(x)}{dx^2} + 2 \left(\frac{\alpha}{2} + \beta x \right) \frac{d \mathcal{R}_m^{(\beta, \alpha)}(x)}{dx} - m(2\beta + m - 1) \mathcal{R}_m^{(\beta, \alpha)}(x) = 0, \quad (16)$$

which being of the form of the text-book hypergeometric equation [9],[10],[11] can be cast into the self-adjointed Sturm-Liouville form given by

$$\begin{aligned} s(x) \frac{d^2 \mathcal{R}_m^{(\beta, \alpha)}(x)}{dx^2} + \frac{1}{w(x)} \left(\frac{d s(x) w(x)}{dx} \right) \frac{d \mathcal{R}_m^{(\beta, \alpha)}(x)}{dx} + \lambda_m \mathcal{R}_m^{(\beta, \alpha)}(x) = 0, \quad (17) \\ s(x) = 1 + x^2, \quad w^{(\beta, \alpha)}(x) = s(x)^{\beta-1} e^{-\alpha \cot^{-1} x}, \quad \lambda_m = -m(2\beta + m - 1), \\ -\infty < x < \infty. \end{aligned} \quad (18)$$

However, while the standard textbooks consider exclusively $s(x)$ functions which are at most second order polynomials of *real roots*, in which case

$$w(a)s(a)x^l = w(b)s(b)x^l = 0, \quad \forall l = \text{integer}, \quad (19)$$

holds valid, the roots of $s(x)$ in Eq. (16) are *imaginary*. In the former case it is well known that

- $\mathcal{R}_m^{(\beta, \alpha)}(x)$ would be polynomials of order m ,

- λ_m would satisfy

$$\lambda_m = -m \left(K_1 \frac{d \mathcal{R}_1^{(\beta, \alpha)}(x)}{d x} + \frac{1}{2}(m-1) \frac{d^2 s(x)}{d x^2} \right), \quad (20)$$

with K_m being the $\mathcal{R}_m^{(\beta, \alpha)}(x)$ normalization constant,

- the first order polynomial would be defined as

$$\mathcal{R}_1^{(\beta, \alpha)}(x) = \frac{1}{K_1 w(x)} \left(\frac{d s(x) w(x)}{d x} \right), \quad (21)$$

- the latter relation would generalize to any m via the so called Rodrigues formula

$$\mathcal{R}_m^{(\beta, \alpha)}(x) = \frac{1}{K_m w(x)} \frac{d^m}{d x^m} (w(x) s(x)^m), \quad (22)$$

- $w(x)$ would be the weight-function with respect to which the $\mathcal{R}_m^{(\beta, \alpha)}(x)$ polynomials would appear orthogonal.

Within this context the question arises whether the imaginary roots of $s(x) = (1 + x^2)$ in Eq. (16) would prevent the $\mathcal{R}_m^{(\beta, \alpha)}(x)$ functions from being real orthogonal polynomials. The answer to this question is negative. It can be shown that also in the latter case

- the $\mathcal{R}_m^{(\beta, \alpha)}(x)$'s are polynomials of order m ,
- they can also be constructed systematically from a Rodrigues formula in terms of the respecified weight function,
- but only a finite number them will be orthogonal due to the violation of Eq. (19).

From the historical perspective, Eq. (18) has first been brought to attention by the celebrated English mathematician Sir Edward John Routh in Ref. [12] (modulo the unessential difference in the argument of the exponential from the present \cot^{-1} to Routh's \tan^{-1}), the teacher of J. J. Thomson and J. Larmor, among others famous physicists. Routh observed that the weight-function of the Jacobi polynomials, $P_m^{(\mu, \nu)}(x)$, takes the form of Eq. (18) upon the particular complexification of the argument and the parameters according to $\mu \rightarrow \eta = a + ib, \nu \rightarrow \eta^*$, and $x \rightarrow ix$. From that he concluded that $P_m^{(\eta, \eta^*)}(ix)$ is a real polynomial (up to a global phase factor). Later on, in 1929, the prominent Russian mathematician Vsevolod Ivanovich Romanovski, one of the founders of the Tashkent University, studied few more of their properties in [13] and it was him who observed that only a finite number of them appear orthogonal. While the mathematics literature is familiar with such polynomials [14], [15], [16], [17] where they are referred to as finite Romanovski polynomials [18], or, Romanovski-Pseudo-Jacobi polynomials [19], a curious omission from all the standard textbooks on mathematical physics [9],[10] takes place. This might be related to circumstance that the physics problems which call for such polynomials are relatively few. Recently, it has been

reported in the peer physics literature [8], [20] that the Schrödinger equation with the respective hyperbolic Scarf and trigonometric Rosen-Morse potentials is solved exactly precisely in terms of the Romanovski polynomials. Moreover, the latter are also relevant in calculation of gap probabilities in finite Cauchy random matrix ensembles [21]. In the following, we shall adopt the notion of Routh-Romanovski polynomials for obvious reasons.

3.1 The exact spectrum

Back to Eq. (15) we observe that if it is to coincide with Eq. (16) then the coefficient in front of the $1/(x^2+1)$ term has to nullify. This restricts the $C^{(\beta,\alpha)}(x)$ parameters in the Schrödinger wave function to be

$$-\alpha(1-\beta) + 2b = 0, \quad \left(\frac{\alpha}{2}\right)^2 - (1-\beta)^2 + \epsilon = 0. \quad (23)$$

With that Eq. (15) to which one has reduced the original Schrödinger equation amounts to

$$(1+x^2) \frac{d^2 C^{(\beta,\alpha)}(x)}{dx^2} + 2\left(\frac{\alpha}{2} + \beta x\right) \frac{d C^{(\beta,\alpha)}(x)}{dx} + (-\beta(1-\beta) - a(a+1)) C^{(\beta,\alpha)}(x) = 0. \quad (24)$$

The final step is to identify the constant term in the latter equation with the one in Eq. (16) which amounts to a third condition

$$-\beta(1-\beta) - a(a+1) = -m(2\beta + m - 1), \quad (25)$$

which introduces the dependence of the $C^{(\beta,\alpha)}(x)$ functions on the index m , i.e. $C^{(\beta,\alpha)}(x) \rightarrow C_m^{(\beta,\alpha)}(x)$. Remarkably, Eqs. (23) and (25) indeed allow for consistent solutions for α , β , and ϵ and given by (upon renaming m by $(n-1)$):

$$\beta_n = -(n+a) + 1, \quad \alpha_n = \frac{2b}{n+a}, \\ \epsilon_n = (n+a)^2 - \frac{b^2}{(n+a)^2}, \quad n = m + 1, \quad (26)$$

now with $n \geq 1$. In this way Eq. (26) provides the exact tRM spectrum. In effect, the polynomials that define the exact solution of the Schrödinger equation with the trigonometric Rose-Morse potential turn out identical to the Routh-Romanovski polynomials however with indices that depend on n . As we shall see below, this circumstance will become of crucial importance in allowing for an *infinite* number of orthogonal polynomials (as required by the infinite depth of the potential) and thus for avoiding the finite orthogonality of the bare Routh-Romanovski polynomials.

With that all the necessary ingredients for the solution of Eq. (24) have been prepared. In now exploiting the Rodrigues representation (when making the n dependence explicit),

$$C_n^{(\beta_n, \alpha_n)}(x) \equiv \mathcal{R}_n^{(\beta_n, \alpha_n)}(x) = \frac{1}{K_n w^{(\beta_n, \alpha_n)}(x)} \frac{d^{n-1}}{dx^{n-1}} \left(w^{(\beta_n, \alpha_n)}(x) s(x)^{n-1} \right), \quad (27)$$

allows for the systematic construction of the solutions of Eq. (24). Notice that in terms of $w^{(\beta_n, \alpha_n)}(x)$ the wave function is expressed as

$$R_n^{(a,b)}(\cot^{-1} x) = \sqrt{w^{(-(n+a)+1, \frac{2b}{n+a})}(x)} \mathcal{R}_n^{(-(n+a)+1, \frac{2b}{n+a})}(x). \quad (28)$$

Next one can check orthogonality of the physical solutions in z space and obtain it as it should be as

$$\int_0^\pi R_n(z) R_{n'}(z) dz = \delta_{n n'}, \quad (29)$$

The orthogonality of the wave functions $R_n(z)$ implies in x space orthogonality of the $\mathcal{R}_n^{(\beta_n, \alpha_n)}(x)$ polynomials with respect to $w^{(\beta_n, \alpha_n)}(x) \frac{dz}{dx}$ due to the variable change. As long as $\frac{d \cot^{-1} x}{dx} = -1/(1+x^2) \equiv -1/s(x)$ then the orthogonality integral for the polynomials takes the form

$$\int_{-\infty}^{\infty} \frac{dx}{s(x)} \sqrt{w^{(\beta_n, \alpha_n)}(x)} \mathcal{R}_n^{(\beta_n, \alpha_n)}(x) \sqrt{w^{(\beta_{n'}, \alpha_{n'})}(x)} \mathcal{R}_{n'}^{(\beta_{n'}, \alpha_{n'})}(x) = \delta_{n n'}. \quad (30)$$

The existence of an infinite number of orthogonal Routh-Romanovski polynomials was made possible on cost of the n dependence of the parameters which emerged while converting the Schrödinger equation to the polynomial one.

3.2 The degeneracy in the spectra

Inspection of Eq. (26) reveals existence of an intriguing degeneracy in the tRMP spectrum. In order to see it let us assume that the a -parameter in Eq. (13) takes only integer non-negative $a = 0, 1, 2, \dots$ -values. In such a case, one immediately reads off from Eq. (26) that the energy levels for any $\sigma = (m + 1 + a)$ with $\sigma = 1, 2, 3, \dots$ are σ -fold degenerate as a can take all the values between 0 and $(\sigma - 1)$ according to $a = 0, 1, \dots, (\sigma - 1)$ (see Fig. 3). Comparison of the a -degeneracy to the non-strange baryon spectra in Fig. 1 and Eqs. (4) is suggestive of the idea to interpret the non-negative integer a -values as angular momenta and view the $\text{csc}^2\left(\frac{r}{d}\right)$ term as a **non-standard** centrifugal barrier

$$a(a+1) \text{csc}^2\left(\frac{r}{d}\right) \longrightarrow \frac{l(l+1)}{\sin^2\left(\frac{r}{d}\right)}, \quad a \equiv l = 0, 1, 2, \dots \quad (31)$$

In terms of σ the mass formula in Eq. (2) translates to

$$\frac{4(M_{\sigma, I} - M_{1, I} + \frac{1}{4}g_I)}{g_I} \longrightarrow \epsilon_\sigma = -\frac{b^2}{\sigma^2} + \sigma^2, \quad b^2 = \frac{4f_I}{g_I}. \quad (32)$$

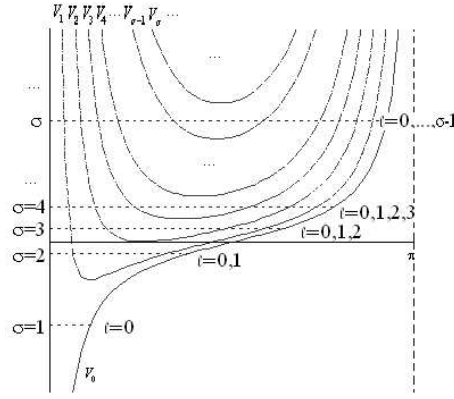


Fig. 3. Degeneracy of energy levels of same σ but different angular momenta in l dependent trigonometric Rosen-Morse potentials. The curves correspond to $b = 60$, a value fitted to the N spectrum.

Non-standard centrifugal barriers of various types have been frequently exploited in the calculation of the spectral properties of collective nuclei. Specifically, in Ref. [22] use has been made of an angular-momentum dependent potential originally suggested by Ginocchio in Refs. [23]. The non-standard centrifugal barrier in this potential asymptotically approaches for certain parameter values the physical centrifugal barrier, $l(l+1)/r^2$ while for another set of parameters it becomes the Pöschel-Teller potential. In our case, for small arguments the \csc^2 term also approaches the physical centrifugal term as evident from Eq. (9) and visualized by Figs. 4. Non-standard centrifugal barriers have the property to couple various multipole modes in nuclei, an example being given more recently in Ref. [24]. From now onward we shall adopt non-negative integer values for the a parameter and view the \csc^2 term as a non-standard centrifugal barrier according to

$$V_l(r) = -2B \cot\left(\frac{r}{d}\right) + \frac{\hbar^2}{2\mu d^2} l(l+1) \csc^2\left(\frac{r}{d}\right). \quad (33)$$

In so doing we are defining a new angular momentum dependent potential, $V_l(r)$, that possesses the dynamical $O(4)$ symmetry. Notice that this does not contradict the statement of Ref. [25] according to which only pure or screened Coulomb-like potentials are $O(4)$ symmetric as the theorem of Ref. [25] refers to potentials with the standard centrifugal barrier only. The b parameter in Eq. (32) now relates to the potential parameter B as

$$b = \frac{2\mu d^2 B}{\hbar^2}. \quad (34)$$

Next we shall bring down the a index, suppress the b index and change notations according to

$$R_n^{((a \equiv l), b)}\left(\frac{r}{d}\right) \longrightarrow R_{\sigma l}\left(\frac{r}{d}\right), \quad \sigma = n + l. \quad (35)$$

The single-particle wave functions within the angular dependent trigonometric Rosen-Morse potential are straightforwardly calculated from Eq. (28). Below we list the first three levels for illustrative purposes:

- ground state $\sigma = 1$:

$$1s: R_{10} \left(\frac{r}{d} \right) = 2 \sqrt{\frac{b(b^2 + 1)}{(1 - e^{-2\pi b})}} e^{-b(\frac{r}{d})} \sin \left(\frac{r}{d} \right), \quad (36)$$

- first excited state, $\sigma = 2$:

$$2s: R_{20} \left(\frac{r}{d} \right) = \sqrt{\frac{2b \left(\left(\frac{b}{4} \right)^2 + 1 \right)}{(1 - e^{-\pi b})}} e^{-b(\frac{r}{2d})} \sin \left(\frac{r}{d} \right) \left(b \sin \left(\frac{r}{d} \right) - 2 \cos \left(\frac{r}{d} \right) \right),$$

$$2p: R_{21} \left(\frac{r}{d} \right) = 2 \sqrt{\frac{2}{3}} \sqrt{\frac{b \left(\left(\frac{b}{2} \right)^2 + 1 \right) \left(\left(\frac{b}{4} \right)^2 + 1 \right)}{(1 - e^{-\pi b})}} e^{-b \frac{r}{2d}} \sin^2 \left(\frac{r}{d} \right), \quad (37)$$

- second excited state $\sigma = 3$:

$$3s: R_{30} \left(\frac{r}{d} \right) = \frac{2}{9\sqrt{3}} \sqrt{\frac{b \left(\left(\frac{b}{9} \right)^2 + 1 \right)}{(1 - e^{-2\pi \frac{b}{3}})}} e^{-b \frac{r}{3d}} \sin \left(\frac{r}{d} \right) \left(2 \left(\left(\frac{b}{3} \right)^2 \sin^2 \left(\frac{r}{d} \right) - b \sin \left(\frac{r}{d} \right) \cos \left(\frac{r}{d} \right) + \cos^2 \left(\frac{r}{d} \right) \right) - 1 \right),$$

$$3p: R_{31} \left(\frac{r}{d} \right) = \left(\frac{2}{3} \right)^{\frac{3}{2}} \sqrt{\frac{b \left(\left(\frac{b}{3} \right)^2 + 1 \right) \left(\left(\frac{b}{9} \right)^2 + 1 \right)}{(1 - e^{-2\pi \frac{b}{3}})}} e^{-b \frac{r}{3d}} \sin^2 \left(\frac{r}{d} \right) \left(b \sin \left(\frac{r}{d} \right) - 6 \cos \left(\frac{r}{d} \right) \right),$$

$$3d: R_{32} \left(\frac{r}{d} \right) = 4 \sqrt{\frac{2}{15}} \sqrt{\frac{b \left(\left(\frac{b}{3} \right)^2 + 1 \right) \left(\left(\frac{b}{6} \right)^2 + 1 \right) \left(\left(\frac{b}{9} \right)^2 + 1 \right)}{(1 - e^{-2\pi \frac{b}{3}})}} e^{-b \frac{r}{3d}} \sin^3 \left(\frac{r}{d} \right).$$

In Figs. 5 we display as an illustrative example the wave functions for the first two σ levels.

4 Discussion and concluding remarks

In this work we made the case that the trigonometric Rosen-Morse potential with the \csc^2 term being reinterpreted as a non-standard centrifugal barrier provides quantum numbers and level splittings of same dynamical $O(4)$ patterns as observed within the $SU(2)_I \times O(4)$ classification scheme of baryons in the light quark sector. Due to local $O(4) \sim O(1, 3)$ isomorphism, the potential $\left(\frac{\kappa}{2}, \frac{\kappa}{2} \right) \otimes \left[\left(\frac{1}{2}, 0 \right) \oplus \left(0, \frac{1}{2} \right) \right]$ levels have as a relativistic image the covariant field theoretical high-spin degrees of freedom, $\psi_{\mu_1 \dots \mu_\kappa}$.

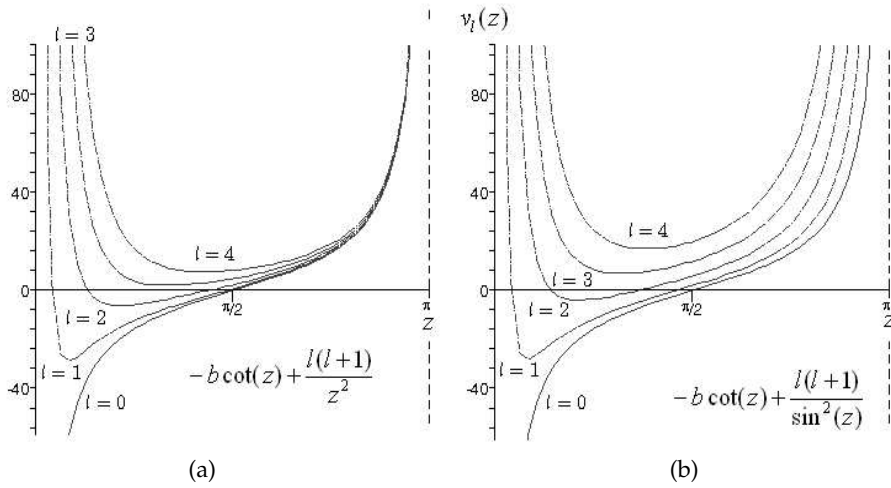


Fig. 4. The $\cot(\frac{z}{a})$ potential with the physical centrifugal barrier (left) and the non-standard one (right).

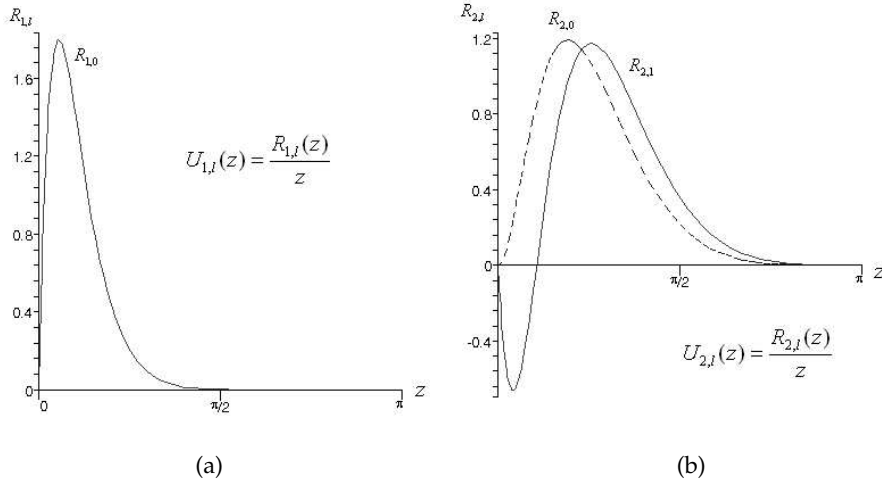


Fig. 5. Wave functions for $\sigma = 1, l = 0$ (left) and $\sigma = 2, l = 0, 1$ (right).

We presented exact energies and wave functions of a particle within the above potential and in so doing put it on equal algebraic footing with the harmonic oscillator and/or the Coulomb potentials of wide spread. In this fashion,

- an element of covariance was brought into the otherwise non-covariant potential picture,
- the algebraic Hamiltonian in Eq. (6) describing the $O(4)$ degeneracy in the N and Δ spectra was translated into a potential model of same dynamical symmetry.

The $O(4)$ degeneracy of the N and Δ spectra seem to speak in favor of quark-diquark as leading configurations of resonance structures. Yet, form factors are known to be more sensitive to configuration mixing effects and may require inclusion of genuine three quark configurations. As long as the tRMP shape captures the essential traits of the quark-gluon dynamics of QCD, we here consider it as a promising candidate for a realistic common quark potential that is worth being employed in the calculations of spectroscopic properties of non-strange resonances.

Acknowledgments

It is a pleasure to thank the organizers for their warm hospitality and the excellent working conditions provided by them during the workshop. We benefited from extended discussions with Hans-Jürgen Weber and Alvaro Pérez Raposo on various aspects of the Romanovski polynomials with emphasis on their orthogonality properties.

Work supported by Consejo Nacional de Ciencia y Tecnología (CONACyT) Mexico under grant number C01-39280.

References

1. M. Kirchbach, *Mod. Phys. Lett. A* **12**, 2373-2386 (1997).
2. W. Rarita, J. Schwinger, *Phys. Rev.* **60**, 61 (1941).
3. M. Kirchbach, *Int. J. Mod. Phys. A* **15**, 1435-1451 (2000).
4. M. Kirchbach, M. Moshinsky, Yu. F. Smirnov, *Phys. Rev. D* **64**, 114005 (2001).
5. R. Bijker, F. Iachello, A. Leviatan, *Ann. Phys.* **236**, 69-116 (1994).
6. C. V. Sukumar, *J. Phys. A:Math. Gen.* **18**, 2917 (1998); C. V. Sukumar, AIP proceedings **744**, eds. R. Bijker et al., *Supersymmetries in physics and applications* (New York, 2005) p. 167.
7. F. Cooper, A. Khare, U. P. Sukhatme, *Supersymmetry in Quantum Mechanics* (World Scientific, Singapore, 2001).
8. C. B. Compean, M. Kirchbach, *J. Phys. A:Math.Gen.* **39**, 547 (2006).
9. M. Abramowitz, I. A. Stegun, *Handbook of Mathematical Functions with Formulas, Graphs and Mathematical Tables*, (Dover, 2nd edition, New York, 1972).
10. G. B. Arfken, H. J. Weber, *Mathematical Methods for Physicists*, 6th ed. (Elsevier-Academic Press, Amsterdam, 2005).
11. Phylippe Dennery, André Krzywicki, *Mathematics for Physicists* (Dover, New York, 1996).
12. E. J. Routh, *Proc. London Math. Soc.* **16** 245 (1884).
13. V. I. Romanovski, *C. R. Acad. Sci. Paris*, **188**, 1023 (1929).
14. A. F. Nikiforov, V. B. Uvarov, *Special Functions of Mathematical Physics* (Birkhäuser, Basel-Boston, 1988).
15. M. E. H. Ismail, *Classical and Quantum Orthogonal Polynomials in One Variable* (Cambridge Univ. Press, 2005).
16. W. Koepf, M. Masjed-Jamei, *Integral Transforms and Special Functions*, **17**, 559 (2006).
17. Yu. A. Neretin, *Beta-Integrals and Finite Orthogonal Systems of Wilson Polynomials*, E-Print Archive: math.CA/0206199.

18. Alejandro Zarzo Altarejos, *Differential Equations of the Hypergeometric Type* (in Spanish), Ph. D. thesis, Faculty of Science, University of Granada (1995).
19. P. A. Lesky, *Sitzungsberichte der Mathematisch-Naturwissenschaftlichen Klasse Abt. II, Österreichische AdW*, **206**, 127 (1997).
20. D. E. Alvarez-Castillo, M. Kirchbach, *Exact Spectrum and Wave Functions of the Hyperbolic Scarf Potential in Terms of Finite Romanovski Polynomials*, E-Print Archive: quant-ph/0603122, v3.
21. N. Witte, P. J. Forrester, *Nonlinearity* **13**, 1965 (2000); E-Print Archive: math-ph/0009022.
22. K. Bennaceur, J. Dobachewski, M. Ploszajczak, *Phys. Rev. C* **60**, 034308 (1999).
23. J. N. Ginocchio, *Ann. Phys. (N.Y.)* **152**, 203 (1984); **159**, 467 (1985).
24. N. Minkov, P. Jotov, S. Drenska, W. Scheid, D. Bonatsos, D. Lenis, D. Petrellis, *Nuclear collective motion with a coherent coupling between quadrupole and octupole modes*, E-Print Archive: nucl-th/0603059.
25. Bei Zeng, Jin-Yan Zeng, *J. Math. Phys.* **43**, Issue 2, 897 (2002).



Separable Dyson-Schwinger model at finite T

D. Blaschke^{a,b}, D. Horvatić^c, D. Klabučar^c, A. E. Radzhabov^b

^aInstitut für Physik, Universität Rostock D-18051 Rostock, Germany

[‡]Bogoliubov Laboratory of Theoretical Physics, Joint Institute for Nuclear Research,
141980 Dubna, Russia

^cPhysics Department, Faculty of Science, University of Zagreb, Bijenička c. 32, Zagreb
10000, Croatia

Abstract. Theoretical understanding of experimental results from relativistic heavy-ion collisions requires a microscopic approach to the behavior of QCD n-point functions at finite temperatures, as given by the hierarchy of Dyson-Schwinger equations, properly generalized within the Matsubara formalism. The technical complexity of related finite-temperature calculations however mandates modeling. We present a model where the QCD interaction in the infrared, nonperturbative domain, is modeled by a separable form. Results for the mass spectrum of light quark flavors at finite temperature are presented.

1 Introduction

While the experiments at RHIC [1,2] advanced the empirical knowledge of the hot QCD matter dramatically, the understanding of the state of matter that has been formed is still lacking. For example, the STAR collaboration's assessment [2] of the evidence from RHIC experiments depicts a very intricate, difficult-to-understand picture of the hot QCD matter. Among the issues pointed out as important was the need to clarify the role of quark-antiquark ($q\bar{q}$) bound states continuing existence above the critical temperature T_c , as well as the role of the chiral phase transition.

Both of these issues are consistently treated within the Dyson-Schwinger (DS) approach to quark-hadron physics. Dynamical chiral symmetry breaking (DChSB) as the crucial low-energy QCD phenomenon is well-understood in the rainbow-ladder approximation (RLA), a symmetry preserving truncation of the hierarchy of DS equations. Thanks to this, the QCD low energy theorems are fulfilled and the behavior of the chiral condensate and pion mass and decay constant are in accord with the Gell-Mann–Oakes–Renner relation, i.e. the Goldstone theorem.

For recent reviews of the DS approach, see, e.g., Refs. [3,4], of which the first [3] also reviews the studies of QCD DS equations at finite temperature, started in [5]. Unfortunately, the extension of DS calculations to non-vanishing temperatures is technically quite difficult. This usage of separable model interactions greatly simplifies DS calculations at finite temperatures, while yielding equivalent results on a given level of truncation [6,7]. A recent update of this covariant

separable approach with application to the scalar σ meson at finite temperature can be found in [8]. Here, we present results for the quark mass spectrum at zero and finite temperature, extending previous work by including the strange flavor.

2 The separable model at zero temperature

The dressed quark propagator $S_q(p)$ is the solution of its DS equation [3,4],

$$S_q(p)^{-1} = i\gamma \cdot p + \tilde{m}_q + \frac{4}{3} \int \frac{d^4\ell}{(2\pi)^4} g^2 D_{\mu\nu}^{\text{eff}}(p-\ell) \gamma_\mu S_q(\ell) \gamma_\nu, \quad (1)$$

while the $q\bar{q}'$ meson Bethe-Salpeter (BS) bound-state vertex $\Gamma_{q\bar{q}'}(p, P)$ is the solution of the BS equation (BSE)

$$-\lambda(P^2) \Gamma_{q\bar{q}'}(p, P) = \frac{4}{3} \int \frac{d^4\ell}{(2\pi)^4} g^2 D_{\mu\nu}^{\text{eff}}(p-\ell) \gamma_\mu S_q(\ell_+) \Gamma_{q\bar{q}'}(\ell, P) S_q(\ell_-) \gamma_\nu, \quad (2)$$

where $D_{\mu\nu}^{\text{eff}}(p-\ell)$ is an effective gluon propagator modeling the nonperturbative QCD effects, \tilde{m}_q is the current quark mass, the index q (or q') stands for the quark flavor (u, d or s), P is the total momentum, and $\ell_\pm = \ell \pm P/2$. The chiral limit is obtained by setting $\tilde{m}_q = 0$. The meson mass is identified from $\lambda(P^2 = -M^2) = 1$. Equations (1) and (2) are written in the Euclidean space, and in the consistent rainbow-ladder truncation.

The simplest separable Ansatz which reproduces in RLA a nonperturbative solution of (1) for any effective gluon propagator in a Feynman-like gauge $g^2 D_{\mu\nu}^{\text{eff}}(p-\ell) \rightarrow \delta_{\mu\nu} D(p^2, \ell^2, p \cdot \ell)$ is [6,7]

$$D(p^2, \ell^2, p \cdot \ell) = D_0 \mathcal{F}_0(p^2) \mathcal{F}_0(\ell^2) + D_1 \mathcal{F}_1(p^2) (p \cdot \ell) \mathcal{F}_1(\ell^2). \quad (3)$$

This is a rank-2 separable interaction with two strength parameters D_i and corresponding form factors $\mathcal{F}_i(p^2)$, $i = 1, 2$. The choice for these quantities is constrained to the solution of the DSE for the quark propagator (1)

$$S_q(p)^{-1} = i\gamma \cdot p A_q(p^2) + B_q(p^2) \equiv Z_q^{-1}(p^2) [i\gamma \cdot p + m_q(p^2)], \quad (4)$$

where $m_q(p^2) = B_q(p^2)/A_q(p^2)$ is the dynamical mass function and $Z_q(p^2) = A_q^{-1}(p^2)$ the wave function renormalization. Using the separable Ansatz (3) in (1), the gap equations for the quark amplitudes $A_q(p^2)$ and $B_q(p^2)$ read

$$B_q(p^2) - \tilde{m}_q = \frac{16}{3} \int \frac{d^4\ell}{(2\pi)^4} D(p^2, \ell^2, p \cdot \ell) \frac{B_q(\ell^2)}{\ell^2 A_q^2(\ell^2) + B_q^2(\ell^2)} = b_q \mathcal{F}_0(p^2), \quad (5)$$

$$[A_q(p^2) - 1] = \frac{8}{3p^2} \int \frac{d^4\ell}{(2\pi)^4} D(p^2, \ell^2, p \cdot \ell) \frac{(p \cdot \ell) A_q(\ell^2)}{\ell^2 A_q^2(\ell^2) + B_q^2(\ell^2)} = a_q \mathcal{F}_1(p^2). \quad (6)$$

Once the coefficients a_q and b_q are obtained by solving the gap equations (5) and (6), the only model parameters remaining are \tilde{m}_q and the parameters of the gluon propagator, to be fixed by meson phenomenology.

3 Extension to finite temperature

The extension of the separable model studies to the finite temperature case, $T \neq 0$, is systematically accomplished by a transcription of the Euclidean quark 4-momentum via $p \rightarrow p_n = (\omega_n, \mathbf{p})$, where $\omega_n = (2n + 1)\pi T$ are the discrete Matsubara frequencies. In the Matsubara formalism, the number of coupled equations represented by (1) and (2) scales up with the number of fermion Matsubara modes included. For studies near and above the transition, $T \geq 100$ MeV, using only 10 such modes appears adequate. Nevertheless, the appropriate number can be more than 10^3 if the continuity with $T = 0$ results is to be verified. The effective $\bar{q}q$ interaction will automatically decrease with increasing T without the introduction of an explicit T -dependence which would require new parameters.

The solution of the DS equation for the dressed quark propagator now takes the form

$$S_q^{-1}(p_n, T) = i\boldsymbol{\gamma} \cdot \mathbf{p} A_q(p_n^2, T) + i\gamma_4 \omega_n C_q(p_n^2, T) + B_q(p_n^2, T), \quad (7)$$

where $p_n^2 = \omega_n^2 + \mathbf{p}^2$ and the quark amplitudes $B_q(p_n^2, T) = \tilde{m}_q + b_q(T)\mathcal{F}_0(p_n^2)$, $A_q(p_n^2, T) = 1 + a_q(T)\mathcal{F}_1(p_n^2)$, and $C_q(p_n^2, T) = 1 + c_q(T)\mathcal{F}_1(p_n^2)$ are defined by the temperature-dependent coefficients $a_q(T)$, $b_q(T)$, and $c_q(T)$ to be determined from the set of three coupled non-linear equations

$$a_q(T) = \frac{8D_1}{9} T \sum_n \int \frac{d^3p}{(2\pi)^3} \mathcal{F}_1(p_n^2) \mathbf{p}^2 [1 + a_q(T)\mathcal{F}_1(p_n^2)] d_q^{-1}(p_n^2, T), \quad (8)$$

$$c_q(T) = \frac{8D_1}{3} T \sum_n \int \frac{d^3p}{(2\pi)^3} \mathcal{F}_1(p_n^2) \omega_n^2 [1 + c_q(T)\mathcal{F}_1(p_n^2)] d_q^{-1}(p_n^2, T), \quad (9)$$

$$b_q(T) = \frac{16D_0}{3} T \sum_n \int \frac{d^3p}{(2\pi)^3} \mathcal{F}_0(p_n^2) [\tilde{m}_q + b_q(T)\mathcal{F}_0(p_n^2)] d_q^{-1}(p_n^2, T). \quad (10)$$

The function $d_q(p_n^2, T)$ is the denominator of the quark propagator $S_q(p_n, T)$, and is given by

$$d_q(p_n^2, T) = \mathbf{p}^2 A_q^2(p_n^2, T) + \omega_n^2 C_q^2(p_n^2, T) + B_q^2(p_n^2, T). \quad (11)$$

The procedure for solving gap equations for a given temperature T is the same as in $T = 0$ case, but one has to control the appropriate number of Matsubara modes as mentioned above.

4 Confinement and Dynamical Chiral Symmetry Breaking

If there are no poles in the quark propagator $S_q(p)$ for real timelike p^2 then there is no physical quark mass shell. This entails that quarks cannot propagate freely, and the description of hadronic processes will not be hindered by unphysical quark production thresholds. This sufficient condition is a viable possibility for realizing quark confinement [7]. A nontrivial solution for $B_q(p^2)$ in the chiral

limit ($\tilde{m}_0 = 0$) signals DChSB. There is a connection between quark confinement realized as the lack of a quark mass shell and the existence of a strong quark mass function in the infrared through DChSB. The propagator is confining if $m_q^2(p^2) \neq -p^2$ for real p^2 , where the quark mass function is $m_q(p^2) = B_q(p^2)/A_q(p^2)$. In the present separable model, the strength $b_q = B_q(0)$, which is generated by solving Eqs. (5) and (6), controls both confinement and DChSB. At finite temperature, the strength $b_q(T)$ for the quark mass function will decrease with T, until the denominator (11) of the quark propagator can vanish for some timelike momentum, and the quark can come on the free mass shell. The connection between deconfinement and disappearance of DChSB is thus clear in the DS approach. Also the present model is therefore expected to have a deconfinement transition at or a little before the chiral restoration transition associated with $b_0(T) \rightarrow 0$.

The following simple choice of the separable interaction form factors,

$$\mathcal{F}_0(p^2) = \exp(-p^2/\Lambda_0^2), \quad \mathcal{F}_1(p^2) = \frac{1 + \exp(-p_0^2/\Lambda_1^2)}{1 + \exp((p^2 - p_0^2)/\Lambda_1^2)},$$

is used to obtain numerical solutions which reproduce very well the phenomenology of the light pseudoscalar mesons and generate an acceptable value for the chiral condensate.

The resulting quark propagator is found to be confining and the infrared strength and shape of quark amplitudes $A_q(p^2)$ and $B_q(p^2)$ are in quantitative agreement with the typical DS studies. Gaussian-type form factors are used as a minimal way to preserve these properties while realizing that the ultraviolet suppression is much stronger than the asymptotic fall off (with logarithmic corrections) known from perturbative QCD and numerical studies on the lattice [9].

5 Results

Parameters of the model are completely fixed by meson phenomenology calculated from the model as discussed in [7,8]. In the nonstrange sector, we work in the isosymmetric limit and adopt bare quark masses $\tilde{m}_u = \tilde{m}_d = 5.5$ MeV and in strange sector we adopt $\tilde{m}_s = 115$ MeV. Then the parameter values

$$\Lambda_0 = 758 \text{ MeV}, \quad \Lambda_1 = 961 \text{ MeV}, \quad p_0 = 600 \text{ MeV}, \quad (12)$$

$$D_0 \Lambda_0^2 = 219, \quad D_1 \Lambda_1^4 = 40, \quad (13)$$

lead, through the gap equation, to $a_{u,d} = 0.672$, $b_{u,d} = 660$ MeV, $a_s = 0.657$ and $b_s = 998$ MeV i.e., to the dynamically generated momentum-dependent mass functions $m_q(p^2)$ shown in Fig. 1. In the limit of high p^2 , they converge to \tilde{m}_u and \tilde{m}_s . However, at low p^2 , the values of $m_u(p^2)$ are close to the typical constituent quark mass scale $\sim m_\rho/2 \sim m_N/3$ with the maximum value at $p^2 = 0$, $m_u(0) = 398$ MeV. The corresponding value for the strange quark is $m_s(0) = 672$ MeV.

Thus, Fig. 1 shows that in the domain of low and intermediate $p^2 \lesssim 1 \text{ GeV}^2$, the dynamically generated quark masses have typical constituent quark mass values.

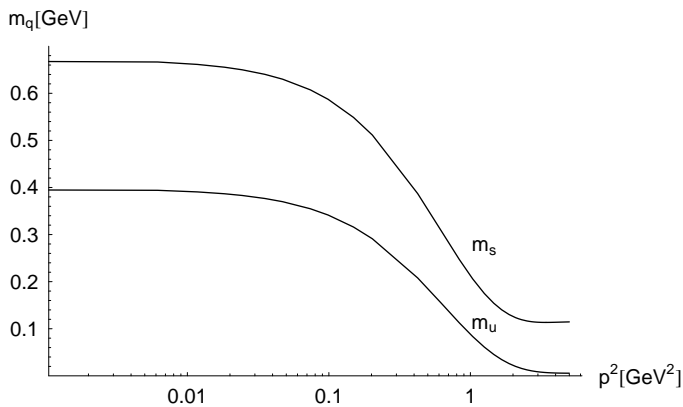


Fig. 1. The p^2 dependence (at $T = 0$) of the dynamically generated quark masses $m_s(p^2)$, $m_u(p^2)$ for, respectively, the strange and the (isosymmetric) nonstrange case.

Thus, the DS approach provides a derivation of the constituent quark model [10] from a more fundamental level, with the correct chiral behavior of QCD.

Obtaining such dynamically generated constituent quark masses, as previous experience with the DS approach shows (see, e.g., Refs. such as [3,4,10]), is essential for reproducing the static and other low-energy properties of hadrons, including decays. (We would have to turn to less simplified DS models for incorporating the correct perturbative behaviors, including that of the quark masses. Such models are amply reviewed or used in, e.g., Refs. [3,4,10,11], but addressing them is beyond the present scope, where the perturbative regime is not important.)

The extension of results to finite temperatures is given in Figs. 2, 3. Very important is the temperature dependence of the chiral-limit quantities $B_0(0)_T$ and $\langle q\bar{q} \rangle_0(T)$, whose vanishing with T determines the chiral restoration temperature T_{Ch} . We find $T_{Ch} = 128$ MeV in the present model.

The temperature dependences of the functions giving the vector part of the quark propagator, $A_{u,s}(0)_T$ and $C_{u,s}(0)_T$, are depicted in Fig. 4. Their difference is a measure of the $O(4)$ symmetry breaking with the temperature T .

The presented model, when applied in the framework of the Bethe-Salpeter approach to mesons as quark-antiquark bound states, produces a very satisfactory description of the whole light pseudoscalar nonet, both at zero and finite temperatures [12].

Acknowledgments We thank M. Bhagwat, Yu.L. Kalinovsky and P.C. Tandy for discussions. A.E.R. acknowledges support by RFBR grant No. 05-02-16699, the Heisenberg-Landau program and the HISS Dubna program of the Helmholtz Association. D.H. and D.K. were supported by MZT project No. 0119261. D.B. is grateful for support by the Croatian Ministry of Science for a series of guest lectures held in the Physics Department at University of Zagreb, where the present

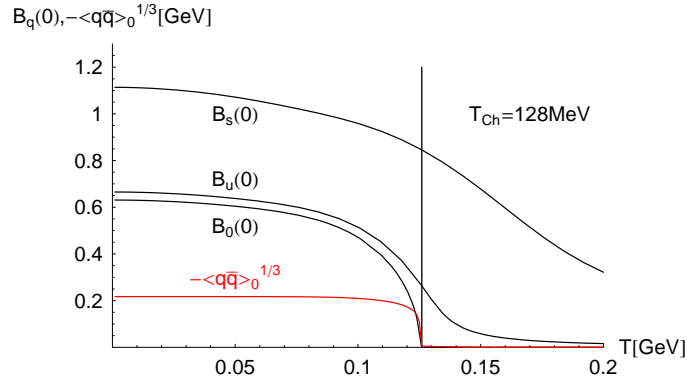


Fig. 2. The temperature dependence of $B_s(0)$, $B_u(0)$ and $B_0(0)$, the scalar propagator functions at $p^2 = 0$, for the strange, the nonstrange and the chiral-limit cases, respectively. The temperature dependence of the chiral quark-antiquark condensate, $-\langle q\bar{q} \rangle_0^{1/3}$, is also shown (by the lowest curve). Both chiral-limit quantities, $B_0(0)$ and $-\langle q\bar{q} \rangle_0^{1/3}$, vanish at the chiral-symmetry restoration temperature $T_{\text{Ch}} = 128$ MeV.

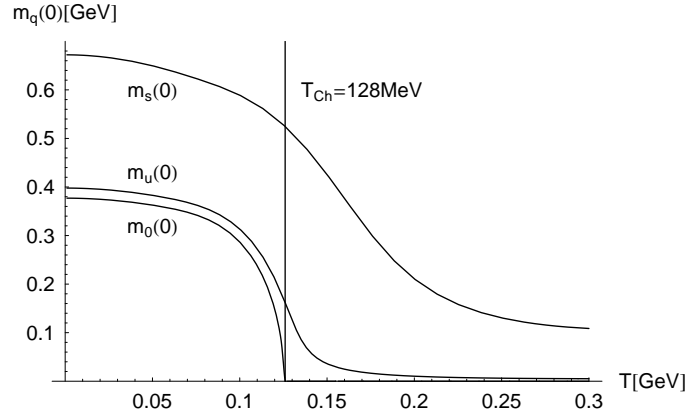


Fig. 3. The temperature dependence of $m_s(0)$, $m_u(0)$ and $m_0(0)$, the dynamically generated quark masses at $p^2 = 0$ for the strange, the nonstrange and the chiral-limit cases, respectively.

work has been completed. D.K. acknowledges the partial support of Abdus Salam ICTP at Trieste, where a part of this paper was written.

References

1. B. Müller and J. L. Nagle, arXiv:nucl-th/0602029.
2. J. Adams *et al.* [STAR Collaboration], Nucl. Phys. A **757** (2005) 102.
3. C. D. Roberts and S. M. Schmidt, Prog. Part. Nucl. Phys. **45** (2000) S1.
4. R. Alkofer and L. von Smekal, Phys. Rept. **353** (2001) 281.
5. A. Bender, D. Blaschke, Y. Kalinovsky and C. D. Roberts, Phys. Rev. Lett. **77** (1996) 3724.

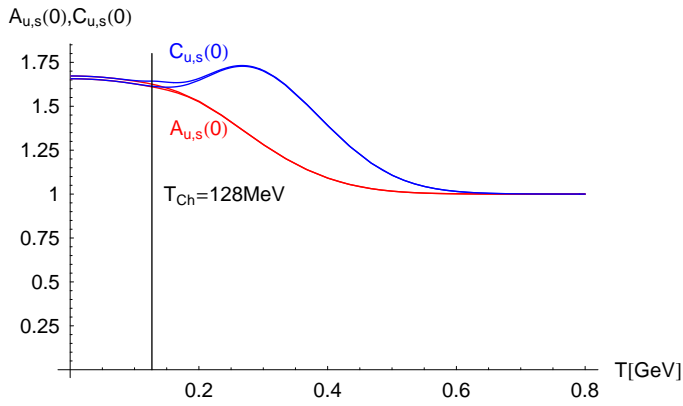


Fig. 4. The violation of $O(4)$ symmetry with T is exhibited on the example of $A_{u,s}(0)_T$ and $C_{u,s}(0)_T$.

6. C. J. Burden, L. Qian, C. D. Roberts, P. C. Tandy and M. J. Thomson, *Phys. Rev. C* **55** (1997) 2649 [arXiv:nucl-th/9605027].
7. D. Blaschke, G. Burau, Yu. L. Kalinovsky, P. Maris and P. C. Tandy, *IJMPA* **16** (2001) 2267.
8. D. Blaschke, Yu. L. Kalinovsky, A. E. Radzhabov and M. K. Volkov, *Phys. Part. Nucl. Lett.* **3** (2006) 327.
9. M. B. Parappilly, P. O. Bowman, U. M. Heller, D. B. Leinweber, A. G. Williams and J. B. Zhang, *Phys. Rev. D* **73** (2006) 054504
10. D. Kekez, B. Bistrovic and D. Klabučar, *IJMPA* **14** (1999) 161.
D. Kekez, D. Klabučar and M. D. Scadron, *J. Phys. G* **26** (2000) 1335.
11. D. Klabučar and D. Kekez, *Phys. Rev. D* **58** (1998) 096003.
D. Kekez and D. Klabučar, *Phys. Rev. D* **65** (2002) 057901.
D. Kekez and D. Klabučar, *Phys. Rev. D* **73** (2006) 036002.
12. D. Blaschke, D. Horvatić, D. Klabučar and A. E. Radzhabov, Zagreb University preprint ZTF-06-10-1.



Bosonic contractions

William H. Klink

Department of Physics and Astronomy University of Iowa, Iowa City, Iowa

1 Introduction

In point form field theory all interactions are in the four-momentum operator and Lorentz transformations are kinematic. Interactions are introduced via vertices, products of local free fields, which are integrated over the forward hyperboloid to give the interacting four-momentum operator. The natural variable that arises in point form is the four-velocity, the four-momentum divided by the bare mass of underlying constituents; to make a point form field theory discrete, it is the four-velocity that is made discrete [1].

The four-momentum operator P^μ is written as the sum of free and interacting four-momentum operators, $P^\mu = P^\mu(fr) + P^\mu(I)$. To guarantee the relativistic covariance of the theory, it is required that

$$[P^\mu, P^\nu] = 0, \quad (1)$$

$$U_\Lambda P^\mu U_\Lambda^{-1} = (\Lambda^{-1})^\mu_\nu P^\nu, \quad (2)$$

where U_Λ is the unitary operator representing the Lorentz transformation Λ . These "point form" equations [2], in which all of the interactions are in the four-momentum operator and the Lorentz transformations are kinematic, lead to the eigenvalue problem

$$P^\mu |\Psi_p\rangle = p^\mu |\Psi_p\rangle, \quad (3)$$

where p^μ is the four-momentum eigenvalue and $|\Psi_p\rangle$ the eigenvector of the four-momentum operator, which acts in generalized fermion-antifermion-boson Fock spaces. Then the physical vacuum and physical bound and scattering states should all arise as the appropriate solutions of the eigenvalue Eq.(3). What is unusual in Eq.(3) is that the momentum operator has interaction terms. But since the momentum and energy operators commute and can be simultaneously diagonalized, they have common eigenvectors. One of the important properties of the point form is that the Lorentz generators have no interactions, so that global Lorentz transformations on operators and states are easily written out.

With the exception of QCD and gravitational self couplings, all of the fundamental particle interactions have the form of bilinears in fermion and antifermion creation and annihilation operators times terms linear in boson creation and annihilation operators. For example QED is a theory bilinear in electron and positron

creation and annihilation operators and linear in photon creation and annihilation operators. The well-known nucleon-antinucleon-meson interactions are of this form as are the weak interactions. These interactions differ of course in the way the fermions are coupled to the bosons, including the way in which internal symmetries are incorporated. An exception is QCD, where due to the $SU(3)_{\text{color}}$ symmetry which generates gluon self coupling terms, the gluon sector is no longer linear in creation and annihilation operators. The other exception occurs with gravitons; since they carry energy and momentum, they also can couple to themselves.

If a^\dagger , b^\dagger and c^\dagger denote respectively, fermion, antifermion and boson creation operators, the aforementioned trilinear interactions can all be written as $(a^\dagger + b)(a + b^\dagger)(c^\dagger + c)$, while the "relativistic energy" terms are of the form $a^\dagger a - bb^\dagger + c^\dagger c$. Written in this way the fermion-antifermion bilinears $a^\dagger a$, bb^\dagger , $a^\dagger b^\dagger$, and ba close to form a Lie algebra which is related to the the Lie algebra of the unitary groups. Similarly the boson operators $c^\dagger c$, c^\dagger and c close to form a Lie algebra related to the semidirect product of unitary groups with the Heisenberg group. Then the aforementioned trilinear interactions can all be viewed as products of these two Lie algebras; some concluding remarks will be made about generalizations to QCD.

One of the main problems that arises in trying to solve continuum field theory eigenvalue equations such as Eq.(3) is that the interacting four-momentum operator takes elements out of the generalized fermion-antifermion-boson Fock space. Difficulties arise in three ways, from the infinite Lorentz volume, from the possibility of creating infinite numbers of bare fermion-antifermion pairs, and from the possibility of creating infinite numbers of bare bosons. If the number of fermion-antifermion modes is made finite, the first two kinds of problems disappear. As shown in reference [1], for a finite number of modes, N , there is an underlying fermion-antifermion symmetry generated by the Lie algebra of the group $U(2N)$.

But even with a finite number N of modes, it is still possible to have indefinitely large numbers of bare bosons in each mode. To keep the number of bare bosons finite, the algebra of bosonic operators, the semidirect product of unitary with Heisenberg algebras, will be given as a contraction limit of unitary algebras; before the contraction limit is taken, the number of bare bosons in any mode is finite. Then the eigenvalue problem, Eq.(3) becomes a problem in diagonalizing matrices. The maximum number of bare bosons is controlled by a number M , which, going to infinity as the contraction parameter goes to zero, gives the full boson algebra.

For theories like QCD there are also boson self coupling terms. In that case the $c^\dagger c$ terms in the free four-momentum operator are supplemented by the self energy terms. But the boson contraction limit is still valid with these self coupling terms, only now, of course, the matrices to be diagonalized are more complicated.

Consider then the Hamiltonian

$$H = m \sum_{i=1}^N (e_i (a_i^\dagger a_i - b_i b_i^\dagger + \kappa c_i^\dagger c_i) + \alpha A(X_i) c_i + \alpha A(X_i^\dagger) c_i^\dagger) \quad (4)$$

resulting from making the number of four-velocity modes finite; the first two terms in Eq.(4) give the discrete version of the fermion-antifermion relativistic energy. That is, the free fermionic relativistic four-momentum can be written in terms of the four-velocity as $m \int \frac{d^3v}{v_0} v^\mu a_\nu^\dagger a_\nu$, where $v = \frac{\mathbf{p}}{m}$ is the four-velocity, \mathbf{p} the four-momentum ($v \cdot v := v_0^2 - \mathbf{v} \cdot \mathbf{v} = 1$) and m is the bare mass of the fermions (spin and internal symmetry labels are suppressed here). When the four-velocity is made discrete and finite (with a total of N modes), for $\mu = 0$ the free relativistic energy, with $e_i = \sqrt{1 + \mathbf{v}_i \cdot \mathbf{v}_i}$, takes the form given in the first term in Eq.(4).

The bare mass κm of the bosons need not be the same as the bare mass m of the fermions. κ is a dimensionless constant relating the boson bare mass to the fermion bare mass. Similarly α is a bare dimensionless coupling constant giving the strength of the trilinear vertex. $\mathcal{A}(X_i) := \sum_{\mu, \nu=1}^{2N} A_\mu^\dagger X_{\mu\nu}(i) A_\nu$, with $A_\mu^\dagger = (a_i^\dagger, b_i)$, generates the four fermion bilinears $a^\dagger a$, $a^\dagger b^\dagger$, bb^\dagger , and ba , which form the basis for a fermionic Lie algebra related to the group $U(2N)$. $X_{\mu\nu}(i)$ is a matrix coupling the four fermion-antifermion bilinears to the bosons and depends on the nature of the coupling (for example, electromagnetic or pion-nucleon coupling). The antifermion relativistic energy is written as bb^\dagger rather than in the usual normal order because it is an element of the $U(2N)$ Lie algebra.

The goal is to find the eigenvectors and eigenvalues of H for finite N and then investigate the limit as N goes to infinity. But even for finite N , there can be indefinitely many bosons in each mode. The goal of this contribution to the Bled 2006 Workshop is to sketch how to make the number of bosons in each mode finite, and then recover the infinite number of bosons limit by Lie algebra contraction[3].

2 Bosonic Contractions

Consider the bosonic Lie algebra consisting of the creation and annihilation operators, c_i^\dagger, c_i . Adjoin to this the elements $L_{ij} := c_i^\dagger c_j$ (which itself generates a $U(N)$ Lie algebra), so that the commutation relations of the four types of elements are

$$[L_{ij}, c_k^\dagger] = c_i^\dagger \delta_{jk} \quad (5)$$

$$[L_{ij}, c_k] = -c_i \delta_{jk} \quad (6)$$

$$[L_{ij}, \mathbb{1}] = 0 \quad (7)$$

$$[c_i, c_j^\dagger] = \mathbb{1} \delta_{ij} \quad (8)$$

$$[c_i, \mathbb{1}] = 0 \quad (9)$$

The commutation relations are those of the semidirect product of the unitary algebra with the Heisenberg algebra, and the elements are those appearing in the bosonic part of the Hamiltonian, Eq.(4).

Actually, only the diagonal parts of L_{ij} occurs in Eq.(4), so each mode can be treated separately:

$$[L, c^\dagger] = c^\dagger \quad (10)$$

$$[L, c] = -c \quad (11)$$

$$[c, c^\dagger] = I, \quad (12)$$

which is the usual harmonic oscillator algebra for each mode (all other commutators are zero).

Consider next a U(2) Lie algebra, with elements J_1 , J_2 , and J_\pm and the following commutation relations:

$$[J_1, J_2] = 0 \quad (13)$$

$$[J_1, J_\pm] = \pm J_\pm \quad (14)$$

$$[J_2, J_\pm] = (-) \pm J_\pm \quad (15)$$

$$[J_-, J_+] = J_2 - J_1 \quad (16)$$

Now modify the basis of this Lie algebra by defining

$\tilde{J}_\pm := \rho J_\pm$ and $\tilde{J}_2 := \rho^2 J_2$, with ρ a positive number; then the Lie algebra becomes

$$[J_1, \tilde{J}_2] = 0 \quad (17)$$

$$[J_1, \tilde{J}_\pm] = \pm \tilde{J}_\pm \quad (18)$$

$$[\tilde{J}_2, \tilde{J}_\pm] = \pm (-\rho^2) \tilde{J}_\pm \quad (19)$$

$$[\tilde{J}_-, \tilde{J}_+] = \tilde{J}_2 - \rho^2 J_1 \quad (20)$$

$$(21)$$

In the contraction limit when $\rho \rightarrow 0$ this Lie algebra agrees with the one mode bosonic algebra (\tilde{J}_2 plays the role of the identity operator in this contraction)

Consider next a concrete realization of the U(2) Lie algebra, with

$$J_1 \rightarrow z \frac{\partial}{\partial z}$$

$$J_2 \rightarrow w \frac{\partial}{\partial w}$$

$$J_+ \rightarrow z \frac{\partial}{\partial w}$$

$$J_- \rightarrow w \frac{\partial}{\partial z}$$

on the holomorphic Hilbert space of two complex variables[4]. Then the bosonic representations of the Lie algebra of U(2), labelled $(M,0)$, are the homogeneous polynomials of degree M , with an orthonormal basis given by $|M, n \rangle = \frac{z^n w^{M-n}}{\sqrt{n!(M-n)!}}$. In order that such a basis be holomorphic, the total number of bosons in any mode is restricted by M . Further

$$\begin{aligned} \tilde{J}_+ |M, n \rangle &= \frac{\rho(M-n)z^{(n+1)}w^{(M-n-1)}}{\sqrt{n!(M-n)!}} \\ &= \sqrt{n+1} \sqrt{\rho^2(M-n)} |n+1 \rangle. \end{aligned} \quad (22)$$

When $M \rightarrow \infty, \rho \rightarrow 0$ such that $M\rho^2 = 1$, the usual boson calculus result is recovered.

To see how such contraction limits are used to solve eigenvalue problems, consider the simple example of a one mode Hamiltonian. For one mode the sums in Eq.(4) reduce to one term. If now in the one mode Hamiltonian the bosonic operators are replaced by their U(2) algebra analogs, the following matrix eigenvalue problem results:

$$H|\Psi\rangle = \lambda|\Psi\rangle, \quad (23)$$

$$H = a^\dagger a - b b^\dagger + \kappa J_1 + \alpha \mathcal{A}(X) J_- + \alpha \mathcal{A}(X^\dagger) J_+, \quad (24)$$

$$|\Psi\rangle = f_1(J_+) a^\dagger b^\dagger |0\rangle + f_2(J_+) |0\rangle, \quad (25)$$

$$f_\mu(J_+) = \sum_{n=0}^M f_\mu^{(n)}(J_+)^n; \quad (26)$$

here the f 's are coefficients to be determined from the eigenvalue problem and $\mu = 1, 2$. The J 's act on the $M+1$ dimensional boson space with basis given in Eq.(22). If Eqs.(24), (25), and (26) are substituted into Eq.(23), a set of coupled equations for the f 's results, in which all of the f 's except one can be eliminated. Choose $f_\mu^{(0)}$ (amplitude for finding no bare bosons); then the resulting continued fraction (or iterated resolvent[5]) solution to the eigenvalue equation has the form

$$E f + X \frac{M\alpha^2}{\lambda - \kappa - E - X \frac{2(M-1)\alpha^2}{\lambda - 2\kappa - E - \dots} X^\dagger} X^\dagger f = \lambda f. \quad (27)$$

Here $f := f_\mu^{(0)}$ and $E = \text{diag}(1, -1)$. To bring in the contraction algebra elements, Eq.(18), it is simply necessary to replace the coupling constant by $\rho\alpha$; then as $M \rightarrow \infty$ and $\rho \rightarrow 0$, such that $M\rho^2 \rightarrow 1$, Eq.(27) tends to the infinite continued fraction limit, which is the formal solution to the eigenvalue problem of the Hamiltonian given by Eq.(4) for one mode.

Generalizing to N modes, it follows that boson contraction is equivalent to truncating an infinite continued fraction series (that is, let $\alpha \rightarrow \rho\alpha$ so that $M\alpha^2 \rightarrow M\rho^2\alpha^2 \rightarrow \alpha^2$ when $M\rho^2 \rightarrow 1$). The value of M determines where the truncation occurs.

When there is bosonic self-coupling, as with gluons in QCD or gravitons, it no longer suffices to consider each mode separately, as the self-coupling terms couple the different modes. In that case the bosonic algebra is the full algebra given in Eqs.(5) through (9) and is the contraction limit of the Lie algebra of $U(N+1)$; in this case the representations are the so-called symmetric representations [4], written $(M, 0 \dots 0)$, with M again controlling the maximum number of bosons. The analysis of $U(N+1)$, its symmetric representations, and how the Lie algebra contracts to the full bosonic algebra will be discussed in a future paper dealing with the QCD Hamiltonian.

References

1. W. H. Klink, "Quantum Field Theory on Four-Velocity Lattices, preprint.

2. Point Form equations for finite degree of freedom systems are analyzed in W. Klink, *Phys. Rev. C* 58 (1998), 3587.
3. Lie group and Lie algebra contractions are discussed in various texts; see for example, R. D. Talman, *Special Functions; a Group Theoretical Approach*, New York, W. A. Benjamin, 1968. The original article on space-time contractions is given in E. Inonu and E. Wigner, *Proc. Nat. Acad. Sci.* 39 (1953) 520; for a more general discussion see E. Saletan, *Jour. Math. Phys.* 2 (1961) 15.
4. See S. Gliske, W. H. Klink, T. Ton-That, *Algorithms for Computing Generalized U(N) Racah Coefficients*, *Acta Applicandae Mathematica* (2005)88,229, section 2 for an introduction to the representation theory used here. The underlying Borel-Weil theory is discussed in A. Knapp, *Representation Theory of Semisimple Lie Groups*, Princeton University Press, Princeton NJ, 1986, page 143.
5. Iterated resolvents are discussed in the paper by H. C. Pauli, *Eur. Phys. Jour. C* 7 (1999) 289, and references cited therein. See also A. Krassnigg, W. Schweiger, W. Klink, *Phys. Rev. C* 67 (2003) 064003.



Electromagnetic currents in deuteron and NN-system induced by intermediate dibaryon*

V. I. Kukulín, I. T. Obukhovskiy and V. N. Pomerantsev

Institute of Nuclear Physics, Moscow State University, 119899 Moscow, Russia

Abstract. New, s -channel electromagnetic isoscalar currents in the NN system induced by intermediate dressed six-quark dibaryon are introduced and discussed with application to some observables in deuteron. Among these a special attention has been paid to the deuteron magnetic moment, magnetic form factor $B(Q^2)$ in the area of diffraction minimum and the circular polarization of the γ -quanta in the process $n p \rightarrow d \gamma$ at thermal neutron energies which could not be explained previously within the framework of the traditional NN force models based on the meson exchange concept. The isoscalar current in NN system has been shown to provide a new nontrivial window to the low-energy QCD, which is free from many complications of high-energy physics.

1 Modern puzzles in electromagnetic structure of NN system

From the first glance it appears that the electromagnetic structure of NN system (including deuteron) have been explored and understood in preceding years quite well. Almost all of the respective theoretical results have been obtained within conventional meson-exchange models for nuclear force and electromagnetic currents (including one-, two- and three-body currents) [1-5]. However more careful and detailed analysis of the field discloses immediately that many modern experimental data still cannot be interpreted consistently and without arbitrary assumptions. It concerns especially with the interpretation of the spin-polarization observables. To be definite, we point here to a few most evident disagreements:

- (i) Precise recent calculation [6] for the deuteron magnetic moment μ_d with inclusion of the pair currents and relativistic effects has led to a strong disagreement with well known experimental result, i.e. $\mu_{\text{theor}} = 0.8875$ n.m. vs. $\mu_{\text{exp}} = 0.85744$ n.m.
- (ii) The photon-induced spin polarization, P_γ , of emitted neutron in low-energy deuteron photo-disintegration $d(\gamma, n)p$ calculated very recently [7] with incorporation of all basic pair-current contributions revealed surprisingly large deviation from respective experiment. Moreover, inclusion of the MEC contributions even renders the disagreement larger [7].

* Talk delivered by V. Kukulín

- (iii) Cross sections and vector analyzing powers in bremsstrahlung $pp \rightarrow ppy$ process at $E_p \geq 190$ MeV in the kinematical region where relative energy of two-proton pair in final state is minimal [8]. This kinematics corresponds to the condition when γ -quantum is emitted into most backward direction. The authors [8] examined carefully all the basic MEC contributions and found no resources to improve the amount of disagreement which reaches as large as 60 – 100%!
- (iv) There are still two older unsolved problems in the field, these are the deuteron magnetic form factor $B(q^2)$ in the region near its diffraction minimum ($q_m^2 \sim 2 \text{ GeV}^2$), and
- (v) The circular polarization, P_γ , of γ -quanta emitted in radiative capture of spin-polarized neutrons in hydrogen at thermal energies $n + p \rightarrow d + \gamma$ [9]. The experimental data for the latter quantity could not be explained within conventional NN force models [10], disagreement with the data are being around 50%.

It should be emphasized that the above puzzles seem to be well within the scope of applicability of the basic non-relativistic NN potential models (with some possible minor relativistic corrections [6]). All these puzzles look to be hardly removable within conventional NN force and current models. Moreover, all the above puzzles are intimately related to the nature of short-range NN interaction which is still poorly understood up to date. So that the most radical and natural way to resolve the puzzles seems to replace the conventional Yukawa-like mechanism used in conventional force and current models used in description of the short- and intermediate-range NN interaction with some basically different model. Such a different concept for intermediate- and short-range NN interaction has been developed by our joint group from Moscow and Tübingen universities [11-15].

2 Dibaryon model for intermediate- and short-range nuclear force and new s -channel currents in NN system

The dibaryon model has already been discussed in full detail in refs. [14,15] (see also the previous Workshops of this series [16]), so that we present here only a short sketch of the model. According to the model, the intermediate- and short-range NN interaction is described by the diagram in Fig. 1:

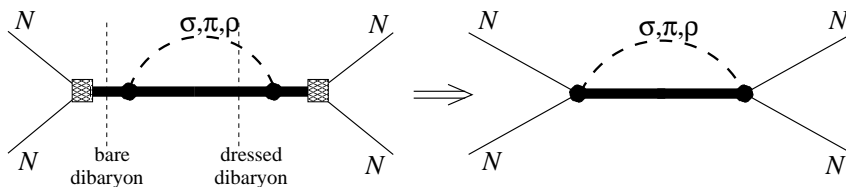


Fig. 1. Intermediate- and short-range NN interaction in the model.

where the intermediate six-quark bag dressed with a scalar σ -meson and propagating in s -channel plays a dominant role in the intermediate-range attraction. This s -channel graph replaces the conventional t -channel σ -exchange which has been demonstrated recently [17] to lead to a *strong NN repulsion rather than intermediate-range attraction* as has been assumed a long time in all conventional NN potential models [1-3]. In fact, the above s -channel dibaryon model describes the QCD string of color field with multi-quark clusters at its ends. In general, this string may vibrate and rotate and can be described quite well by a relativistic (Dirac) or even non-relativistic oscillator with size of the quantum of energy $\hbar\omega \simeq 350$ MeV [15].

The respective NN-potential, which has been derived from this picture, may have relativistic or non-relativistic form and in both cases are highly non-local and energy-dependent [14,15]. In general case, when the NN collision energy is well above 1 GeV one should take into account a few excited states of the string and the respective NN "potential" includes a few separable terms each of those being corresponds to one excited string state [15]. In the low-energy case $E_{NN} < 1$ GeV the inclusion of $2\hbar\omega$ -states will be quite sufficient to describe NN scattering amplitudes, and thus we get two-term separable potential (e.g. for uncoupled 1S_0 -channel):

$$V_{NqN}(\mathbf{q}, \mathbf{q}'; E) = g_{00}(\mathbf{q})\lambda_0 g_{00}(\mathbf{q}') + g_{22}(\mathbf{q})\lambda_2(E)g_{22}(\mathbf{q}'),$$

where $\lambda_0 \rightarrow \infty$ while $\lambda_2(E)$ corresponds to the dressed dibaryon propagator and taken from loop integral shown in Fig. 1 [14,15] and the potential form factors $g_{mn}(\mathbf{q})$ are the harmonic oscillator wave functions (relativistic or nonrelativistic).

The enhancement of the scalar field in the symmetric six-quark configuration $s^6[6]_x$ implies some rearrangement of quark-gluon fields in the region where two nucleons are totally overlapping. The emergence of a strong scalar-isoscalar field in the six-quark bag induces automatically an isoscalar exchange current in the multi-quark system.

The σ -meson loops originate mainly from "non-diagonal" transitions from the mixed-symmetry $2\hbar\omega$ -excited configurations $|s^4 p^2 [f_x][f_{CS}] \rangle$ to the unexcited fully symmetric configuration $|s^6 [6]_x \rangle$ in the six-quark system with emission of a (virtual or real) σ -meson. In turn, the strongly attractive interaction between the scalar-isoscalar σ -field and the multi-quark bag results in an enhancement of the very short-range diquark attractive correlations in the multi-quark system. Thus, as a net result of all these highly non-linear effects the mass of the intermediate dibaryon surrounded by the σ -field gets much lower as compared to the respective bare dibaryon.

This picture of the 6q-bag dressing (associated with the emergence of scalar-isoscalar field) is similar to the 3q-bag dressing for Roper resonance (B.Golli, S.Sirča). The scalar interaction can be presented not only through the σ -meson exchange but also through a quark confinement or another force including even the four-quark instanton-induced interaction of t'Hooft's type (Fig. 2) [18].

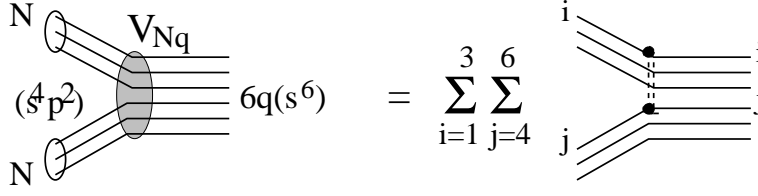


Fig.2. Graphical illustration for $NN \rightarrow DB$ transition in terms of quark microscopic model. The double-dashed line denotes some scalar exchange which can induce the $NN \rightarrow DB$ transition.

In six-quark microscopic model with above scalar exchange the transition operator V_{Nq} can be written in the form

$$V_{Nq} = \sum_{i=1}^3 \sum_{j=4}^6 g_s^2 v_s(r_{ij}), \quad (1)$$

where $v_s(r_{ij})$ is a scalar qq interaction. This operator should be substituted into the transition matrix element (2) - see below. The particular form of the scalar operator (1) and its origin are not significant here. The DBS-induced effective NN interaction generated by the scalar-exchange transition operator can be rewritten in the following constrained form:

$$V_{NqN}(\mathbf{r}, \mathbf{r}'; E) \simeq \sum_{ff'} \{ \langle N(123) | \langle N(456) \rangle | s^4 p^2 \{f\} \rangle \langle s^4 p^2 \{f\} | V_{Nq} | s^6 [6]_x \rangle G_{DB}(E) \\ \times \langle s^6 [6]_x | V_{Nq} | s^4 p^2 \{f'\} \rangle \langle s^4 p^2 \{f'\} | \{ |N(123)\rangle | N(456)\rangle \} \} \quad (2)$$

where $\{ \langle N(123) | \langle N(456) \rangle | s^4 p^2 \{f\} \rangle = C_f \varphi_{2S}(\mathbf{r})$.

The nucleon wave function $N(ijk)$ in such an approach is described by the pure s^3 configuration of the CQM,

$$|N(123)\rangle = |s^3 [3]_x \{f_{ST}\}\rangle = \psi_N(\rho_1, \rho_2) | [2^3]_C [3]_{ST} \rangle,$$

where $\psi_N(\rho_1, \rho_2) = \mathcal{N} \exp \left[-\frac{1}{2b^2} (\rho_1^2/2 + 2\rho_2^2/3) \right]$, the parameter b being the scale parameter of the CQM, with $b \simeq 0.5 - 0.6$ fm; the relative coordinates are $\rho_1 = \mathbf{r}_1 - \mathbf{r}_2$ and $\rho_2 = (\mathbf{r}_1 + \mathbf{r}_2)/2 - \mathbf{r}_3$.

Then, using the 2S function for the transition $NN \rightarrow DB$ vertex, i.e. substituting $\varphi(\mathbf{r}) = \varphi_{2S}(\mathbf{r})$, one gets in our simple ansatz Eq. (1) using the qq pair interaction $v_s(r_{ij})$ the transition matrix element:

$$\langle NN(s^4 p^2) | V_{Nq} | DB(s^6) \rangle = g_s^2 \langle v \rangle \varphi_{2S}(\mathbf{r}), \text{ and } \lambda(E) = g_s^4 \langle v \rangle^2 G_{DB}(E), \quad (3)$$

where $\langle v \rangle$ is a superposition (with the algebraic coefficients C_f) of the quark shell-model transition matrix elements $\langle s^4 p^2 | \sum_{i=1}^3 \sum_{j=4}^6 v_s(ij) | s^6 \rangle$.

As a result, the total wavefunction of the two-nucleon system Ψ_{tot} is defined in the direct sum of two Hilbert spaces $\mathcal{H}_{NN} \oplus \mathcal{H}_{DB}$, so that deuteron state in the dibaryon model reads

$$|d\rangle = \begin{pmatrix} \cos \theta_{Nq} |d(NN)\rangle \\ \sin \theta_{Nq} |DB\rangle \end{pmatrix}, \quad (4)$$

where the mixing angle θ_{Nq} is calculated on the basis of coupled channel equations [14,15] with the transition operator V_{Nq} taken as a coupling potential.

The modeling of the $NN \rightarrow DB$ transition by scalar exchanges between quarks makes it possible to consider the “contact” $\gamma NN \rightarrow DB$ vertices in terms of CQM with *the minimal electromagnetic interaction* of the constituent quarks, i.e. with the quark current

$$j_q^\mu(\mathbf{q}) = \sum_{i=1}^6 \hat{e}_i F_q(q^2) \bar{u}(p'_i) \gamma_i^\mu u(p_i),$$

where $q = p' - p$, $\hat{e}_i = \frac{1}{6} + \frac{1}{2} \tau_z^{(i)}$ and $F_q(q^2)$ is a form factor of the constituent quark which is important only at intermediate momentum transfer $Q^2 \gtrsim 1 \text{ GeV}^2/c^2$. Here $F_q(Q^2) = 1/(1 + Q^2/\Lambda_q^2)$, where the parameter Λ_q is expected to be constrained by the chiral symmetry scale $\Lambda_\chi \simeq 4\pi f_\pi \simeq 1 \text{ GeV}$. In the limit $q_0 \rightarrow 0$, the singular terms $\sigma_i^{\mu\nu} q_\nu \varepsilon_\mu^{(\lambda)*} m_q / (p'_i \cdot q)$ and $\sigma_i^{\mu\nu} q_\nu \varepsilon_\mu^{(\lambda)*} m_q / (-p_i \cdot q)$ cancel each other in sum $M_{ij(a)}^\lambda + M_{ij(b)}^\lambda$, so that one obtains in the non-relativistic approximation $q_0/m_q \ll 1$ the three-dimensional operator

$$\begin{aligned} V_{Nq\gamma} = & \frac{ie g_s^2}{2m_q} \sum_{i=1}^3 \sum_{j=4}^6 \epsilon^{(\lambda)*} \cdot \left\{ v_s(\mathbf{k}_j^2) \left(\frac{\hat{\mathbf{q}} \cdot \mathbf{k}_i}{m_q} [\boldsymbol{\sigma}_i \times \hat{\mathbf{q}}] - \frac{[\boldsymbol{\sigma}_i \times \mathbf{k}_i]}{m_q} \right) \right. \\ & \left. + v_s(\mathbf{k}_i^2) \left(-\frac{\hat{\mathbf{q}} \cdot \mathbf{k}_j}{m_q} [\boldsymbol{\sigma}_j \times \hat{\mathbf{q}}] - \frac{[\boldsymbol{\sigma}_j \times \mathbf{k}_j]}{m_q} \right) \right\} \\ & \times (2\pi)^3 \delta^3(\mathbf{p}_i + \mathbf{p}_j - \mathbf{p}'_i - \mathbf{p}'_j - \mathbf{q}) \end{aligned}$$

defined on non-relativistic quark wavefunctions of the CQM. This operator describes the transition between the NN- to the 6q-bag-channel with emission of a M1 γ -quantum, i.e. a “contact” $NN \rightarrow DB + \gamma$ interaction, schematically shown in Fig. 3.

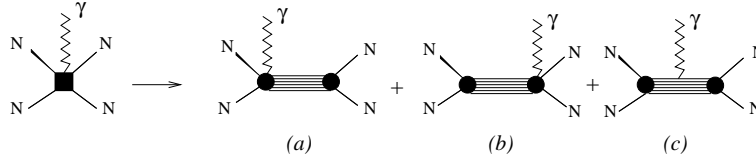


Fig. 3. Schematic representation of the new electromagnetic currents induced by intermediate dibaryon generation.

After integrating over 3q-wavefunctions of both nucleons one gets the $NqN\gamma$ (contact) term searched for (as the sum of two graphs, (a) and (b), in the above

figure)

$$V_{NqN\gamma}^{(\lambda)}(\mathbf{q}; r, r') = \frac{eZ}{2M_N} \left\{ i \left[\frac{\boldsymbol{\sigma}_p + \boldsymbol{\sigma}_n}{2} \times \mathbf{q} \right] \cdot \boldsymbol{\epsilon}^{(\lambda)*} G_M^S(q^2) \right. \\ \left. + i \left[\frac{\boldsymbol{\sigma}_p - \boldsymbol{\sigma}_n}{2} \times \mathbf{q} \right] \cdot \boldsymbol{\epsilon}^{(\lambda)*} G_M^V(q^2) \right\} \\ \times \left\{ \frac{1}{q} j_1(qr/2) \frac{d\varphi_{2S}(r)}{dr} \frac{\lambda(E')}{2M_N} \varphi_{2S}(r') + \varphi_{2S}(r) \frac{\lambda(E)}{2M_N} \frac{1}{q} j_1(qr'/2) \frac{d\varphi_{2S}(r')}{dr'} \right\},$$

where $G_M^S(0) = \mu_p + \mu_n$ and $G_M^V(0) = \mu_p - \mu_n$. Additional factor Z here incorporates the possible relativistic effects and quark boost contributions which should be essential at $Q^2 \sim 1 \text{ GeV}^2/c^2$, and other contact terms with inclusion of pseudo-scalar and vector-meson exchanges. It is felt that the value $Z \approx 1 \pm 0.3$ is reasonable since a precision of 10 - 30% is typical for standard quark model evaluations of the hadron magnetic moments. As will be demonstrated below when choosing a reasonable value $Z = 0.7$ for a single free constant the above contact term leads to a considerable improvement in description of the whole isoscalar magnetic properties of the deuteron.

3 The deuteron magnetic moment and the deuteron magnetic form factor $B(q^2)$

In our model the deuteron magnetic form factor takes the form:

$$G_M^d(q^2) = \sqrt{\frac{2}{3}} \frac{\sqrt{-q^2}}{2M_N} \left\{ \cos^2 \theta_{Nq} G_{M(NN)}^d(q^2) \right. \\ \left. + \cos^2 \theta_{Nq} \mu_{NqN} F_{NqN}(q^2) + \sin^2 \theta_{Nq} \mu_{s^6} F_{s^6}(q^2) \right. \\ \left. + 2 \cos \theta_{Nq} \sin \theta_{Nq} \mu_{s^6-s^4p^2} F_{s^6-s^4p^2}(q^2) \right\},$$

where the first term in the brackets represents the purely nucleonic current contribution while the second one corresponds to the isoscalar component of contact $NN \Leftrightarrow NN\gamma$ vertex

$$\mu_{NqN} F_{NqN}(q^2) = G_M^S(q^2) 2Z \int_0^\infty \int_0^\infty dr dr' u(r) u(r') \varphi_{2S}(r) \frac{\lambda(0)}{2M_N} \frac{j_1(qr'/2)}{q} \frac{d\varphi_{2S}(r')}{dr'}.$$

Here, $F_{NqN}(0) = 1$ by definition and thus the value μ_{NqN} is equal to that of right-hand side integral at $q = 0$. As a result, the dressed bag gives a real contribution to the deuteron magnetic moment only due to contact $NN \Leftrightarrow NN\gamma$ -vertex, and this contribution is equal to

$$\Delta\mu_d^{DB} = \cos^2 \theta_{Nq} \mu_{NqN}.$$

In all the present calculations for the deuteron magnetic moment and the structure function $B(q^2)$ the published parameters of the Moscow-Tübingen (MT) NN-model have been employed [14]. These parameters allow to fit the NN phase shifts in the very large energy interval 0 - 1000 MeV. The mixing parameter θ_{Nq}

calculated with the MT model is $\sin \theta_{Nq} = -0.13886$. The sum of the single-nucleon and bare 6q-bag contributions to the deuteron magnetic moment amounts to $\mu_d = \cos^2 \theta_{Nq} \mu_d(NN) + \sin^2 \theta_{Nq} \mu_d(6q) = 0.8489$ n.m. Then we should add the $NN \rightleftharpoons NN\gamma$ contact term contribution to this value. With $Z = 0.7$ one can reproduce exactly the deuteron magnetic moment, so that we fix it for all our subsequent calculations. We consider the accurate experimental value for this quantity as a stringent test for any new isoscalar current contribution. Further, with the fixed renormalization constant as above we calculate the deuteron magnetic form factor $B(q^2)$ and the circular polarization P_γ in $n + p \rightarrow d + \gamma$ process. We display the results of these calculations for $B(q^2)$ in Fig. 4. It is evident from the figure that the contribution of new isoscalar current makes it possible to describe quantitatively the $B(q^2)$ behaviour in all area of transfer momenta q measured up to date.

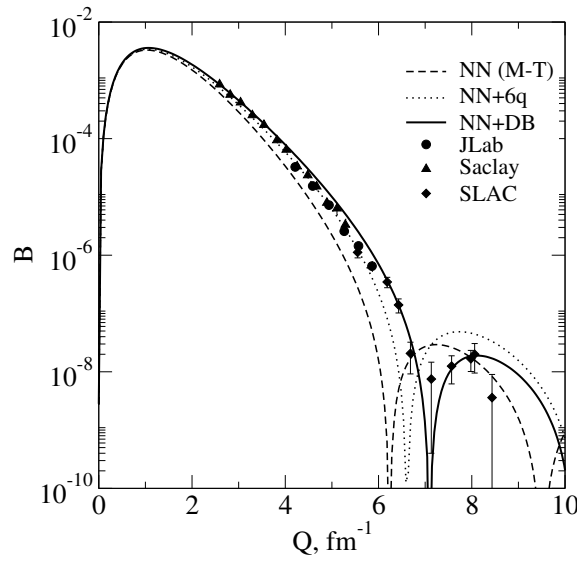


Fig. 4. The structure function $B(Q)$ of elastic e-d scattering. The impulse approximation (IA) result for the Moscow-Tübingen potential model is shown by the dashed line. The sum of IA and the diagonal ($s^6 \rightarrow s^6$) and non-diagonal ($s^6 \rightarrow s^4 p^2$) bare 6q-contributions is shown by the dotted line. The total contribution of the IA+ bare dibaryon + DB (contact term) contribution is represented by the solid line. The data are taken from (Saclay), (SLAC) and (JLab).

4 The $n + p \rightarrow d + \gamma$ reaction cross section and γ -quantum circular polarization

The total $np \rightarrow d\gamma$ reaction cross section for unpolarized neutrons can be expressed through the respective amplitudes in the following way

$$\sigma_{\text{unpol}}^{\text{tot}} = \frac{m_n}{p_n} \alpha |q| \frac{q^2}{4m_N^2} \frac{4\pi}{3} \sum_{MM'} \sum_{\lambda=\pm 1} \left[|M1_{MM',I=1}^{(\lambda)}|^2 + |M1_{MM',I=0}^{(\lambda)}|^2 + |E2_{MM'}^{(\lambda)}|^2 \right]$$

The helicity dependent cross section has a form:

$$\sigma_\lambda(\lambda_n) = \frac{m_n}{p_n} \alpha |q| \frac{q^2}{4m_N^2} \frac{1}{2} \sum_{\lambda_p} \sum_{M'} \left| \sum_M \left(\frac{1}{2} \lambda_p \frac{1}{2} \lambda_n |00\rangle M1_{MM',I=1}^{(\lambda)} + \left(\frac{1}{2} \lambda_p \frac{1}{2} \lambda_n |1M\rangle \left[M1_{MM',I=0}^{(\lambda)} + E2_{MM'}^{(\lambda)} \right] \right) \right|^2.$$

where $M1_{MM'}^{(\lambda)}$ and $E2_{MM'}^{(\lambda)}$ are the respective matrix elements. The $M1_{MM',I=0}^{(\lambda)}$ matrix element includes both the single-nucleon and s -channel new currents while the $M1_{MM',I=1}^{(\lambda)}$ and $E2_{MM'}^{(\lambda)}$ elements are related to the nucleonic currents only (in the present calculation).

Using the above general formulas for the helicity dependent cross sections one can find the circular polarization $P_\gamma(\lambda_n)$ for the fixed initial values of λ_n (or λ_n, λ_p)

$$P_\gamma(\lambda_n) = \frac{\sigma_{\lambda=1}(\lambda_n) - \sigma_{\lambda=-1}(\lambda_n)}{\sigma_{\text{unpol}}} = \frac{\sum_{\lambda=\pm 1} \lambda \sigma_\lambda(\lambda_n)}{\frac{1}{2} \sum_{\lambda_n} \sum_{\lambda=\pm 1} \sigma_\lambda(\lambda_n)}.$$

It is important to stress, that the dependence of the $M1$ - and $E2$ -transition matrix elements upon the momentum transfer q in these formulas is rather weak at low energies and becomes quite significant only for e - d scattering in the region of moderate and high momenta transfer. The eventual expression for P_γ takes the form: $P_\gamma(\lambda_n) = (-1)^{1/2+\lambda_n} P_\gamma$ with $P_\gamma = 2\text{Re} \{ M1_0^{\text{total}}/M1_1 + E2_0^{\text{total}}/M1_1 \}$.

Table 1. Circular polarization of γ quanta in the $n + p \rightarrow d + \gamma$ reaction

Model	$P_\gamma(M1)$.10 ³	$P_\gamma(E2)$.10 ³	$P_\gamma(NN)$.10 ³	$P_\gamma(DB)$.10 ³	p_γ^{total} .10 ³
Reid 93	-1.761	0.699	-1.062	0	-1.062
Moscow-Tübingen	-1.791	0.657	-1.134	-0.261	-1.395
Experiment					-1.5±0.3

The results of P_γ calculation are shown in Table 1 together with comparison with the similar results found with a conventional NN-force model (RSC93) and respective experimental value. As it evident from the Table, our parameter-free calculation gives (in a first time) a good agreement with the experimental result.

Summarizing all the above material one can conclude that the dibaryon model for basic NN force leads to a good description for deuteron magnetic properties at low and high momentum transfer and also to explanation of very tiny polarization effects in $n + p \rightarrow d + \gamma$ process. These facts may serve as strong additional arguments in favor of the dibaryon model of nuclear force, together with optimistic results found previously [11-15] with the above model.

Acknowledgment This work was partially supported by the Russian Foundation for Basic Research (grants 05-02-04000 and 05-02-17407) and the Deutsche Forschungsgemeinschaft (grant 436 RUS 113/790/).

References

1. R. Schiavilla and D.O.Riska, Phys. Rev. C **43**, 437 (1991).
2. E. Hummel and J.A. Tjon, Phys. Rev. Lett. **63**, 1788 (1989).
3. L.E. Marcucci, D.O.Riska and R. Schiavilla, Phys. Rev. C **58**, 3069 (1998).
4. D.R. Phillips, nucl-th/0304046.
5. A. Buchmann, Y. Yamauchi, and A. Faessler, Nucl. Phys. **A496**, 621 (1989).
6. H. Arenhövel, F. Ritz, and T. Wilbois, Phys. Rev. **C61**, 034002 (2000).
7. R. Schiavilla, Phys. Rev. **C72**, 034001 (2005).
8. M Cozma, O. Scholten, R.G.E. Timmermans and J.E. Tjon, Phys. Rev. **C68**, 044003 (2003).
9. A. Bazhenov *et al*, Phys.Lett. B **289**, 17 (1992); V.A. Vesna *et al*, Nucl. Phys. **A352**, 181 (1981).
10. A.P. Burichenko and I.B. Khriplovich, Nucl. Phys. **A515**, 139 (1990).
11. V.I. Kukulin, I.T. Obukhovskiy, V.N. Pomerantsev, and A. Faessler, J.Phys. G: Nucl. Part. Phys. **27**, 1851 (2001).
12. V.I. Kukulin, I.T. Obukhovskiy, V.N. Pomerantsev and A. Faessler, Physics of Atomic Nucl. **64**, 1748 (2001).
13. V.I. Kukulin, V.N. Pomerantsev, M. Kaskulov, and A. Faessler, J. Phys. G **30**, 287 (2004); V.I. Kukulin, V.N. Pomerantsev, and A. Faessler, J. Phys. G **30**, 309 (2004).
14. V.I. Kukulin, I.T. Obukhovskiy, V.N. Pomerantsev, and A. Faessler, Int. J. Mod. Phys. E **11**, 1 (2002).
15. A. Faessler, V.I. Kukulin, and M.A. Shikhalev, Ann. Phys. (NY) **320**, 71 (2005).
16. V.I. Kukulin, in Bled Workshops in Physics, vol.6, N1, "Exciting Hadrons", p.8 (2005).
17. E. Oset *et al.*, Progr. Theor. Phys. **103**, 351 (2000); M.M. Kaskulov and H. Clement, Phys. Rev. **C70**, 014002 (2004).
18. V.I. Kukulin, I.T. Obukhovskiy, V.N. Pomerantsev, and A. Faessler, nucl-th/0607001.



Hadronic decays and baryon structure^{*}

T. Melde, W. Plessas, and B. Sengl

Theoretical Physics, Institute for Physics, University of Graz
Universitätsplatz 5, A-8010 Graz, Austria

Abstract. Relativistic constituent quark models generally describe three-quark systems with particular interactions. The corresponding invariant mass eigenvalue spectra and pertinent eigenstates should exhibit the multiplet structure anticipated for baryon resonances. Taking into account the flavour content, spin structure, and spatial distribution of the baryon wave functions together with mass relations of the eigenvalues and decay properties of the eigenstates, we can link the theoretical mass eigenstates with the experimentally measured resonances. The resulting classification of baryon resonances differs in some respects from the one suggested by the Particle Data Group. With regard to the hadronic decay widths of light and strange baryon resonances a consistent picture emerges only, if the classification includes two-star resonances.

1 Introduction

Constituent quark models (CQMs) for light and strange baryons have seen a number of important new developments over the last few years. Generally, CQMs are specified by a confining interaction and an interaction responsible for the hyperfine splitting of the baryon spectra. There has been a number of different implementations of hyperfine (and confining) interactions, and some prominent models are based on one-gluon-exchange (OGE) [1], instanton-induced (II) [2,3], and Goldstone-boson-exchange (GBE) dynamics [4,5].

Recently, we have presented relativistic calculations of π and η decay widths of N and Δ resonances within the point-form spectator model (PFSM), and it has been seen that the experimental data are systematically underestimated [6]. Similar characteristics of these decay widths have been found by the Bonn group following a completely different relativistic approach, namely with the II CQM in the framework of the Bethe-Salpeter equation [7,8]. Previous studies of mesonic baryon decays along CQMs essentially employed nonrelativistic or relativised methods [9–15]. Our investigations of hadronic decays within the point form have now been extended to the nonstrange decays of strange resonances [16]. The corresponding decay widths exhibit similar characteristics as the ones in the light sector [6]. A specific interpretation has been reached with regard to the three $\frac{1}{2}^-$ Σ levels produced by CQMs (below 2 GeV): Only the third excitation (in the GBE CQM) should be identified with the measured $\Sigma(1750)$ resonance.

^{*} Talk delivered by T. Melde.

2 Classification in Flavour Multiplets

Motivated by the consistent picture that arose from the PFSM results for hadronic decay widths we undertook a classification of the mass-operator eigenstates into flavour multiplets according to their most congruent behaviour of spatial densities, spin as well as flavour content, mass relations, and decay properties. A natural pattern of flavour multiplets emerges that comprises also experimentally less well established (i.e., two-star) resonances. The resulting multiplets are summarized in Table 1. In the first column the total spin and parity J^P of the flavour multiplet members are given as well as the total orbital angular momenta L and total spins S specifying their wave functions in the rest frame. The bold-face entries denote states where our classification differs from the one by the PDG [18], and the last column refers to the multiplet number according to the classification of Guzey and Polyakov [17]. This classification is nearly identical to ours. The only exception is the $\Lambda(1810)$, which turns out to be a flavour singlet (with a percentage of 92%) rather than a flavour octet.

Table 1. Suggested classification of experimentally seen baryons. The last column denotes the multiplet number according to Guzey and Polyakov [17]. The superscripts denote the percentages of octet, singlet, and decuplet flavour contributions in the respective states (specifically in case of the GBE CQM).

$(LS)J^P$				#	
Octets					
$(0\frac{1}{2})\frac{1}{2}^+$	$N(939)^{100}$	$\Lambda(1116)^{100}$	$\Sigma(1193)^{100}$	$\Xi(1318)^{100}$	1
$(0\frac{1}{2})\frac{1}{2}^+$	$N(1440)^{100}$	$\Lambda(1600)^{96}$	$\Sigma(1660)^{100}$	$\Xi(\mathbf{1690})^{100}$	3
$(0\frac{1}{2})\frac{1}{2}^+$	$N(1710)^{100}$		$\Sigma(\mathbf{1880})^{99}$		4
$(1\frac{1}{2})\frac{1}{2}^-$	$N(1535)^{100}$	$\Lambda(1670)^{72}$	$\Sigma(\mathbf{1560})^{94}$		9
$(1\frac{3}{2})\frac{1}{2}^-$	$N(1650)^{100}$	$\Lambda(1800)^{100}$	$\Sigma(\mathbf{1620})^{100}$		14
$(1\frac{1}{2})\frac{3}{2}^-$	$N(1520)^{100}$	$\Lambda(1690)^{72}$	$\Sigma(1670)^{94}$	$\Xi(1820)^{97}$	8
$(1\frac{3}{2})\frac{3}{2}^-$	$N(1700)^{100}$		$\Sigma(1940)^{100}$		11
$(1\frac{3}{2})\frac{5}{2}^-$	$N(1675)^{100}$	$\Lambda(1830)^{100}$	$\Sigma(1775)^{100}$	$\Xi(\mathbf{1950})^{100}$	12
Singlets					
$(0\frac{1}{2})\frac{1}{2}^+$		$\Lambda(\mathbf{1810})^{92}$			4
$(1\frac{1}{2})\frac{1}{2}^-$		$\Lambda(1405)^{71}$			6
$(1\frac{1}{2})\frac{3}{2}^-$		$\Lambda(1520)^{71}$			7
Decuplets					
$(0\frac{3}{2})\frac{3}{2}^+$	$\Delta(1232)^{100}$	$\Omega(1672)^{100}$	$\Sigma(1385)^{100}$	$\Xi(1530)^{100}$	2
$(0\frac{3}{2})\frac{3}{2}^+$	$\Delta(1600)^{100}$		$\Sigma(\mathbf{1690})^{99}$		5
$(1\frac{1}{2})\frac{1}{2}^-$	$\Delta(1620)^{100}$		$\Sigma(\mathbf{1750})^{94}$		10
$(1\frac{1}{2})\frac{3}{2}^-$	$\Delta(1700)^{100}$				13

The PDG suggests a classification of baryons without consideration of one- and two-star resonances [18]. The proposed scheme closely resembles the one by Samios et al. [19] postulated already in 1974, when many of the resonances known today have not yet been confirmed. In the context of modern relativistic CQMs one learns that also less well established resonances of two-star status should be included into a classification of flavour multiplets. A prominent example is the $\Sigma(1750)$, which is to be identified only with the third $\frac{1}{2}^-$ excitation in CQMs and turns out to be in a flavour decuplet.

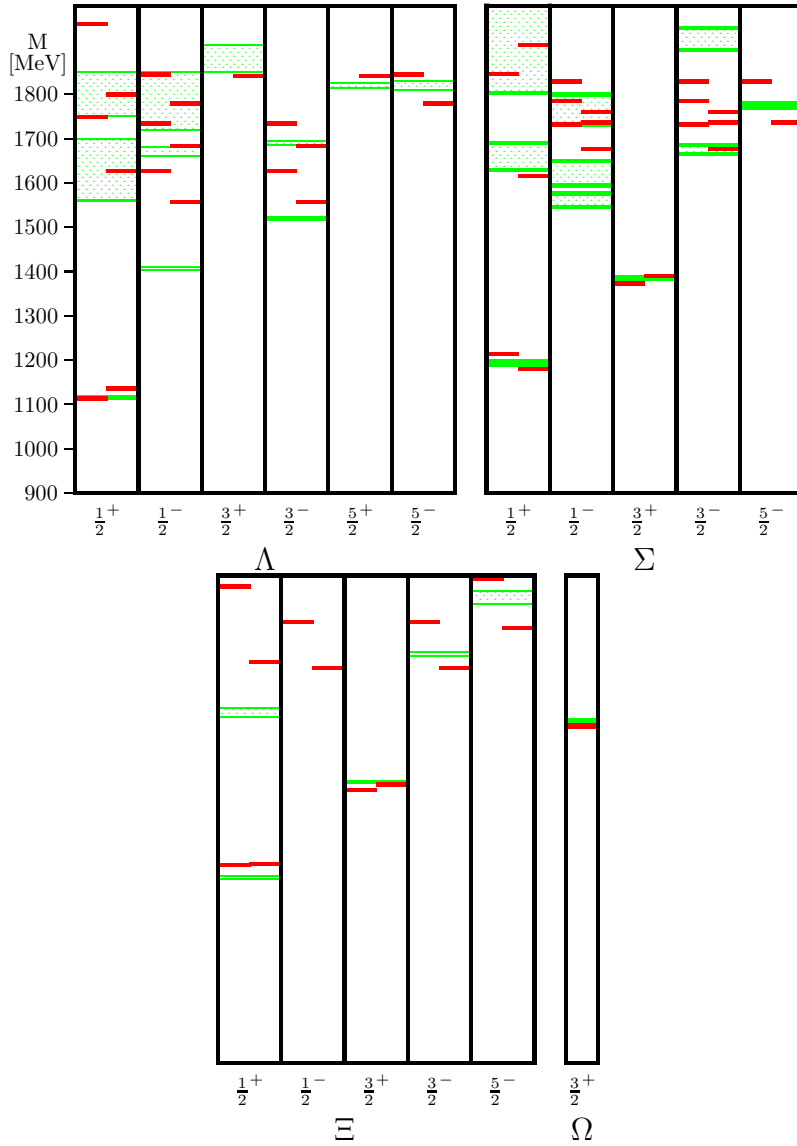


Fig. 1. Λ , Σ , Ξ , and Ω spectra for OGE (left) and GBE (right) CQMs.

The octet states in Table 1 have a pure or very predominant octet flavour content, with the notable exceptions of the $\Lambda(1670)$ and $\Lambda(1690)$; the latter couple strongly to singlet states. The state $\Lambda(1810)$ is identified as a (nearly pure) singlet state in concordance with a recent large- N_c study [20]. The other two singlets exhibit considerable admixtures of octet contributions, congruent with the singlet contributions of their partners in the octet multiplets. It should also be noted that the classification of the $\Xi(1950)$ as $J^P = \frac{5}{2}^-$ is different from a recent one by Zhou and Ma [21], who classified it as a $J^P = \frac{3}{2}^-$.

In Fig. 1 we show all the experimental resonance states (shadowed boxes) employed for the classification of the mass eigenstates produced by the GBE and OGE CQMs (horizontal lines). Specifically in the Σ excitation spectrum with $J^P = \frac{1}{2}^-$ a natural explanation of the states is found, if in addition to the $\Sigma(1750)$ also the two lower lying states are included, which are seen in experiment as two-star resonances. It is interesting to note that the ordering of the three Σ states with $J^P = \frac{1}{2}^-$ is different in the two CQMs, namely octet-decuplet-octet for the OGE and octet-octet-decuplet for the GBE. Only in the Σ spectrum with $J^P = \frac{3}{2}^-$ and the Ξ spectrum with $J^P = \frac{1}{2}^-$ we still observe more theoretical states than experimentally seen resonances. However, at least in case of the Σ the PDG expects a resonance in the relevant mass range.

3 Summary

We have investigated the properties of the light and strange baryons obtained with the relativistic OGE and GBE CQMs. It has been found that the CQMs provide a high degree of systematics with regard to the spectroscopy: The invariant mass eigenstates yield a consistent pattern of flavour multiplets. In particular, the $\Sigma(1750)$ is identified as a flavour decuplet. Additional two-star resonances can be interpreted consistently. A new classification is reached differing in some respects from the one by the PDG [18].

On the other hand, one faces difficulties in the description of baryon reactions. In particular, the predictions of covariant decay widths along the PFSM cannot explain all of the experimental results. Further relativistic studies are necessary. In particular, investigations on the intricacies of the PFSM construction [22] might be of further relevance. For a more refined approach the inclusion of explicit mesonic degrees of freedom appears mandatory. Investigative coupled-channel calculations in a Poincaré-invariant quantum-mechanical framework have already been performed in the meson sector [23,24]. However, the complexity of this approach still prevents the application to baryons. For including mesonic degrees of freedom in the description of baryons, a promising first step would be to take into account appropriate contributions (similar to the ones derived in Ref. [25]) directly on the baryon-meson level.

Acknowledgment This work was supported by the Austrian Science Fund (Projects FWF-P16945 and FWF-P19035). B. S. acknowledges support through the

Doktoratskolleg Graz "Hadrons in Vacuum, Nuclei and Stars" (FWF-DK W1203). We like to thank F. Stancu for pointing out the classification of the $\Lambda(1810)$ as a singlet in the study of Ref [20].

References

1. S. Capstick and N. Isgur, Phys. Rev. D **34**, 2809 (1986).
2. U. Loering, B. C. Metsch, and H. R. Petry, Eur. Phys. J. A **10**, 395 (2001).
3. U. Loering, B. C. Metsch, and H. R. Petry, Eur. Phys. J. A **10**, 447 (2001).
4. L. Y. Glozman, W. Plessas, K. Varga, and R. F. Wagenbrunn, Phys. Rev. D **58**, 094030 (1998).
5. L. Y. Glozman *et al.*, Phys. Rev. C **57**, 3406 (1998).
6. T. Melde, W. Plessas, and R. F. Wagenbrunn, Phys. Rev. C **72**, 015207 (2005); Erratum, *ibid.* to appear .
7. B. Metsch, U. Loering, D. Merten, and H. Petry, Eur. Phys. J. A **18**, 189 (2003).
8. B. Metsch, AIP Conf. Proc. **717**, 646 (2004).
9. F. Stancu and P. Stassart, Phys. Rev. D **39**, 343 (1989).
10. S. Capstick and W. Roberts, Phys. Rev. D **49**, 4570 (1994).
11. P. Geiger and E. S. Swanson, Phys. Rev. D **50**, 6855 (1994).
12. E. S. Ackleh, T. Barnes, and E. S. Swanson, Phys. Rev. D **54**, 6811 (1996).
13. A. Krassnigg *et al.*, Few Body Syst. Suppl. **10**, 391 (1999).
14. W. Plessas *et al.*, Few Body Syst. Suppl. **11**, 29 (1999).
15. L. Theussl, R. F. Wagenbrunn, B. Desplanques, and W. Plessas, Eur. Phys. J. A **12**, 91 (2001).
16. B. Sengl, T. Melde, and W. Plessas, contribution to these proceedings
17. V. Guzey and M. V. Polyakov, hep-ph/0512355 (2005).
18. W.-M. Yao *et al.*, J. Phys. G **33**, 1 (2006).
19. N. P. Samios, M. Goldberg, and B. T. Meadows, Rev. Mod. Phys. **46**, 49 (1974).
20. N. Matagne and F. Stancu, Phys. Rev. D **74**, 034014 (2006).
21. Q. Zhou and B.-Q. Ma, Eur. Phys. J. A **28**, 345 (2006).
22. T. Melde, L. Canton, W. Plessas, and R. F. Wagenbrunn, Eur. Phys. J. A **25**, 97 (2005).
23. A. Krassnigg, W. Schweiger, and W. H. Klink, Phys. Rev. C **67**, 064003 (2003).
24. A. Krassnigg, Phys. Rev. C **72**, 028201 (2005).
25. L. Canton, T. Melde, and J. P. Svenne, Phys. Rev. C **63**, 034004 (2001).



Baryons in relativistic constituent quark models

W. Plessas

Theoretical Physics, Institute for Physics, University of Graz
Universitätsplatz 5, A-8010 Graz, Austria

The performance of relativistic constituent quark models in baryon physics is reviewed. First, the invariant mass spectra of light, strange as well as charmed baryons are addressed. For the baryons containing only u , d , and s quarks three types of relativistic constituent quark models existing in the literature are considered, namely, the ones whose hyperfine interaction is based on one-gluon-exchange [1], Goldstone-boson-exchange [2], and instanton-induced dynamics [3]. With regard to charmed baryons it is in particular examined, which kind of hyperfine interaction between light and heavy (c) quarks is more promising. For this purpose two variants of extensions of the Goldstone-boson-exchange constituent quark model from the (u,d,s) to the charm sector are examined; the first one employs one-gluon exchange and the second one Goldstone-boson exchange between the light and heavy quarks [4]. It is found that both of them are capable of reproducing the spectra of the charmed baryons as measured hitherto in about the same quality, and like it is achieved also by the instanton-induced constituent quark model [5]. Additional experimental data would be necessary in order to discriminate between different hyperfine interactions for light and heavy quarks.

Subsequently the relativistic predictions for the elastic electroweak structure of the nucleons and the other light and strange baryon ground states as produced by the various constituent quark models are discussed. With regard to the one-gluon-exchange as well as Goldstone-boson-exchange constituent quark models the covariant results obtained with the current operators of the point-form spectator model are found to be very similar to each other and to the results of the instanton-induced model (obtained within the Bethe-Salpeter approach) and to be everywhere in remarkable good agreement with experiments [6,7]. On the contrary, the analogous results in the instant-form spectator model appear to be deficient. Neither are they frame-independent nor can they reach a good reproduction of experiment.

With regard to hadronic reactions involving baryons we refer to the contributions of B. Sengl and T. Melde in these proceedings [8,9]. Therein, relativistic results for the π decays of light and strange baryons are discussed, as calculated with the point-form spectator-model decay operator. From the pattern of mesonic decays useful conclusions can be drawn on the classification of baryons into flavor multiplets.

References

1. L. Theussl, R. F. Wagenbrunn, B. Desplanques, and W. Plessas, *Eur. Phys. J. A* **12**, 91 (2001).
2. L. Y. Glozman, W. Plessas, K. Varga, and R. F. Wagenbrunn, *Phys. Rev. D* **58**, 094030 (1998).
3. U. Loering, B. C. Metsch, and H. R. Petry, *Eur. Phys. J. A* **10**, 395 (2001); *ibid.* **10**, 447 (2001).
4. D. Prieling, Diploma Thesis, University of Graz (2006).
5. S. Migura, D. Merten, B. Metsch and H. R. Petry, *Eur. Phys. J. A* **28**, 41 (2006).
6. S. Boffi, L. Y. Glozman, W. Klink, W. Plessas, M. Radici and R. F. Wagenbrunn, *Eur. Phys. J. A* **14**, 17 (2002).
7. K. Berger, R. F. Wagenbrunn and W. Plessas, *Phys. Rev. D* **70**, 094027 (2004).
8. B. Sengl, T. Melde, and W. Plessas, contribution to these proceedings.
9. T. Melde, W. Plessas, and B. Sengl, contribution to these proceedings.



The hypercentral CQM and the electromagnetic form factors

Elena Santopinto

I.N.F.N. and Dipartimento di Fisica dell'Università di Genova, Italy

Abstract. The electromagnetic transition form factors from the nucleon to the resonances are studied in the framework of the hypercentral Constituent Quark Model. Discrepancies between data and theoretical predictions at low Q^2 are discussed and since, this also seems to be a common feature of other versions of CQMs, it is shown to lead to conclusions regarding the lack of degrees of freedom, in particular of explicit effects of quark-antiquark pairs.

1 Introduction

The fact that QCD equations cannot be solved at the hadronic scale has given rise to many effective models of the hadrons, such as bag models, constituent quark models, soliton models etc. , but also to lattice formulation of QCD. Constituent Quark Models based on the effective degrees of freedom of three constituent quarks, have been proposed in several versions: the Capstick and Isgur model, CI, [1], the algebraic U(7)-model, U(7), [2] the hypercentral formulation [3], the chiral Boson Exchange Model, χ CQM, [4,5] and the Bonn Instanton Model, Bonn IM [6]. While these models display important and peculiar differences, they have main features, in common: they all are based on the effective degrees of freedom of three constituent quarks and on the SU(6) spin-flavour symmetry; they also contain a long-range linear confining potential and an SU(6)-breaking term, even though the form and the advocated origin of this last term may be different (as in the one-gluon-exchange-inspired hyperfine interaction and in the Goldstone Boson Exchange SU(6)-breaking interaction used in the chiral model). There is also another limit-class of Constituent Models based on the diquark and quark effective degrees of freedom, since we can think of the diquark as two correlated quarks. Recently, a new diquark model has been proposed for which the electromagnetic transition form factors have also been calculated and have shown a good power-low behaviour. This is an Interacting Quark-Diquark Model [7] based on a coulomb plus linear confining potential and an exchange potential. It has been shown that the presence of a coulomb potential with its O(4)-dynamical symmetry not only helps in the reproduction of the experimental spectrum, but is also responsible for the good power-low behaviour of the electromagnetic form factors. This limit class model will not be discussed further in this paper.

2 The CQMs

The experimental 4– and 3–star non-strange resonances can be arranged in $SU_{sf}(6)$ -multiplets (see Fig. 1). This means that the quark dynamics has a dominant $SU_{sf}(6)$ -invariant part which accounts for the average multiplet energies. In order to reproduce the spectrum, a model will first of all have to reproduce more or less the general trend of the averaged $SU_{sf}(6)$ (spin-flavour) multiplets and then, by means of an $SU_{sf}(6)$ -breaking term, the splitting inside each of them. Thus, although the different CQMs are quite different, we can, for each of them, split the potential into an $SU_{sf}(6)$ -invariant part plus an $SU_{sf}(6)$ -breaking term, which is spin-dependent and can also be flavour-dependent. In the early LQCD calculations, the presence of a long range spin-flavour independent potential was already proved [8].

In the various CQM versions, this is realized as follows: in the CI model the confinement is provided by a three-body term corresponding to a string-like Y-shaped configuration, while the $SU(6)$ -breaking potential is of the OGE-inspired type. In the $U(7)$ model the Hamiltonian can be described as a string-like collective model that describes vibrations and rotations of a string-like Y-shaped configuration, while the energy splittings are produced by a Guersy and Radicati mass formula, thus depending also on flavour and not only spin. In the χ CQM the confinement interaction is of a linear type (a two-body linear potential), while the $SU(6)$ -breaking potential is provided by a meson-exchange potential, since at low energies the Goldstone Bosons are important degrees of freedom. This is formulated in Point Form dynamics. The Bonn IM is relativistic, since it is based on a Bethe-Salpeter approach for the description of the three-body problem. The confinement is provided by a linear term depending on a collective variable. The $SU(6)$ -breaking term is provided by a two-body 't Hooft residual interaction, based on QCD-instanton effects. Finally, the hypercentral CQM can be considered a very simple schematization of linear plus coulomb like terms in the hypercentral approximation plus an $SU(6)$ -breaking term originally only spin-dependent, in a new version also spin-and flavour-dependent.

3 The hypercentral CQM

The relative configurations of three objects can be described by means of the Jacobi coordinates ρ and λ , i.e. (ρ, Ω_ρ) and $(\lambda, \Omega_\lambda)$; however, they can also be described by means of the so-called hyperspherical coordinates. This means using, instead of the modulus of ρ and the modulus of λ , the root-mean-square of the sum of their squares, $x = \sqrt{\rho^2 + \lambda^2}$ and their ratio $\xi = \arctg(\frac{\rho}{\lambda})$, keeping the standard angles Ω_ρ and Ω_λ .

In the hCQM the $SU(6)$ invariant potential is assumed to be hypercentral that is of the type that depends only on the collective coordinate called hyperradius, x , and in particular of hypercoulomb plus linear type [3]

$$V(x) = -\frac{\tau}{x} + \alpha x. \quad (1)$$

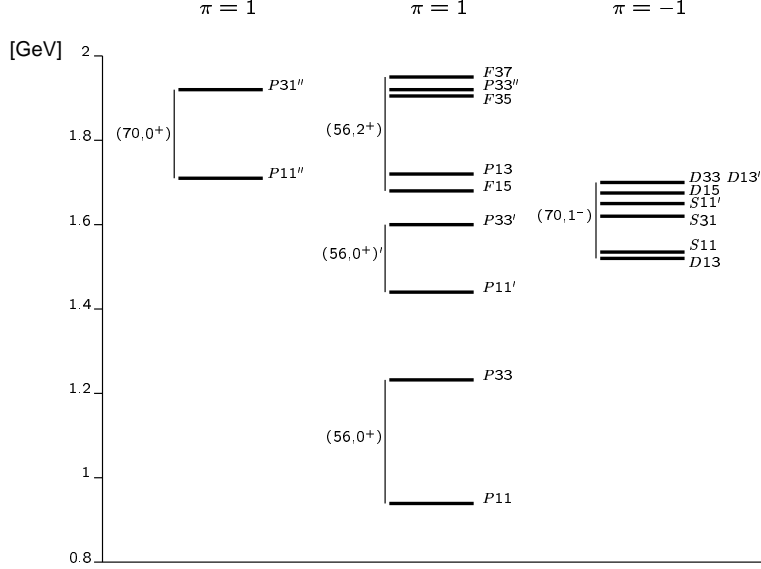


Fig. 1. The experimental spectrum of the 4- and 3-star non strange resonances. On the left the standard assignments to the SU(6) multiplets is reported, with the total orbital angular momentum and the parity too.

Interactions of the type linear plus Coulomb-like have long been used for the meson sector (*e.g.* the Cornell potential). This form has been supported by recent Lattice QCD calculations for static sources [10].

In the case of baryons, a so-called hypercentral approximation has been introduced [11,12], which amounts to averaging all the two-body potentials for the three-quark system over the hyperangle ξ , and works quite well, especially for the lower part of the spectrum [13]. In this respect, the hypercentral potential Eq.1 can be regarded as the hypercentral approximation of the Lattice QCD potential. On the other hand, the hyperradius x is a collective coordinate and therefore the hypercentral potential also contains three-body effects.

The hypercoulomb term $1/x$ has important features [3,14]: it can be solved analytically and the resulting form factors have a power-law behaviour, unlike the widely used harmonic oscillator; moreover, the negative parity states are exactly degenerate with the first positive parity excitation, providing a good starting point for the description of the spectrum. This degeneracy is a signature of a higher symmetry; in this case it can be interpreted as an O(7) symmetry.

The splittings within the multiplets are produced by a perturbative SU(6)-breaking term, which as a first approximation can be assumed to be the standard hyperfine interaction H_{hyp} [15]. It has, however, been extended to a flavour-dependence by means of a Guersey and Radicati SU(6)-breaking term [9]. The three quark Hamiltonian for the hCQM in its simplest form is then [3]:

$$H = \frac{p_\lambda^2}{2m} + \frac{p_\rho^2}{2m} - \frac{\tau}{x} + \alpha x + H_{\text{hyp}}, \quad (2)$$

where m is the quark mass (taken as $1/3$ of the nucleon mass). The strength of the hyperfine interaction is determined in order to reproduce the $\Delta - N$ mass difference and the remaining two free parameters are fitted to the spectrum, reported in Fig. 2, leading to the following values:

$$\alpha = 1.61 \text{ fm}^{-2}, \quad \tau = 4.59. \quad (3)$$

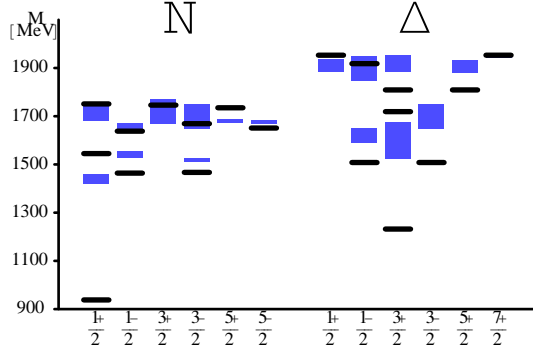


Fig. 2. The spectrum obtained with the hypercentral model Eq. (3) and the parameters Eq. (4) (full lines)), compared with the experimental data of PDG [16] (grey boxes).

Keeping these parameters fixed, the model has been applied to calculating various physical quantities of interest: photocouplings [17], electromagnetic transition amplitudes [18], elastic nucleon form factors [19] and the ratio between the electric and magnetic proton form factors [20]. Some results of such parameter-free calculations are presented in the next section.

4 Electromagnetic transition form factors.

The electromagnetic transition amplitudes, are defined as the matrix elements of the electromagnetic interaction between the nucleon, N , and the resonance, B , states:

$$\begin{aligned} A_{1/2} &= \langle B, J', J'_z = \frac{1}{2} | H_{\text{em}}^t | N, J = \frac{1}{2}, J_z = -\frac{1}{2} \rangle \zeta \\ A_{3/2} &= \langle B, J', J'_z = \frac{3}{2} | H_{\text{em}}^t | N, J = \frac{1}{2}, J_z = \frac{1}{2} \rangle \zeta, \\ S_{1/2} &= \langle B, J', J'_z = \frac{3}{2} | H_{\text{em}}^l | N, J = \frac{1}{2}, J_z = \frac{1}{2} \rangle \zeta \end{aligned} \quad (4)$$

where ζ is the sign of the $N\pi$ decay amplitude.

The photocouplings of the hCQM [17] (i.e. Eq. (4) calculated at the photon point), in comparison with other calculations with other CQMs, see Table 2 of Ref. [17], and references therein, have the same overall behaviour, having the same $SU(6)$ structure in common, but in many cases they all show a lack of strength.

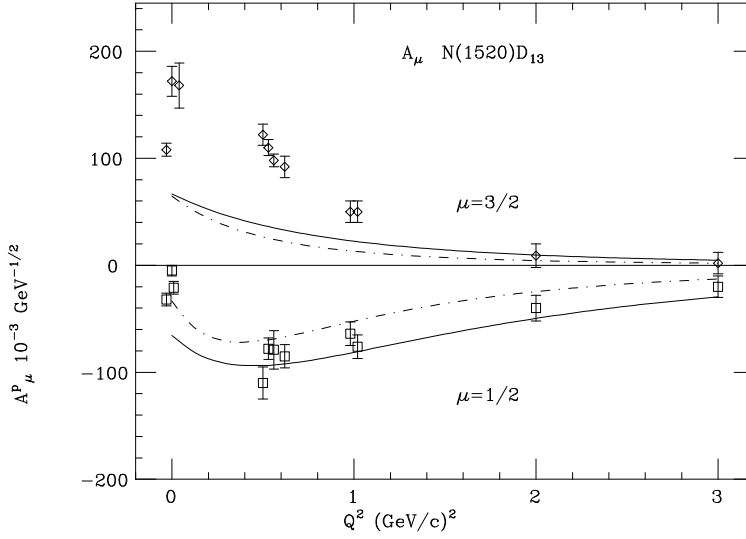


Fig. 3. The transverse helicity amplitudes for the $D_{13}(1520)$ resonance, calculated with the hCQM of Eqs. (3) (full curve, [18]). The dashed curve is obtained with the analytical version of the hCQM ([14]), where the behaviour of the quark wave function is determined mainly by the hypercoulomb potential. The data are from the compilation of ref. [23]

Taking into account the Q^2 -behaviour of the transition matrix elements of Eq. (4), one can calculate the hCQM helicity amplitudes in the Breit frame [18]. The hCQM results for the $D_{13}(1520)$ [17] is given in Fig. 3. We have completed our program in order to systematically calculate the helicity amplitudes, both transverse and longitudinal, for all the 3 and 4 star resonances [21]. In general the Q^2 -behaviour is reproduced, except for discrepancies at small Q^2 . These discrepancies, as those observed in the photocouplings, can be ascribed either to the non-relativistic character of the model or to the lack of explicit quark-antiquark configurations, which may be important at low Q^2 . The kinematical relativistic corrections at the level of boosting the nucleon and the resonance states to a common frame are not responsible for these discrepancies, as we have demonstrated in Ref. [24]. Similar results are obtained for the other negative parity resonances [18]. It should be mentioned that the r.m.s. radius of the proton corresponding to the parameters of Eq. (3) is 0.48 fm, which is the value obtained in [22] in order to reproduce the D_{13} photocoupling. Therefore, the missing strength at low Q^2 can be ascribed to the lack of quark-antiquark effects, which are probably more important in the outer region of the nucleon. These considerations are supported, see Fig. 4, by the comparison between our results and the MAID [25] results, where the pion cloud contributions, evaluated by means of a dy-

namical model [26], are also reported. Their importance decreases with increasing Q^2 , going rapidly to zero, as expected. This feature is quite general, since it happens systematically also for the excitation of higher resonances, such as $P_{11}(1440)$, $S_{11}(1535)$, $D_{13}(1520)$, $F_{15}(1680)$ as we have shown in Ref. [27].

If we compare our results with the predictions obtained with other versions of CQMs for which the helicity amplitudes are available, again we can see that the overall trend is reproduced; however the problem of missing strength at low Q^2 is present in all these versions of CQMs.

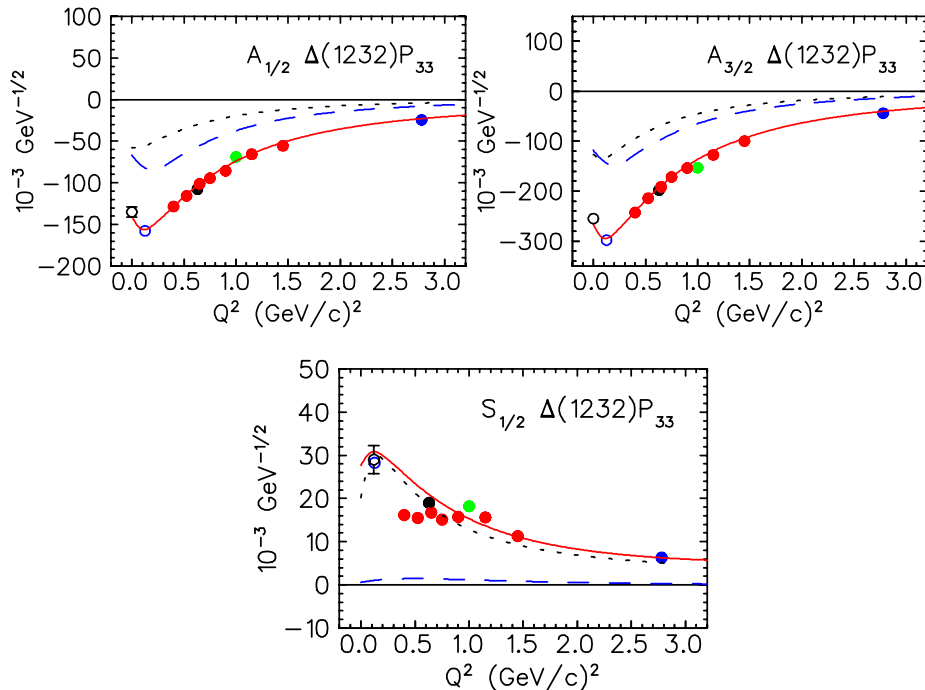


Fig. 4. The Q^2 dependence of the $N \rightarrow \Delta$ helicity amplitudes: superglobal fit performed with MAID [25] (solid curve), predictions of the hypercentral Constituent Quark Model [3,18,27] (dashed curve), pion cloud contributions calculated with the Mainz dynamical model [26] (dotted curve). The data points at finite Q^2 are the results of single- Q^2 fits [27] on recent data (see Ref.[27] for the references to the experimental data).

Acknowledgment

The author gratefully acknowledges the warm atmosphere of the Workshop and the interesting discussions with Prof. Mitja Rosina.

References

1. S. Capstick and N. Isgur, Phys. Rev. D **34**,2809 (1986)

2. R. Bijker, F. Iachello and A. Leviatan, *Ann. Phys. (N.Y.)* **236**, 69 (1994)
3. M. Ferraris, M.M. Giannini, M. Pizzo, E. Santopinto and L. Tiator, *Phys. Lett.* **B364**, 231 (1995).
4. L. Ya. Glozman and D.O. Riska, *Phys. Rep.* **C268**, 263 (1996).
5. L. Ya. Glozman, Z. Papp, W. Plessas, K. Varga and R. F. Wagenbrunn, *Phys. Rev.* **C57**, 3406 (1998); L. Ya. Glozman, W. Plessas, K. Varga and R. F. Wagenbrunn, *Phys. Rev.* **D58**, 094030 (1998).
6. U. Löring, K. Kretzschmar, B. Ch. Metsch, H. R. Petry, *Eur. Phys. J.* **A10**, 309 (2001); U. Löring, B.Ch. Metsch, H. R. Petry, *Eur. Phys. J.* **A10**, 395 (2001); 447 (2001).
7. E. Santopinto, *Phys. Rev. C* **72** (2005) 022201.
8. A. De Rújula, H. Georg, S.L. Glashow, *Phys. Rev.* **D12**, 147 (1975)
9. M. M. Giannini, E. Santopinto and A. Vassallo, *Eur. Phys. J. A* **25** (2005) 241.
10. Gunnar S. Bali et al., *Phys. Rev.* **D62**, 054503 (2000); Gunnar S. Bali, *Phys. Rep.* **343**, 1 (2001); C. Alexandrou, P. de Forcrand, O. Jahn, *Nucl. Phys. Proc. Suppl.* **119**, 667 (2003).
11. P. Hasenfratz, R.R. Horgan, J. Kuti and J.M. Richard, *Phys. Lett.* **B94**, 401 (1980)
12. J.-M. Richard, *Phys. Rep. C* **212**, 1 (1992)
13. M. Fabre de la Ripelle and J. Navarro, *Ann. Phys. (N.Y.)* **123**, 185 (1979).
14. E. Santopinto, F. Iachello and M.M. Giannini, *Nucl. Phys.* **A623**, 100c (1997); E. Santopinto, F. Iachello and M.M. Giannini, *Eur. Phys. J.* **A1**, 307 (1998); R. Bijker, F. Iachello and E. Santopinto, *J. Phys. A* **31** (1998) 9041.
15. N. Isgur and G. Karl, *Phys. Rev.* **D18**, 4187 (1978); *Phys. Rev.* **D19**, 2653 (1979).
16. Particle Data Group, *Eur. Phys. J.* **C15**, 1 (2000).
17. M. Aiello, M. Ferraris, M.M. Giannini, M. Pizzo and E. Santopinto, *Phys. Lett.* **B387**, 215 (1996).
18. M. Aiello, M. M. Giannini and E. Santopinto, *J. Phys. G: Nucl. Part. Phys.* **24**, 753 (1998)
19. M. De Sanctis, E. Santopinto and M.M. Giannini, *Eur. Phys. J.* **A1**, 187 (1998).
20. M. De Sanctis, M.M. Giannini, L. Repetto and E. Santopinto, *Phys. Rev.* **C62**, 025208 (2000).
21. M. M. Giannini and E. Santopinto to be published.
22. L. A. Copley, G. Karl and E. Obryk, *Phys. Lett.* **29**, 117 (1969).
23. V. D. Burkert, private communication
24. M. De Sanctis, E. Santopinto and M.M. Giannini, *Eur. Phys. J.* **A2**, 403 (1998).
25. D. Drechsel, O. Hanstein, S.S. Kamalov, L. Tiator, *Nucl. Phys.* **A645**, 145 (1999).
26. S. Kamalov, S.N. Yang, D. Drechsel, O. Hanstein, L. Tiator, *Phys. Rev.* **C64**, 032201 (2001).
27. L. Tiator, D. Drechsel, S. Kamalov, M.M. Giannini, E. Santopinto, A. Vassallo, *Eur. Phys. J.* **A19**, s01, 55 (2004).



Relativistic calculation of hadronic baryon decays*

B. Sengl, T. Melde and W. Plessas

Theoretical Physics, Institute for Physics, University of Graz
Universitätsplatz 5, A-8010 Graz, Austria

Abstract. The description of baryon resonance decays represents a major challenge of strong interaction physics. We will report on a relativistic approach to mesonic decays of light and strange baryon resonances within constituent quark models. The calculations are performed in the point-form of relativistic quantum mechanics, specifically focusing on the strange sector. It is found that the relativistic predictions generally underestimate the experimental data. The nonrelativistic approximation of the approach leads to the decay operator of the elementary emission model. It is seen that the nonrelativistic reduction has considerable effects on the decay widths.

There is already a long tradition in studying mesonic decays of baryon resonances within constituent quark models (CQMs). However, most of the studies hitherto have been performed within nonrelativistic or so-called relativised models [1–5]. Recently, the Graz group has presented relativistic CQM calculations for π and η decays of N and Δ resonances employing a decay operator along the point-form spectator model (PFSM) in the framework of relativistic (Poincaré-invariant) quantum mechanics [6]. A similar relativistic study following a Bethe-Salpeter approach has been reported by the Bonn group [7,8]. In this contribution we report results for π decays of strange baryon resonances by the relativistic Goldstone-boson exchange (GBE) and one-gluon exchange (OGE) CQMs of Refs. [9] and [5], respectively. The nonstrange decays of strange baryon resonances have not found much attention in the past. So far there are no covariant results but only the studies in Refs. [10–12]. In addition to the relativistic predictions we also present the decay widths resulting from the nonrelativistic reduction of the PFSM decay operator, which corresponds to the elementary emission model (EEM).

The decay width of a baryon resonance is defined by the expression

$$\Gamma_{i \rightarrow f} = \frac{|\mathbf{q}|}{4M^2} \frac{1}{2J+1} \sum_{M_J, M_{J'}} \frac{1}{2T+1} \sum_{M_T, M_{T'}, M_{T_m}} |F_{i \rightarrow f}|^2 \quad (1)$$

with the transition amplitude $F_{i \rightarrow f}$ given by the matrix element of the reduced (four-momentum conserving) decay operator \hat{D}_{rd}^m between incoming and outgoing baryon states

$$F_{i \rightarrow f} = \langle V', M', J', M_{J'}, T', M_{T'} | \hat{D}_{rd}^m | V, M, J, M_J, T, M_T \rangle. \quad (2)$$

* Talk delivered by B. Sengl.

Here, the index m refers to the particular mesonic decay mode and $q_\mu = (q_0, \mathbf{q})$ denotes the four-momentum of the outgoing meson in the rest-frame of the decaying baryon resonance $|V, M, J, M_J, T, M_T\rangle$; the latter is characterized by the eigenvalues of the velocity V , mass M , intrinsic spin J with z -component M_J , and isospin T with z -projection M_T . Correspondingly the outgoing baryon state is denoted by the primed eigenvalues. Representing the baryon eigenstates in a suitable basis, the matrix element in Eq. (2) leads to the integral

$$\begin{aligned}
 & \langle V', M', J', M_{J'}, T', M_{T'} | \hat{D}_{rd}^m | V, M, J, M_J, T, M_T \rangle \\
 &= \frac{2}{MM'} \sum_{\sigma_i \sigma'_i} \sum_{\mu_i \mu'_i} \int d^3 \mathbf{k}_2 d^3 \mathbf{k}_3 d^3 \mathbf{k}'_2 d^3 \mathbf{k}'_3 \\
 & \times \sqrt{\frac{(\sum_i \omega'_i)^3}{\prod_i 2\omega'_i}} \Psi_{M'J'M_{J'}T'M_{T'}}^*(\mathbf{k}'_i; \mu'_i) \prod_{\sigma'_i} D_{\sigma'_i \mu'_i}^{*\frac{1}{2}} \{R_W [k'_i; B(V')]\} \\
 & \times \langle p'_1, p'_2, p'_3; \sigma'_1, \sigma'_2, \sigma'_3 | \hat{D}_{rd}^m | p_1, p_2, p_3; \sigma_1, \sigma_2, \sigma_3 \rangle \\
 & \times \prod_{\sigma_i} D_{\sigma_i \mu_i}^{\frac{1}{2}} \{R_W [k_i; B(V)]\} \sqrt{\frac{(\sum_i \omega_i)^3}{\prod_i 2\omega_i}} \Psi_{MJM_JTM_T}(\mathbf{k}_i; \mu_i), \quad (3)
 \end{aligned}$$

where $\Psi_{MJM_JTM_T}(\mathbf{k}_i; \mu_i)$ is the rest-frame wave function of the incoming baryon and analogously $\Psi_{M'J'M_{J'}T'M_{T'}}^*(\mathbf{k}'_i; \mu'_i)$ the one of the outgoing baryon. Both wave functions result from the velocity-state representation of the baryon eigenstates. The momentum representation of the decay operator follows from the PFSM construction [6,13], where one assumes that only one of the quarks directly couples to the emitted meson:

$$\begin{aligned}
 & \langle p'_1, p'_2, p'_3; \sigma'_1, \sigma'_2, \sigma'_3 | \hat{D}_{rd}^m | p_1, p_2, p_3; \sigma_1, \sigma_2, \sigma_3 \rangle \\
 &= -3 \left(\frac{M}{\sum_i \omega_i} \frac{M'}{\sum_i \omega'_i} \right)^{\frac{3}{2}} \frac{ig_{qqm}}{2m_1} \frac{1}{\sqrt{2\pi}} \bar{u}(p'_i, \sigma'_i) \gamma_5 \gamma^\mu \mathcal{F}^m u(p_1, \sigma_1) q_\mu \\
 & \quad \times 2p_{20} \delta^3(\mathbf{p}_2 - \mathbf{p}'_2) \delta_{\sigma_2 \sigma'_2} 2p_{30} \delta^3(\mathbf{p}_3 - \mathbf{p}'_3) \delta_{\sigma_3 \sigma'_3}. \quad (4)
 \end{aligned}$$

Here, g_{qqm} is the quark-meson coupling constant, m_1 the mass of the active quark, \mathcal{F}^m the flavor-transition operator specifying the particular decay mode, and $u(p_1, \sigma_1)$ the quark spinor. All details of the formalism and the notation can be found in Ref. [14]. The form of the decay operator is congruent with the calculations in Ref. [6] and also consistent with the baryon charge normalisation and time-reversal invariance of the electromagnetic form-factors [15]. The non-relativistic approximation of the PFSM decay operator leads to the traditional EEM [14].

In Table 1 we present the direct predictions of the GBE and OGE CQMs for the π decay modes of the strange baryon decay resonances and compare with the latest compilation of the PDG [16]. Both the covariant PFSM results as well as the nonrelativistic EEM results have been calculated with theoretical and experimental masses as input. It is immediately evident that the relativistic predictions usually underestimate the experimental data or at most reach them from below.

Table 1. Theoretical predictions for π decay widths by the GBE and OGE CQMs in comparison to experiment [16]. The relativistic calculations follow from the PFSM, while the EEM results represent their nonrelativistic limits.

Decay	J^P	Exp. [MeV]	Theoretical Mass				Experimental Mass			
			Relativistic		Nonrel. EEM		Relativistic		Nonrel. EEM	
			GBE	OGE	GBE	OGE	GBE	OGE	GBE	OGE
$\rightarrow \Sigma\pi$										
$\Lambda(1405)$	$\frac{1}{2}^-$	(50 ± 2)	55	78	320	611	15	17	76	112
$\Lambda(1520)$	$\frac{3}{2}^-$	$(6.55 \pm 0.16)_{-0.04}^{+0.04}$	5	9	5	8	2.8	3.1	2.1	2.3
$\Lambda(1600)$	$\frac{1}{2}^+$	$(53 \pm 38)_{-10}^{+60}$	3	33	2	34	3	17	1.2	15
$\Lambda(1670)$	$\frac{1}{2}^-$	$(14.0 \pm 5.3)_{-2.5}^{+8.3}$	69	103	620	1272	68	94	572	1071
$\Lambda(1690)$	$\frac{3}{2}^-$	$(18 \pm 6)_{-2}^{+4}$	19	25	24	28	18	21	23	22
$\Lambda(1800)$	$\frac{1}{2}^-$	seen	68	101	473	1175	70	95	485	1095
$\Lambda(1810)$	$\frac{1}{2}^+$	$(38 \pm 23)_{-10}^{+40}$	3.8	2.1	55	150	4.1	5.0	55	94
$\Lambda(1830)$	$\frac{5}{2}^-$	$(52 \pm 19)_{-12}^{+11}$	14	19	16	24	16	20	22	24
$\rightarrow \Lambda\pi$										
$\Sigma(1385)$	$\frac{3}{2}^+$	$(4.2 \pm 0.5)_{-0.5}^{+0.7}$	3.1	0.5	6.5	1.1	2.0	2.1	4.1	4.8
$\Sigma(1660)$	$\frac{1}{2}^+$	seen	10	24	2	15	12	14	2.4	6.9
$\Sigma(1670)$	$\frac{3}{2}^-$	$(27 \pm 9)_{-6}^{+12}$	15	23	21	32	13	17	17	21
$\Sigma(1750)^1$	$\frac{1}{2}^-$	$(3.6 \pm 3.6)_{-0}^{+5.6}$	58	102	480	1249	63	102	574	1402
$\Sigma(1750)^2$	$\frac{1}{2}^-$	$(3.6 \pm 3.6)_{-0}^{+5.6}$	32	44	135	312	32	38	136	262
$\Sigma(1750)^3$	$\frac{1}{2}^-$	$(3.6 \pm 3.6)_{-0}^{+5.6}$	10	1.0	116	34	10	0.9	110	32
$\Sigma(1775)$	$\frac{5}{2}^-$	$(4.2 \pm 1.8)_{-0.3}^{+0.8}$	1.9	3.8	2.9	6.9	2.2	3.2	3.5	5.3
$\Sigma(1940)$	$\frac{3}{2}^-$	seen	2.2	3.7	0.5	1.1	4.9	5.8	1.6	2.4
$\rightarrow \Xi\pi$										
$\Xi(1385)$	$\frac{3}{2}^+$	$(31.3 \pm 0.5)_{-4.3}^{+4.4}$	11	11	25	28	14	13	31	32
$\Xi(1660)$	$\frac{1}{2}^+$	seen	8	5	6	0.02	10	3	8	0.05
$\Xi(1670)$	$\frac{3}{2}^-$	$(6 \pm 3)_{-1}^{+3}$	2.5	2.0	5.5	5.1	2.7	1.5	6.0	3.2
$\Xi(1750)^1$	$\frac{1}{2}^-$	seen	1.6	1.5	43	67	0.8	1.4	49	70
$\Xi(1750)^2$	$\frac{1}{2}^-$	seen	19	25	160	422	18	25	169	359
$\Xi(1750)^3$	$\frac{1}{2}^-$	seen	1.0	2.8	18	105	0.9	3	18	97
$\Xi(1775)$	$\frac{5}{2}^-$	$(20 \pm 4)_{-2}^{+3}$	6	10	10	21	8	8	15	15
$\Xi(1940)$	$\frac{3}{2}^-$	seen	0.2	0.4	1.7	3.5	0.5	0.5	5.9	6.1

A similar finding was already made for the π decay widths of N and Δ resonances [6]. Here, there appear only two exceptions, namely the widths of $\Lambda(1405)$ and $\Lambda(1670)$. In case of the former it is caused by the (theoretical) mass, which is far too high for both CQMs; the overprediction disappears when the experimental mass is used. On the other hand the resonance mass of the $\Lambda(1670)$ is more or less well reproduced in accordance with experiment. In this case we may suspect the large decay width to result from another reason, possibly a coupling of resonance states.

For the $\Sigma(1750)$ the CQMs offer three states that can be identified with this resonance. In Table 1 we present the decay widths of all theoretical levels (in the entries distinguished by the superscripts 1, 2, and 3). It is seen that the decay width of the third state $\Sigma(1750)^3$ is pretty consistent with the magnitude of the experimental data and it should be identified with the measured $\Sigma(1750)$. The other two states can then be interpreted with lower lying resonances (such as the $\Sigma(1620)$ and $\Sigma(1560)$) not so well established by experiment. Regarding the classification of these states see also Ref. [17].

From the comparison of the PFSM results with experimental masses as input one learns that the effects from different hyperfine interactions generally play a minor role. Considerable influences are seen only in $\Sigma\pi$ and $\Lambda\pi$ decays of $\Lambda(1600)$, $\Sigma(1750)^3$, and $\Sigma(1660)$.

The nonrelativistic results corresponding to the EEM scatter below and above the experimental data. The effect of the nonrelativistic reduction is strongly dependent on the decaying resonance. It is governed essentially by the truncation in the spin couplings as well as the elimination of the Lorentz boosts.

We have reported the first covariant results for π decays of strange baryon resonances within CQMs. Obviously the approach needs further improvements. In the first instance, one might think of a coupled-channel formulation. The importance of additional Fock components has already been seen in a PFSM calculation of mesons decays [18,19] and also recent studies of baryon resonances [20,21].

Acknowledgment This work was supported by the Austrian Science Fund (Projects FWF-P16945 and FWF-P19035). B. Sengl acknowledges support by the Doktoratskolleg Graz "Hadrons in Vacuum, Nuclei and Stars" (FWF-DK W1203). The authors are grateful to L. Canton, A. Krassnigg, and R. F. Wagenbrunn for useful discussions.

References

1. F. Stancu and P. Stassart, Phys. Rev. D **39**, 343 (1989).
2. S. Capstick and W. Roberts, Phys. Rev. D **49**, 4570 (1994).
3. P. Geiger and E. S. Swanson, Phys. Rev. D **50**, 6855 (1994).
4. E. S. Ackleh, T. Barnes, and E. S. Swanson, Phys. Rev. D **54**, 6811 (1996).
5. L. Theussl, R. F. Wagenbrunn, B. Desplanques, and W. Plessas, Eur. Phys. J. A **12**, 91 (2001).
6. T. Melde, W. Plessas, and R. F. Wagenbrunn, Phys. Rev. C **72**, 015207 (2005); Erratum, *ibid.* to appear .

7. B. Metsch, U. Loering, D. Merten, and H. Petry, *Eur. Phys. J.* **A18**, 189 (2003).
8. B. Metsch, *AIP Conf. Proc.* **717**, 646 (2004).
9. L. Y. Glozman, W. Plessas, K. Varga, and R. F. Wagenbrunn, *Phys. Rev. D* **58**, 094030 (1998).
10. S. Capstick and W. Roberts, *Phys. Rev. D* **58**, 074011 (1998).
11. A. Krassnigg *et al.*, *Few Body Syst. Suppl.* **10**, 391 (1999).
12. W. Plessas *et al.*, *Few Body Syst. Suppl.* **11**, 29 (1999).
13. T. Melde, L. Canton, W. Plessas, and R. F. Wagenbrunn, *Eur. Phys. J. A* **25**, 97 (2005).
14. B. Sengl, Dissertation, University of Graz, 2006.
15. R. F. Wagenbrunn, T. Melde, and W. Plessas, hep-ph/0509047 (2005).
16. W.-M. Yao *et al.*, *J. Phys. G* **33**, 1+ (2006).
17. T. Melde, W. Plessas, and B. Sengl, Bled Proceedings, Baryon Structure (2006).
18. A. Krassnigg, W. Schweiger, and W. H. Klink, *Phys. Rev. C* **67**, 064003 (2003).
19. A. Krassnigg, *Phys. Rev. C* **72**, 028201 (2005).
20. Q. B. Li and D. O. Riska, *Phys. Rev. C* **73**, 035201 (2006).
21. Q. B. Li and D. O. Riska, *Phys. Rev. C* **74**, 015202 (2006).



Baryon resonances in large N_c QCD*

N. Matagne and Fl. Stancu

Institute of Physics, B5, University of Liège, Sart Tilman, 4000 Liège 1, Belgium

Abstract. The baryon spectra are discussed in the context of the $1/N_c$ expansion approach, with emphasis on mixed symmetric states. The contributions of the spin dependent terms as a function of the excitation energy are shown explicitly. At large energies these contributions are expected to vanish.

1 Introduction

At energies corresponding to a length scale of the order of the hadron size the standard perturbative QCD cannot be applied, because the coupling constant is too large. In the nonperturbative regime one can use the so-called $1/N_c$ expansion approach which is based on the 32 years old idea of 't Hooft [1], who suggested a perturbative expansion of QCD in terms of the parameter $1/N_c$ where N_c is the number of colors. The double line diagrammatic method proposed by 't Hooft has been implemented by Witten [2] to describe hadrons by using convenient power counting rules for Feynman diagrams. According to Witten's intuitive picture, a baryon containing N_c quarks is seen as a bound state in an average self-consistent potential of a Hartree type and the corrections to the Hartree approximation are of order $1/N_c$ which means that in the $N_c \rightarrow \infty$ limit the Hartree approximation is exact. Ground state baryons correspond to the ground state of the average potential.

Ten years after 't Hooft's work, Gervais and Sakita [3] and independently Dashen and Manohar in 1993 [4] discovered that QCD has an exact contracted $SU(2N_f)_c$ symmetry when $N_c \rightarrow \infty$, N_f being the number of flavors. The contracted algebra generators acting in the spin-flavour space X^{ia} are related to the $SU(2N_f)$ generators G^{ia} in the limit $N_c \rightarrow \infty$ by

$$X^{ia} = \lim_{N_c \rightarrow \infty} \frac{G^{ia}}{N_c}. \quad (1)$$

For ground state baryons the $SU(2N_f)$ symmetry is broken by corrections proportional to $1/N_c$. Applications to ground state QCD baryons ($N_c = 3$) were considered since 1993-1994. Presently the $1/N_c$ expansion provides a systematic method to analyze baryon properties such as masses, magnetic moments, axial currents, etc.

* Talk delivered by Fl. Stancu

The $1/N_c$ expansion method has been extended to excited states since 1997 in the spirit of the Hartree approximation developed by Witten [8]. It was shown that the $SU(2N_f)$ breaking occurs at order N_c^0 , at variance with the ground state. This conflict generated a conceptual problem, presently under investigation.

Here we are concerned with baryon spectra only. If the $SU(N_f)$ symmetry is exact, the baryon mass operator is a linear combination of terms

$$M = \sum_i c_i O_i, \quad (2)$$

with the operators O_i having the general form

$$O_i = \frac{1}{N_c^{n-1}} O_\ell^{(k)} \cdot O_{SF}^{(k)}, \quad (3)$$

where $O_\ell^{(k)}$ is a k -rank tensor in $SO(3)$ and $O_{SF}^{(k)}$ a k -rank tensor in $SU(2)$, but invariant in $SU(N_f)$. The latter is expressed in terms of $SU(N_f)$ generators. For the ground state one has $k=0$. The first factor gives the order $\mathcal{O}(1/N_c)$ of the operator in the series expansion and reflects Witten's power counting rules. The lower index i represents a specific combination of generators, see examples below. In the linear combination, Eq. (2), each term of type (3) is multiplied by an unknown coefficient c_i which is a reduced matrix element. All these coefficients encode the QCD dynamics and are obtained from a fit to the existing data. It is important to find regularities in their behaviour, as shown below. Additional terms are needed if $SU(N_f)$ is broken, as it is the case for $N_f = 3$ [15].

2 The ground state

A considerable amount of work has been devoted to ground state baryons summarized in several review papers as, for example, [5–7]. The ground state is described by the symmetric representation $[N_c]$. For $N_c = 3$ this becomes [3] or [56] in an $SU(6)$ dimensional notation. Let us consider below the simple case of two flavours, *i.e.* $SU(4)$. Its algebra is

$$\begin{aligned} [S_i, S_j] &= i\epsilon_{ijk} S_k, & [T_a, T_b] &= i\epsilon_{abc} T_c, \\ [G_{ia}, G_{jb}] &= \frac{i}{4}\delta_{ij}\epsilon_{abc} T_c + \frac{i}{2}\delta_{ab}\epsilon_{ijk} S_k. \end{aligned} \quad (4)$$

As $SU(4)$ is a group of rank 3 it has three invariants: S^2 , I^2 and G^2 . *i.e.* three operators of type (3). But for the ground state one can take $I^2 = S^2$ in $SU(4)$. Moreover due to the operator identity [6]

$$\{J^i, J^i\} + \{I^a, I^a\} + 4\{G^{ia}, G^{ia}\} = \frac{3}{2}N_c(N_c + 4) \quad (5)$$

the invariant G^2 can be expressed in terms of S^2 and I^2 . So, one is left with one linearly independent operator, which we choose to be S^2 . Accordingly, the mass formula takes the following simple form

$$M = m_0 N_c + m_2 \frac{1}{N_c} S^2 + m_4 \frac{1}{N_c^3} (S^2)^2 + \dots + m_{N_c-1} \frac{1}{N_c^{N_c-2}} (S^2)^{N_c-3}. \quad (6)$$

This describes a tower of large N_c baryon states with $S = 1/2, \dots, N_c/2$, which collapses into a degenerate state when $N_c \rightarrow \infty$. One can see that the splitting starts at order $1/N_c$ when $SU(2N_f)$ is broken. The coefficients $c_i = m_i$ must be fitted from the data.

3 The excited states

One expects 't Hooft's suggestion [1] to hold in all QCD regimes. Accordingly, the applicability of the $1/N_c$ expansion method to excited states is a subject of current investigation. The experimental facts indicate a small breaking of $SU(6)$ which make the $1/N_c$ studies of excited states entirely plausible. The general form of a mass operator is given by Eq. (2) with O_i defined as in Eq. (3). For simplicity, here we discuss nonstrange baryons where $SU(4)$ symmetry is exact.

Excited baryons can be divided into $SU(6)$ multiplets, as in the constituent quark model. If an excited baryon belongs to the [56]-plet the mass problem can be treated similarly to the ground state in the flavour-spin degrees of freedom, but one has to take into account the presence of an orbital excitation in the space part of the wave function [9,10]. If the baryon belongs to the mixed symmetric representation [21], or [70] in $SU(6)$ notation, the treatment becomes much more complicated. In particular, the resonances up to 2 GeV belong to [70, 1⁻], [70, 0⁺] or [70, 2⁺] multiplets.

There is one standard way to study the [70]-plets which is related to the Hartree approximation [8]. This consists in reducing the description of an excited baryon to that of an excited quark coupled to a symmetric core, see *e.g.* [11–13,15]. In that case the core can be treated in a way similar to that of the ground state. In this method each $SU(2N_f) \times O(3)$ generator is split into two terms

$$S^i = s^i + S_c^i; \quad T^a = t^a + T_c^a; \quad G^{ia} = g^{ia} + G_c^{ia}, \quad \ell^i = \ell_q^i + \ell_c^i, \quad (7)$$

where s^i, t^a, g^{ia} and ℓ_q^i are the excited quark operators and S_c^i, T_c^a, G_c^{ia} and ℓ_c^i the corresponding core operators. As an example, we discuss the latest in date results, for nonstrange baryons belonging to the [70, ℓ^+] multiplets with $\ell = 0$ and 2. The list of the dominant operators up to order $1/N_c$ is given in Table 1 together with the values of the coefficients c_i obtained from the data. It is customary to drop corrections of order $1/N_c^2$. In this list, the first is the trivial operator of order $\mathcal{O}(N_c)$. The second is the 1-body part of the spin-orbit operator of order $\mathcal{O}(1)$ which acts on the excited quark. The third is a composite 2-body operator formally of order $\mathcal{O}(1)$ as well. It involves the tensor operator

$$\ell_q^{(2)ij} = \frac{1}{2} \{ \ell_q^i, \ell_q^j \} - \frac{1}{3} \delta_{i,-j} \ell_q \cdot \ell_q, \quad (8)$$

acting on the excited quark and the $SU(6)$ generators g^{ia} acting on the excited quark and G_c^{ja} acting on the core. The latter is a coherent operator which introduces an extra power N_c so that the order of O_3 is $\mathcal{O}(1)$.

In this procedure, there are two major drawbacks, related to each other. The first is that the number of linearly independent operators constructed from the

Operator	Fitted coef. (MeV)
$O_1 = N_c \mathbb{1}$	$c_1 = 555 \pm 11$
$O_2 = \ell_q^i s^i$	$c_2 = 47 \pm 100$
$O_3 = \frac{3}{N_c} \ell_q^{(2)ij} g^{ia} G_c^{ja}$	$c_3 = -191 \pm 132$
$O_4 = \frac{1}{N_c} (S_c^i S_c^i + s^i S_c^i)$	$c_4 = 261 \pm 47$

Table 1. List of operators and the coefficients resulting from the fit of nonstrange baryon masses assumed to belong to the $[70, 0^+]$ - and $[70, 2^+]$ -plets. The fit gave $\chi_{\text{dof}}^2 \simeq 0.83$ [13].

generators given in the right-hand side of Eqs. (7) increases tremendously so that the number of coefficients to be determined becomes much larger than the experimental data available. Consequently, in selecting the most dominant operators one has to make an arbitrary choice, as we did in Table 1, similarly to previous literature. The second drawback is related to the truncation of the available basis vector space. Among the basis vectors of the irreducible representation $[N_c - 1, 1]$ of S_{N_c} , in this procedure only the vector corresponding to the normal Young tableau is kept, the reason being to decouple the system into a symmetric core and an excited quark. In a normal Young tableau this can be easily done by removing the N_c -th particle from the second row. The terms represented by the other possible Young tableaux, needed to construct a symmetric orbital-flavour-spin state are neglected, *i.e.* antisymmetry is ignored. As a result the procedure brings in terms of order N_c^0 , which is in conflict with the $1/N_c$ expansion for the ground state.

A solution to this problem has been found in Ref. [16], where the separation into a symmetric core and an excited quark is avoided through the calculation of the matrix elements of the $SU(4)$ generators by using a generalized Wigner-Eckart theorem [17]. In this way the antisymmetry is properly taken into account. The result is that the $1/N_c$ expansion starts at order $1/N_c$, as for the ground state.

Based on group theory arguments it is expected that the mass splitting starts at order $1/N_c$, as a general rule, irrespective of the angular momentum and parity of the state and also of the number of flavours, provided $SU(N_f)$ is an exact symmetry.

Despite the drawbacks of the splitting method, the application of the $1/N_c$ expansion method gave useful results, as a first approximation. They predicted the behaviour of the coefficients c_i in the mass formula as a function of the excitation energy. This is illustrated in Fig. 1. This figure suggests that the spin-orbit and the spin-spin terms vanish with the excitation energy, bringing a strong support to constituent quark models and that the spin-spin term is dominant among all the other spin dependent terms. Note that in a quark model picture, the coefficient c_1 would correspond to the additional contribution of a free mass term, the kinetic energy and the confinement. It is not thus surprising that it raises with the excitation energy.

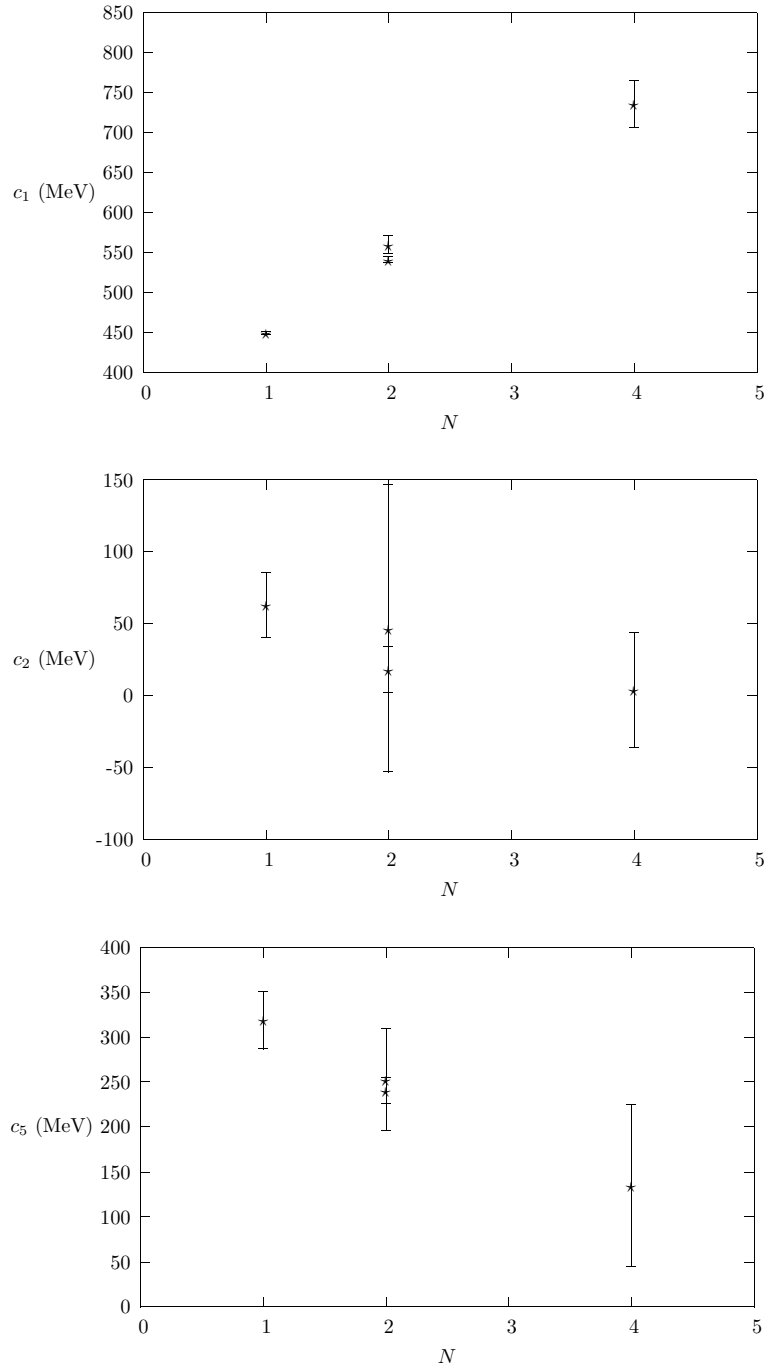


Fig. 1. The coefficients c_i vs N from various sources: for $N = 1$ from Ref. [12] for $N = 2$ from Refs. [9] (lower values) and [13] (upper values), for $N = 4$ from Ref. [10].

4 Conclusion

The $1/N_c$ expansion method provides a powerful theoretical tool to analyze the spin-flavour symmetry of baryons and explains the success of models based on spin-flavor symmetry.

References

1. G. 't Hooft, Nucl. Phys. **72** (1974) 461.
2. E. Witten, Nucl. Phys. **B160** (1979) 57.
3. J. L. Gervais and B. Sakita, Phys. Rev. Lett. **52** (1984) 87; Phys. Rev. **D30** (1984) 1795.
4. R. Dashen and A. V. Manohar, Phys. Lett. **B315** (1993) 425; *ibid* **B315** (1993) 438.
5. R. F. Dashen, E. Jenkins and A. V. Manohar, Phys. Rev. **D51** (1995) 3697.
6. E. Jenkins, Ann. Rev. Nucl. Part. Sci. **48** (1998) 81 [arXiv:hep-ph/9803349].
7. E. Jenkins, arXiv:hep-ph/0111338.
8. J. L. Goity, Phys. Lett. **B414** (1997) 140 [arXiv:hep-ph/9612252].
9. J. L. Goity, C. Schat and N. N. Scoccola, Phys. Lett. **B564** (2003) 83 [arXiv:hep-ph/0304167].
10. N. Matagne and F. Stancu, Phys. Rev. **D71** (2005) 014010. [arXiv:hep-ph/0409261].
11. C. E. Carlson, C. D. Carone, J. L. Goity and R. F. Lebed, Phys. Rev. **D59** (1999) 114008.
12. J. L. Goity, C. L. Schat and N. N. Scoccola, Phys. Rev. **D66** (2002) 114014.
13. N. Matagne and F. Stancu, Phys. Lett. **B631** (2005) 7 [arXiv:hep-ph/0505118].
14. N. Matagne and F. Stancu, Phys. Rev. **D73** (2006) 114025 [arXiv:hep-ph/0603032].
15. N. Matagne and F. Stancu, Phys. Rev. **D74** (2006) 034014 [arXiv:hep-ph/0604122].
16. N. Matagne and F. Stancu, arXiv:hep-ph/0610099.
17. K. T. Hecht and S. C. Pang, J. Math. Phys. **10** (1969) 1571.



Mesons and diquarks in Coulomb-gauge QCD

R. F. Wagenbrunn

Institut für Physik, Fachbereich Theoretische Physik, Karl-Franzens-Universität Graz,
Universitätsplatz 5, A-8010 Austria

Abstract. I demonstrate how confinement in Coulomb-gauge QCD makes quark-quark states of the color anti-triplet (diquarks) move out of the physical spectrum. Mesons as color singlet quark-antiquark states, on the other hand have finite masses and for highly excited states in the meson spectra effective restoration of chiral symmetry can be observed.

In Coulomb-gauge QCD the 00-component of the gluon propagator $D_{\mu\nu}(\mathbf{x}, t)$ has an instantaneous part $V_C(\mathbf{x})\delta(t)$ and confinement means that $-V_C(\mathbf{x}) \rightarrow \infty$ for $|\mathbf{x}| \rightarrow \infty$. It was shown that Coulomb confinement is a necessary condition for confinement, i.e., that the gauge invariant quark-antiquark potential $V_W(r)$ goes to infinity for $r \rightarrow \infty$ [1]. An almost linearly rising Coulomb potential has been suggested [2], which was also confirmed by results from the lattice [3]. In momentum space it becomes

$$V_C(|\mathbf{k}|) = \frac{\sigma_C}{|\mathbf{k}|^4}, \quad (1)$$

where σ_C is the Coulomb string tension. Based on previous works [4] we performed a study of the mechanism of Coulomb confinement in the Dyson-Schwinger-Bethe-Salpeter framework [5] in Rainbow-ladder approximation [6]. We took into account only the Coulomb potential (1) and neglected transverse gluons and non-instantaneous contributions to D_{00} . In that way all integrals over k_0 can be performed analytically and one has to deal with three-dimensional integral equations only. (1) has also an unrealistic ultraviolet (UV) behavior. However, it has the advantage that it produces no UV divergences, thus making renormalization not necessary. Due to all these approximations some physics is lost and the model is not expected to provide realistic quantitative results but some qualitative insight into the physics of confinement in QCD. Since the axial-vector Ward-Takahashi identity is satisfied, chiral symmetry and its dynamical breaking are respected. In particular the pion mass becomes zero in the chiral limit, i.e., for vanishing current quark mass. The potential (1) causes infrared (IR) divergences which are regulated by introducing an IR regulator μ_{IR} and replacing $k^2 \rightarrow k^2 + \mu_{\text{IR}}^2$ (here and in the following $k = |\mathbf{k}|$). The IR limit is then taken by means of $\mu_{\text{IR}} \rightarrow 0$. The essential point is that the integral

$$\frac{1}{2\pi^2} \int d^3q \frac{1}{((\mathbf{p} - \mathbf{q})^2 + \mu_{\text{IR}}^2)^2} = \frac{1}{2\mu_{\text{IR}}} \quad (2)$$

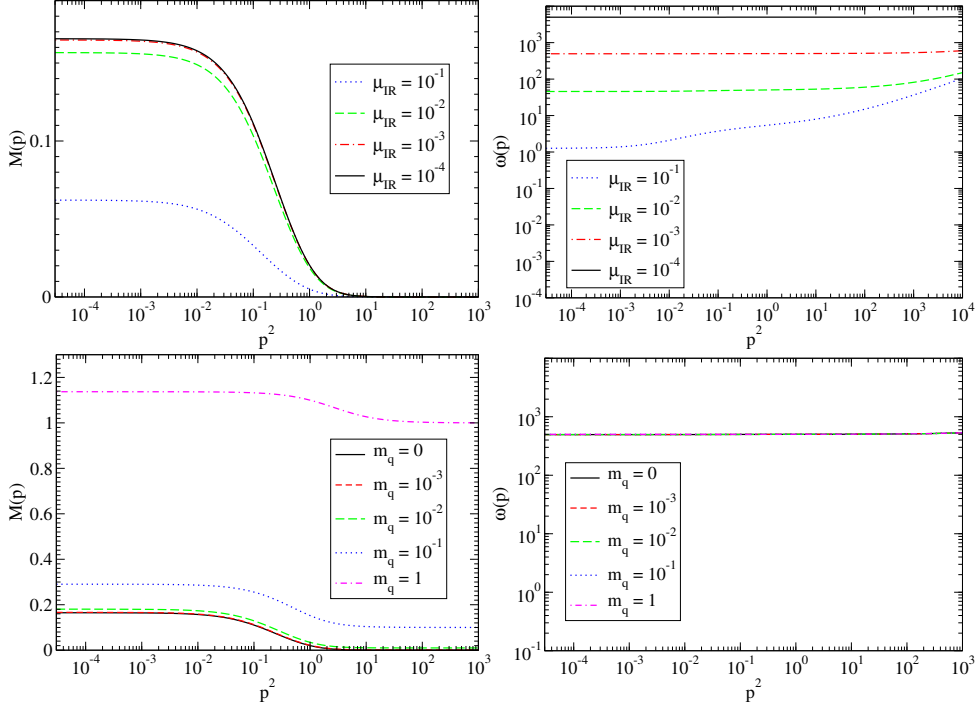


Fig. 1. Mass function $M(p)$ (left plots) and $\omega(p)$ (right plots): In the upper plots the IR behavior for current quark mass $m = 0$ and in the lower plots the results for different current quark masses at constant $\mu_{\text{IR}} = 10^{-3} \sqrt{\sigma_C}$ is shown.

diverges in the IR limit and one can write

$$\frac{1}{2\pi^2} \int d^3q V_C(|\mathbf{p} - \mathbf{q}|) f(q) = \frac{\sigma_C}{2\mu_{\text{IR}}} \int d^3q \delta(\mathbf{p} - \mathbf{q}) f(q) + \text{IR finite term.} \quad (3)$$

For the gap equation of the quark propagator $S(p)$ the ansatz

$$S^{-1}(p) = -i(\gamma_0 p_0 - \boldsymbol{\gamma} \cdot \mathbf{p} C(p) - B(p)) \quad (4)$$

leads to a coupled system of two integral equations

$$B(p) = m + \frac{1}{2\pi^2} \int d^3q V_C(|\mathbf{p} - \mathbf{q}|) \frac{M(q)}{\bar{\omega}(q)} \quad (5)$$

$$C(p) = 1 + \frac{1}{2\pi^2} \int d^3q V_C(|\mathbf{p} - \mathbf{q}|) \hat{\mathbf{p}} \cdot \hat{\mathbf{q}} \frac{q}{p \bar{\omega}(q)}, \quad (6)$$

where $\hat{\mathbf{p}} = \mathbf{p}/p$, m is the current-quark mass, $\bar{\omega}(p) = \sqrt{M^2(p) + p^2}$ and $M(q) = \frac{B(q)}{C(q)}$ is called the quark mass function. Using (3) yields

$$B(p) = \frac{\sigma_C}{2\mu_{\text{IR}}} \frac{M(p)}{\bar{\omega}(p)} + \text{IR finite term} = \frac{\sigma_C}{2\mu_{\text{IR}}} \frac{B(p)}{\omega(p)} + \text{IR finite term}, \quad (7)$$

$$C(p) = \frac{\sigma_C}{2\mu_{\text{IR}}} \frac{1}{\bar{\omega}(p)} + \text{IR finite term} = \frac{\sigma_C}{2\mu_{\text{IR}}} \frac{C(p)}{\omega(p)} + \text{IR finite term}, \quad (8)$$

with

$$\omega(p) = \sqrt{B^2(p) + p^2 C^2(p)} = \frac{\sigma_C}{2\mu_{\text{IR}}} + \text{IR finite term.} \quad (9)$$

The functions $B(p)$ and $C(p)$ diverge like μ_{IR}^{-1} but the mass function is IR finite. The IR behavior for $M(p)$ and $\omega(p)$ for $m = 0$ is demonstrated in the upper plots of Fig. 1, while in the lower plots the same quantities for constant $\mu_{\text{IR}} = 10^{-3} \sqrt{\sigma_C}$ but different current quark masses are shown. The mass function converges to a finite function. For large p it goes to the current quark mass and for small p it gets a dynamical mass which is of approximately the same absolute size for different current quark masses. $\omega(p)\mu_{\text{IR}}$ indeed becomes a constant $\frac{\sigma_C}{2}$, which is independent of the current quark mass.

The Bethe-Salpeter equation (BSE) for a meson with mass M is

$$\chi(p, M) = -i \int \frac{d^4 q}{(2\pi)^4} V_C(|\mathbf{p} - \mathbf{q}|) \gamma_0 S(q_0 + M/2, \mathbf{q}) \chi(q, M) S(q_0 - M/2, \mathbf{q}) \gamma_0.$$

For the pseudoscalar meson (pion with $M = m_\pi$) the Bethe-Salpeter amplitude $\chi(p, m_\pi)$ contains three (pseudoscalar, axial-vector and tensor) components:

$$\chi(p, m_\pi) = P_p(p) \gamma_5 + m_\pi P_A(p) \gamma_0 \gamma_5 + m_\pi P_T(p) \hat{\mathbf{p}} \cdot \boldsymbol{\gamma} \gamma_0 \gamma_5. \quad (10)$$

The BSE is reduced to a coupled system of integral equations

$$\omega(p) h(p) = \frac{1}{2\pi^2} \int d^3 q V_C(|\mathbf{p} - \mathbf{q}|) \left(h(q) + \frac{m_\pi^2}{4\omega(q)} g(q) \right), \quad (11)$$

$$\left(\omega(p) - \frac{m_\pi^2}{4\omega(p)} \right) g(p) = h(p) + \frac{1}{2\pi^2} \int d^3 q V_C(|\mathbf{p} - \mathbf{q}|) \frac{M(p)M(q) + \mathbf{p} \cdot \mathbf{q}}{\bar{\omega}(p)\bar{\omega}(q)} g(q) \quad (12)$$

for the two functions

$$h(p) = \frac{P_p(p)}{\omega(p)}, \quad (13)$$

$$g(p) = \frac{\omega(p)}{\omega^2(p) - \frac{m_\pi^2}{4}} \left[h(p) + 2 \frac{M(p)}{\bar{\omega}(p)} P_A(p) + 2 \frac{\mathbf{p}}{\bar{\omega}(p)} P_T(p) \right]. \quad (14)$$

The IR behavior of Eqs. (11,12) follows by using Eq. (9) on the left and Eq. (3) on the right hand sides, respectively, which yields

$$\frac{\sigma_C}{2\mu_{\text{IR}}} h(p) + \text{IR finite term} = \frac{\sigma_C}{2\mu_{\text{IR}}} h(p) + \text{IR finite term}, \quad (15)$$

$$\frac{\sigma_C}{2\mu_{\text{IR}}} g(p) + \text{IR finite term} = \frac{\sigma_C}{2\mu_{\text{IR}}} g(p) + \text{IR finite term}. \quad (16)$$

Obviously the IR divergences cancel in both equations and all physical observables, in particular the mass, are determined by the IR finite terms. The functions $h(p)$ and $g(p)$ have an IR finite limit, too. This is demonstrated for $m = 0$ in the left plot of Fig. 2.

For two quarks in the $SU(3)_C$ anti-triplet state (diquark) a color factor $\frac{1}{2}$ enters into the BSE kernel. Apart from that for a scalar diquark with mass m_{SD} one

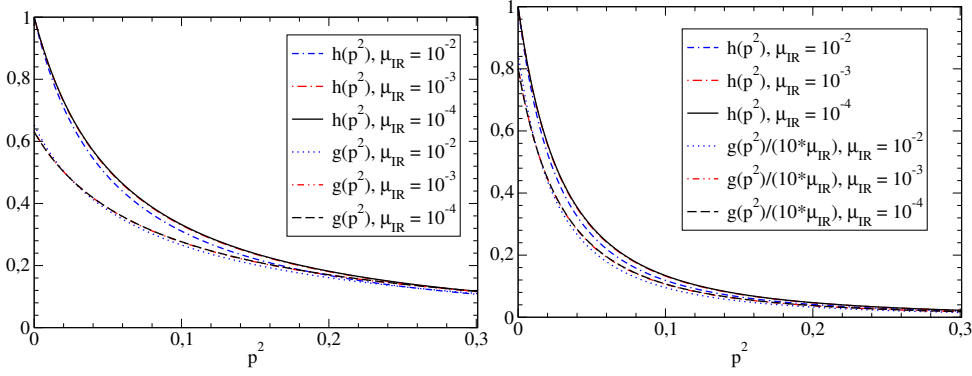


Fig. 2. IR limit of the functions h and g for the pion (left) and the scalar diquark (right) for $m = 0$. In all cases the normalization has been chosen such that $h(0) = 1$.

has the same integral equations as for the pion but the IR divergent terms on the right hand sides of Eqs. (15,16) are reduced to only half their sizes. Thus there must be additional IR divergences. Replacing (15,16) by

$$\begin{aligned} \frac{\sigma_C}{2\mu_{\text{IR}}}h(p) + \text{IR finite term} &= \frac{\sigma_C}{4\mu_{\text{IR}}}h(p) + \frac{m_{\text{SD}}^2}{8}g(p) + \text{IR finite term}, \\ \frac{\sigma_C}{2\mu_{\text{IR}}}g(p) - \frac{m_{\text{SD}}^2\mu_{\text{IR}}}{2\sigma_C}g(p) + \text{IR finite term} &= h(p) + \frac{\sigma_C}{4\mu_{\text{IR}}}g(p) + \text{IR finite term} \end{aligned}$$

and solving for m_{SD} and $g(p)$ yields

$$m_{\text{SD}} = \frac{\sigma_C}{2\mu_{\text{IR}}}, \quad g(p) = \frac{8\mu_{\text{IR}}}{\sigma_C}h(p). \quad (17)$$

The divergences are now balanced by introducing a relation between $h(p)$ and $g(p)$ and making the diquark mass IR divergent. In that way the diquarks are removed from the physical spectrum. This mechanism of confinement applies not only for the scalar diquark but for diquarks of all quantum numbers. Numerically we have reproduced the IR divergence of the mass for scalar and axial-vector diquarks [6]. On the other hand, the shape of the functions $h(p)$ and $g(p)$ converges in the IR limit, which is demonstrated in the right plot of Fig. 2. For that reason not only mesons but also diquarks have IR finite radii. Calculations for the electromagnetic form factor and the charge radius of the pion in Coulomb-gauge QCD have already been performed earlier [7]. Explicitly, the charge radius of the pion is given by

$$\begin{aligned} r_\pi^2 &= \frac{3}{\mathcal{N}_\pi^2} \int \frac{d^3p}{(2\pi)^3} \left\{ -\frac{3}{32\bar{\omega}^4(p)} \left[2\bar{\omega}^2(p) + (M(p) - 2p^2M'(p))^2 \right] g(p)h(p) \right. \\ &\quad \left. + \frac{1}{16} [g'(p)h(p) + g(p)h'(p)] + \frac{p^2}{24} [g(p)h''(p) + g''(p)h(p) - 2g'(p)h'(p)] \right\} \\ &\quad + \mathcal{O}(\mu_{\text{IR}}) \end{aligned}$$

with

$$\mathcal{N}_\pi^2 = 3 \int \frac{d^3p}{(2\pi)^3} g(p)h(p), \quad (18)$$

and of the scalar diquark by

$$r_{\text{SD}}^2 = \frac{3\mu_{\text{IR}}}{\mathcal{N}_{\text{SD}}^2} \int \frac{d^3p}{(2\pi)^3} \left\{ -\frac{7}{6\bar{\omega}^4(p)} \left[2\bar{\omega}^2(p) + (M(p) - 2p^2 M'(p))^2 \right] h^2(p) \right. \\ \left. + 2h(p)h'(p) + \frac{4p^2}{3} \left[h(p)h''(p) - h'^2(p) \right] \right\} + \mathcal{O}(\mu_{\text{IR}})$$

with

$$\mathcal{N}_{\text{SD}}^2 = 48\mu_{\text{IR}} \int \frac{d^3p}{(2\pi)^3} h^2(p). \quad (19)$$

In both cases ' means $\frac{d}{d(p^2)}$. For quark mass $m = 0$ we have obtained the results $r_\pi = 4.3 \sigma_C^{-1/2}$ and $r_{\text{SD}} = 6.0 \sigma_C^{-1/2}$ [6]. Notice that \mathcal{N}_π^2 converges to a finite value while $\mathcal{N}_{\text{SD}}^2$ goes to zero like μ_{IR} . That means that for the diquark only the shape of $h(p)$ converges but its size diverges like $\mu_{\text{IR}}^{-1/2}$. Due to (17), the size of $g(p)$ goes to zero like $\mu_{\text{IR}}^{1/2}$ on the other hand.

Finally I present results for the highly excited meson spectra in the chiral limit [8]. There are certain phenomenological evidences that in highly excited hadrons the chiral $(\text{SU}(2)_L \times \text{SU}(2)_R)$ and $\text{U}(1)_A$ symmetries are approximately restored (for a review see [9]). The states fall into approximate multiplets of $\text{SU}(2)_L \times \text{SU}(2)_R$ and the mass splittings within the multiplets vanish at radial quantum number $n \rightarrow \infty$ and/or spin $J \rightarrow \infty$. Furthermore the splittings within a multiplet become much smaller than between the two subsequent multiplets. The reason for this "effective" symmetry restoration is that excited hadrons gradually decouple from the quark condensates due to a diminishing importance of quantum fluctuations [10]. I restrict the discussion here to scalar and pseudoscalar mesons. Given the complete set of standard quantum numbers I, J^{PC} , the multiplets of $\text{SU}(2)_L \times \text{SU}(2)_R$ for $J = 0$ are [11]

$$(1/2, 1/2)_a : 1, 0^{-+} \longleftrightarrow 0, 0^{++} \text{ and } (1/2, 1/2)_b : 1, 0^{++} \longleftrightarrow 0, 0^{-+}.$$

The BSE for a scalar meson with mass $m_{0^{++}}$ is reduced to the coupled system of integral equations

$$h(p)\omega(p) = \frac{1}{2\pi^2} \int d^3q V_C(|\mathbf{p} - \mathbf{q}|) \frac{pq + M(p)M(q)\hat{\mathbf{p}} \cdot \hat{\mathbf{q}}}{\bar{\omega}(p)\bar{\omega}(q)} \left(h(q) + \frac{m_{0^{++}}^2}{4\omega(q)} g(q) \right), \quad (20)$$

$$g(p) \left(\omega(p) - \frac{m_{0^{++}}^2}{4\omega(p)} \right) = h(p) + \frac{1}{2\pi^2} \int d^3q V_C(|\mathbf{p} - \mathbf{q}|) \hat{\mathbf{p}} \cdot \hat{\mathbf{q}} g(q). \quad (21)$$

For highly excited states the typical momenta of the quarks become large. For large momenta, however, the mass function $M(p)$ becomes small. Setting $M(p) = 0$ in the second equation for the pseudoscalar meson (12) and the first equation for the scalar meson (20) gives just the second equation for the scalar meson (21) and the first equation for the pseudoscalar meson (11), respectively. For large momenta with $M(p) \approx 0$ the two systems of coupled integral equations become

approximately the same. This can explain why pseudoscalar and scalar mesons with large n become approximately degenerate. For states with $J > 0$ similar arguments hold but there are additional states which fall in the multiplets $(0, 0)$ and $(0, 1) \oplus (1, 0)$. The Bethe-Salpeter amplitudes for mesons with large J become strongly suppressed for small momenta and already states with $n = 0$ become approximately degenerate. In our model the numerical results for the meson spectra up to $n, J = 6$ show a very fast restoration of both $SU(2)_L \times SU(2)_R$ and $U(1)_A$ symmetries with increasing J and essentially more slow restoration with increasing n . The excited states lie on approximately linear radial and angular Regge trajectories which is demonstrated in Fig. 3. In the limit $n \rightarrow \infty$ and/or $J \rightarrow \infty$ one observes an approximate degeneracy of all states within the representation $[(0, 1/2) \oplus (1/2, 0)] \times [(0, 1/2) \oplus (1/2, 0)]$ that combines all possible chiral representations for systems of two massless quarks [11].

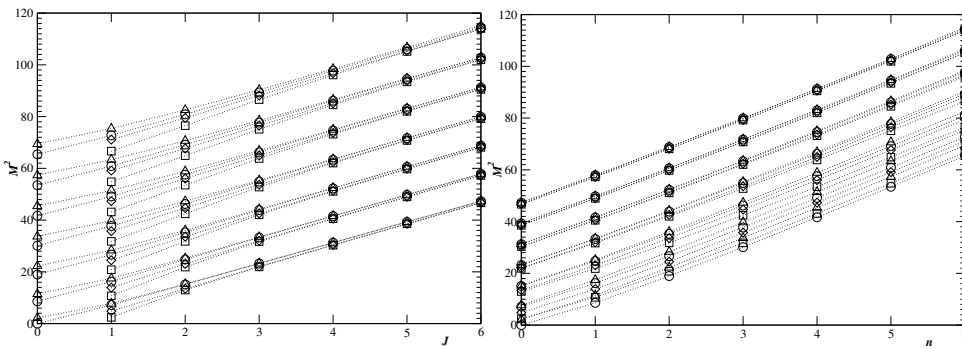


Fig. 3. Angular (left) and radial (right) Regge trajectories for isovector mesons. Mesons of the chiral multiplet $(1/2, 1/2)_a$ are indicated by circles, of $(1/2, 1/2)_b$ by triangles, and of $(0, 1) \oplus (1, 0)$ by squares (J^{++} and J^{--} for even and odd J , respectively) and diamonds (J^{--} and J^{++} for even and odd J , respectively).

Acknowledgment: The results presented in this contribution were obtained in collaboration with R. Alkofer, L. Ya. Glozman, M. Kloker, and A. Krassnigg. I am grateful to the organizers for providing financial support for my participation at the workshop.

References

1. D. Zwanziger, Phys. Rev. Lett. **90**, 102001 (2003).
2. A. P. Szczepaniak and E. S. Swanson, Phys. Rev. D **65**, 025012 (2002); D. Zwanziger, Phys. Rev. D **70**, 094034 (2004); C. Feuchter and H. Reinhardt, Phys. Rev. D **70**, 105021 (2004).
3. J. Greensite, Š. Olejník, and D. Zwanziger, Phys. Rev. D **69**, 074506 (2004); A. Nakamura and T. Saito, Prog. Theor. Phys. **115**, 189 (2006).
4. J. R. Finger and J. E. Mandula, Nucl. Phys. **B199**, 168 (1982); S. L. Adler and A. C. Davis, Nucl. Phys. **B244**, 469(1984); R. Alkofer and P. A. Amundsen, Nucl. Phys. **B306**, 305 (1988).

5. C. D. Roberts and S. M. Schmidt, *Prog. Part. Nucl. Phys.* **45**, S1 (2000); R. Alkofer and L. von Smekal, *Phys. Rep.* **353**, 281 (2001); P. Maris and C. D. Roberts, *Int. J. Mod. Phys. E* **12**, 297 (2003).k
6. R. Alkofer, M. Kloker, A. Krassnigg, and R. F. Wagenbrunn, *Phys. Rev. Lett.* **96**, 022001 (2006).
7. K. Langfeld, R. Alkofer and P. A. Amundsen, *Z. Phys. C* **42**, 159 (1989).
8. R. F. Wagenbrunn and L. Ya. Glozman, hep-ph/0605247, accepted for publication in *Phys. Lett. B*.
9. L. Ya. Glozman, *Int. J. Mod. Phys. A* **21**, 475 (2006).
10. L. Ya. Glozman, A. V. Nefediev, and J. E. F. T. Ribeiro, *Phys. Rev. D* **72**, 094002 (2005).
11. L. Ya. Glozman, *Phys. Lett.* **B587**, 69 (2004).



New resonances and spectroscopy at Belle

M. Bračko^{a,b}, representing the Belle Collaboration

^aUniversity of Maribor, Smetanova ulica 17, SI-2000 Maribor, Slovenia

^bJožef Stefan Institute, P.O.B. 3000, SI-1001 Ljubljana, Slovenia

Abstract. The Belle experiment at the KEKB asymmetric-energy electron-positron collider has proven to be an excellent environment for a wide variety of measurements. Besides its main goal – measurements of CP violation in the system of B mesons – other most important achievements are observations of several yet undiscovered particles and measurements of their properties. The discoveries were often surprising, since only some of the observed states were predicted in various models, while others were not. The existence of these resonances therefore still imposes theoretical questions regarding their nature and also represents a challenge for a proper description in terms of QCD. Selected experimental results together with their possible interpretations are reviewed in this paper.

1 Introduction

The Belle detector [1] at the asymmetric-energy e^+e^- collider KEKB [2] has accumulated around 630 fb^{-1} by July 2006. The KEKB collider is often called the *B-factory*, since it operates at the energy of the $\Upsilon(4S)$ resonance, slightly above the $B\bar{B}$ -production threshold, and thus the accumulated data set contains a large number of $B\bar{B}$ pairs. While the main goal of both B-factories* are measurements of CP violation in the B-meson system, the excellent detector performances also enable searches for new hadronic (bound) states as well as studies of their properties. There are several possible mechanisms of the particle production at B-factories: production in the B-meson decays, fragmentation of quarks in e^+e^- annihilation or creation of C-even states in two photon processes. In this paper, we address some interesting discoveries of new hadronic states, produced by different mechanisms and observed by the Belle collaboration.

2 The X, Y, Z story

Several charmonium-like new states have been recently observed by Belle, namely: X(3872), Z(3930), Y(3940) and X(3940). The naming convention indicates the lack of knowledge about the structure and properties of these particles at the time of their discovery.

* Besides KEKB in Japan, there is a similar collider called PEP-II in the USA, delivering data to the *BABAR* [3] detector.

2.1 Observation and properties of X(3872)

In 2003 Belle reported on the analysis of $B^\pm \rightarrow K^\pm \pi^+ \pi^- J/\psi$ decays, where a narrow charmonium-like state (X(3872)) decaying to $\pi^+ \pi^- J/\psi$ was discovered [4]. For the most recent update from Belle [5], the fitted yield of both, charged and neutral B mesons reconstructed in $B \rightarrow KX(3872)(\rightarrow \pi^+ \pi^- J/\psi)$ decay mode is shown in Fig. 1(a) as a function of the $\pi^+ \pi^- J/\psi$ invariant mass. The observation of X(3872) resonance was later confirmed by the CDF [6], D0 [7] and BABAR [8] experiments. Currently, the world average of the mass is $M(X(3872)) = (3871.2 \pm 0.5) \text{ MeV}/c^2$ [9] and the upper limit on its width, as measured by Belle, is $\Gamma(X(3872)) < 2.3 \text{ MeV}$ [4].

Several interpretations of X(3872) resonance have been suggested, including charmonium hypothesis [10,?], $D^0 \bar{D}^{*0}$ molecule [12] and tetraquarks [13]. Various dedicated studies were performed at Belle in order to determine possible quantum numbers of X(3872) and its nature. In 2005 Belle reported a strong evidence for the radiative decay of $X(3872) \rightarrow \gamma J/\psi$ [14]. The fitted yield of reconstructed B mesons, as obtained from the simultaneous fit to the ΔE and M_{bc} distributions** for $B \rightarrow K\gamma J/\psi$ decay candidates is shown in Fig. 1(b) as a function of the $M(\gamma J/\psi)$. The observed signal with a significance above 4σ can be converted to $\mathcal{B}(X(3872) \rightarrow \gamma J/\psi)/\mathcal{B}(X(3872) \rightarrow \pi^+ \pi^- J/\psi) = 0.14 \pm 0.05$, which is not in agreement with the expectations for charmonium interpretation of X(3872). However, the observation of this radiative decay establishes even charge-conjugation parity (C) of X(3872).

Furthermore, Belle examined possible J^{PC} quantum number assignments of X(3872) by studying angular correlations between the final-state particles in $X(3872) \rightarrow \pi^+ \pi^- J/\psi$ decays [5]. An example is presented in Fig. 1(c): the measured distribution of the angle between the negative of the B meson flight direction and π^+ momentum from X(3872) in the X(3872) frame, is in agreement with the expectation for the 1^{++} state. Additionally, the $\pi^+ \pi^-$ invariant mass distribution for the events in the $X(3872) \rightarrow \pi^+ \pi^- J/\psi$ signal region, shown in Fig 1(d), peaks at the upper kinematic limit indicating the $\rho^0 J/\psi$ intermediate state and favours S-wave over P-wave as the relative orbital angular momentum between the final-state dipion and J/ψ . As a consequence of these studies, $J^{PC} = 1^{++}$ is strongly favoured for the X(3872), but the 2^{++} can not be completely ruled out.

The latter possibility could be ruled out by the recent study [15] of $B \rightarrow KD^0 \bar{D}^0 \pi^0$ decays, where a near-threshold enhancement at the $(3875.4 \pm 0.7(\text{stat.}) \pm 1.1(\text{syst.})) \text{ MeV}/c^2$ for the invariant mass of the $D^0 \bar{D}^0 \pi^0$ system was observed (see Fig. 1(e, f)). If the observed enhancement – whose invariant mass is however about 2σ higher than the world average value for X(3872) – is indeed due to the X(3872), the $J^{PC} = 1^{++}$ quantum number assignment for the X(3872) would again be favoured, since near-threshold decays $X(3872) \rightarrow D^0 \bar{D}^{*0}/D^0 \bar{D}^0 \pi^0$ are expected to be strongly suppressed for $J = 2$.

** Two kinematic variables are used to identify B-meson candidates: $\Delta E \equiv E_B - E_{\text{beam}}$ and $M_{bc} \equiv 1/c^2 \sqrt{E_{\text{beam}}^2 - (p_B c)^2}$, where E_B and p_B are the reconstructed energy and momentum of the B candidate, and E_{beam} is the beam energy, all expressed in the centre-of-mass (CM) frame.

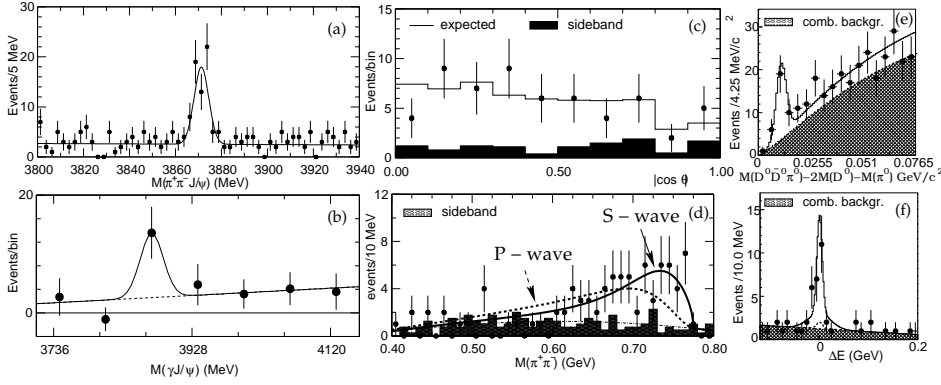


Fig. 1. (a) $\pi^+\pi^-J/\psi$ invariant mass for $B \rightarrow K\pi^+\pi^-J/\psi$ decays [5]; (b) Yield of B mesons for $B \rightarrow K\gamma J/\psi$ decay candidates as a function of $M(\gamma J/\psi)$ [14]; (c) Distribution of angle in $X(3872)$ decays described in the text. The full histogram represents the expectation for $J^{PC} = 1^{++}$ assignment and the hatched histogram is the contribution of background as obtained from the scaled sidebands of $M(\pi^+\pi^-J/\psi)$; (d) $M(\pi^+\pi^-)$ distribution for events in $X(3872)$ signal region. The histogram again indicates the sideband-determined background, while the solid (dashed) curve shows the result of the fit using Breit-Wigner function for $\rho^0 \rightarrow \pi^+\pi^-$, and assuming J/ψ and ρ^0 to be in a relative S-wave (P-wave); (e) and (f) $\Delta M \equiv M(D^0\bar{D}^0\pi^0) - 2M(D^0) - M(\pi^0)$ and ΔE distributions for near-threshold $D^0\bar{D}^0\pi^0$ enhancement in $B \rightarrow KD^0\bar{D}^0\pi^0$ decay [15].

While currently available $X(3872)$ data – the mass, possible 1^{++} quantum numbers and observed decay modes – are in agreement with the hypothesis that $X(3872)$ is a $D^0\bar{D}^{*0}$ molecule [12], some spin assignments corresponding to more conventional interpretations can still not be ruled out (see for example Ref. [16]). Further experimental results and theoretical calculations are thus needed to resolve the puzzle about the nature of the $X(3872)$ resonance.

2.2 $Z(3930)$ resonance

A search for the χ'_{cJ} ($J = 0$ or $J = 2$) states and other C-even charmonium states in the mass range of $3.73 \text{ GeV}/c^2 - 4.3 \text{ GeV}/c^2$ was performed for the two-photon production of $D\bar{D}$ pairs, $\gamma\gamma \rightarrow D\bar{D}$ [17]. The two-photon process was studied in the non-tagged mode, where final-state electron and positron produced in the reaction $e^+e^- \rightarrow e^+e^-D\bar{D}$ are not detected, and the $D\bar{D}$ system has a very small transverse momentum w.r.t. the e^+e^- axis. These requirements help selecting $D\bar{D}$ pairs produced exclusively in collisions of two quasi-real photons. The D mesons were reconstructed in decays of $D^0 \rightarrow K^-\pi^+$, $K^-\pi^+\pi^0$, $K^-\pi^+\pi^-\pi^+$ and $D^+ \rightarrow K^-\pi^+\pi^+$ (and their charge conjugated modes). The obtained $D\bar{D}$ invariant-mass distribution is shown in Fig. 2(a). A clear peak with 5.3σ significance denoted as $Z(3930)$ was observed with mass $(3929 \pm 5(\text{stat.}) \pm 2(\text{syst.})) \text{ MeV}/c^2$ and width $(29 \pm 10(\text{stat.}) \pm 2(\text{syst.})) \text{ MeV}$. A product of the two-photon decay width and branching fraction of the $Z(3930)$ is found to be $\Gamma(Z(3930))\mathcal{B}(Z(3930) \rightarrow D\bar{D}) = 0.18 \pm 0.05 \pm 0.03 \text{ keV}$.

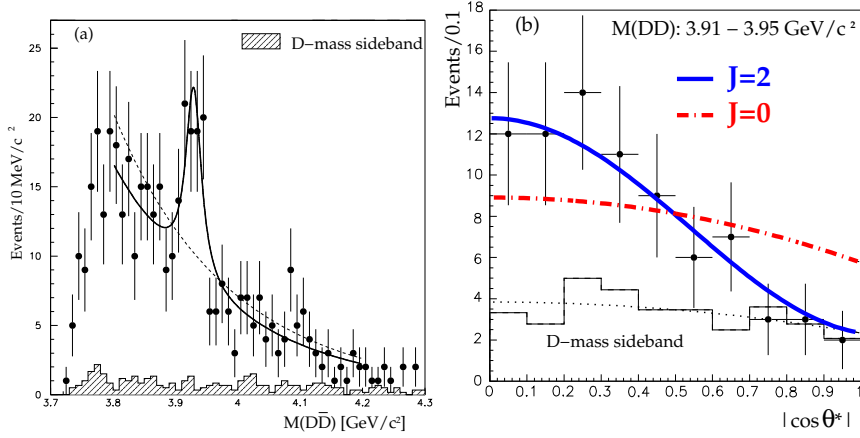


Fig. 2. (a) Invariant mass of $D\bar{D}$ pairs produced in non-tagged two-photon reactions. The curves indicate the result of the fit with a resonant component (solid) and without it (dashed). (b) The $|\cos \theta^*|$ distribution for $Z(3930) \rightarrow D\bar{D}$ decays. Expected predictions for $J = 2$ and $J = 0$ are shown as a solid and a dash-dotted line, respectively, and contain the non-peaking background shown separately by the dotted curve.

An angular analysis was also performed by Belle collaboration [17]. Efficiency corrected $\cos \theta^*$ distribution, where θ^* is the angle between D meson and the beam axis in the $\gamma\gamma$ rest frame, shows that the spin-2 assignment for the observed resonance is strongly favoured over spin-0 assignment. All performed $Z(3930)$ measurements are thus consistent with the expectations for the χ'_{c2} , a radial excitation of 3P_2 charmonium.

2.3 Two new states at $M \approx 3940 \text{ MeV}/c^2$

After the observation of a sub-threshold decay of $X(3872) \rightarrow \omega J/\psi$ [14], using $B \rightarrow KJ/\psi\pi^+\pi^-\pi^0$ decays in a similar way as described for $B \rightarrow KJ/\psi\pi^+\pi^-$ decays in Sec. 2.1, Belle performed an analysis of the $\omega J/\psi$ system produced in exclusive $B \rightarrow K\omega J/\psi$ decays [18], selecting events with $M(\pi^+\pi^-\pi^0) \approx m_\omega$. Events with $M(K\omega) < 1.6 \text{ GeV}/c^2$ are rejected in order to suppress $K_X \rightarrow K\omega$ contribution, where K_X denotes resonances such as $K_1(1270)$, $K_1(1400)$, and $K_2(1400)$ that are known to decay to $K\omega$. The events clustering near the bottom of the Dalitz plot shown in Fig. 3(a) are responsible for a strong enhancement above the phase space expectation, which can be observed in the plot of signal yield of B decays, as obtained from the fit to the M_{bc} distribution, in bins of $M(\omega J/\psi)$ (see Fig. 3(b)). The fit with an S-wave Breit-Wigner function yields (58 ± 11) events with a statistical significance above 8σ , corresponding to a new resonance named $Y(3940)$ with a mass of $(3943 \pm 11(\text{stat.}) \pm 13(\text{syst.})) \text{ MeV}/c^2$ and a total width $\Gamma = (87 \pm 22(\text{stat.}) \pm 26(\text{syst.})) \text{ MeV}$. The measured fraction for this state is $\mathcal{B}(B \rightarrow KY(3940))\mathcal{B}(Y(3940) \rightarrow \omega J/\psi) = (7.1 \pm 1.3(\text{stat.}) \pm 3.1(\text{syst.})) \cdot 10^{-5}$.

Due to rather intriguing properties, the nature of $Y(3940)$ is still mysterious. Namely, any charmonium state with a mass around $3940 \text{ MeV}/c^2$ is expected to

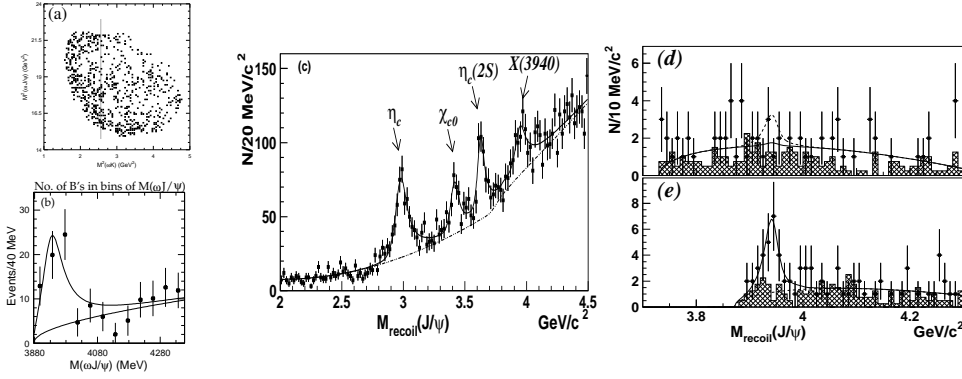


Fig. 3. (a) $M^2(\omega J/\psi)$ vs. $M^2(\omega K)$ Dalitz plot for $B \rightarrow K\omega J/\psi$ decays. Vertical line indicates the region selected by the requirement $M(K\omega) \geq 1.6 \text{ GeV}/c^2$. (b) Yield of B mesons in $B \rightarrow K\omega J/\psi$ decays as a function of $M(\omega J/\psi)$. (c) Spectrum of mass recoiling against the J/ψ . Same recoil mass for events tagged as (d) $J/\psi D\bar{D}$ and (e) $J/\psi D\bar{D}^*$.

dominantly decay to $D\bar{D}$ and/or $D\bar{D}^*$, which for $Y(3940)$ have not been observed yet. Adding that for a $c\bar{c}$ charmonium the hadronic transition to $\omega J/\psi$ should be heavily suppressed, one can conclude that the $Y(3940)$ resonance is probably not a conventional radially excited P-wave charmonium state. As an alternative interpretation, it has been suggested that $Y(3940)$ is one of $c\bar{c}$ -gluon hybrid charmonium states that were first predicted in 1978 [19] and are expected to be produced in B meson decays [20]. It has been shown that $D^{(*)}\bar{D}^{(*)}$ decays for these exotic states are forbidden or heavily suppressed [21], so that such a hybrid state with a mass equal to that of the $Y(3940)$ would have a large branching fraction for decays to J/ψ or ψ' plus light hadrons [22]. However, while this interpretation is able to explain $Y(3940)$ decay modes, predicted masses for $c\bar{c}$ -gluon hybrid states are between 4300 and 4500 GeV/c^2 [23], substantially higher than the measured $Y(3940)$ mass.

Another resonance with a similar mass above $D\bar{D}^{(*)}$ threshold – denoted as $X(3940)$ – was also discovered by the Belle collaboration. This state was observed in the J/ψ recoil mass spectrum for inclusive $e^+e^- \rightarrow J/\psi X$ processes [24]. The mass recoiling against the $J/\psi \rightarrow \ell^+\ell^-$ is determined as $M_{\text{recoil}}(J/\psi) = \sqrt{(E_{\text{CM}} - E_{J/\psi}^*)^2 - (cp_{J/\psi}^*)^2}/c^2$, where E^* is the J/ψ CM energy and E_{CM} is the CM energy of the event. The new peak can be seen in a recoil mass spectrum at about 3940 MeV/c^2 , together with three known peaks corresponding to η_c , χ_{c0} and $\eta_c(2S)$ (see Fig. 3(c)).

Searches for two exclusive decay modes of this newly observed state were performed: $X(3940) \rightarrow D\bar{D}^{(*)}$ and $X(3940) \rightarrow \omega J/\psi$. For the former search, only a single D meson besides the J/ψ was reconstructed to increase the efficiency. Only events with the recoil mass $M_{\text{recoil}}(DJ/\psi)$ close to $D^{(*)}$ mass were retained for the analysis. The resulting mass recoiling against the J/ψ – corresponding to the invariant mass of the $D\bar{D}$ and $D\bar{D}^*$ system – is shown in Fig. 3(d, e)). While no significant signal was observed at the mass of about 3940 MeV/c^2 for the $e^+e^- \rightarrow$

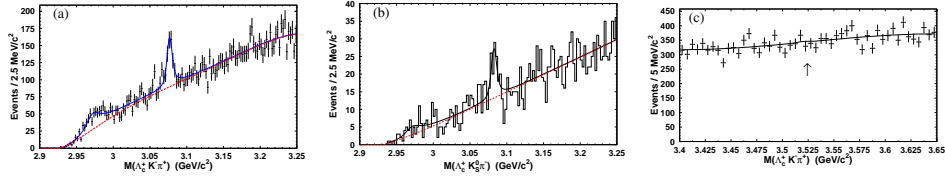


Fig. 4. Distributions of the invariant masses (a) $M(\Lambda_c^+ K^- \pi^+)$ and (b) $M(\Lambda_c^+ K_S^0 \pi^-)$ (both shown as points with error bars) together with the fitting function (the solid line). The dashed lines indicate the background contributions in both cases. (c) The distribution of $\Lambda_c^+ K_S^0 \pi^-$ invariant mass (points with error bars) in the region around the value of 3.52 GeV (marked with an arrow), shown together with the fit result (depicted as a solid line).

$J/\psi D\bar{D}$ events, there is a clear peak for events tagged as $e^+ e^- \rightarrow J/\psi D\bar{D}^*$. The mass of the $X(3940)$ resulting from the fit shown in Fig. 3(e) is $(3943 \pm 6(\text{stat.}) \pm 6(\text{syst.})) \text{ MeV}/c^2$ and the upper limit on the $X(3940)$ total width is 52 MeV at the 90% confidence level.

No significant signal was found for $X(3940) \rightarrow \omega J/\psi$ decays. Since $X(3940)$ state does not share decay modes with the $Y(3940)$, these two states appear not to be the same. A possible interpretation is that $X(3940)$ state is a radially excited charmonium state $\eta_c(3S)$.

3 Observation of $\Xi_{cx}(2980)$ and $\Xi_{cx}(3077)$

Early this year, using the data sample of 461.5 fb^{-1} the Belle collaboration reported the first observation of two charmed baryons [25]. These two baryons, denoted as $\Xi_{cx}(2980)^+$ and $\Xi_{cx}(3077)^+$, are found to be decaying into a $\Lambda_c^+ K^- \pi^+$ final state (see Fig. 4 (a)). Assuming that these states carry charm and strangeness, the above observation would represent the first example of a baryonic decay in which the initial c and s quarks are carried away by two different final state particles. Most naturally, these two states could be interpreted as excited charm-strange baryons Ξ_c . This interpretation could be further justified by positive results of the search for neutral isospin related partners of the above states, performed in events with the $\Lambda_c^+ K_S^0 \pi^-$ final state. The latter search results in the observation of the $\Xi_{cx}(3077)^0$ together with a broad enhancement near the threshold, i.e. in the mass region corresponding to the $\Xi_{cx}(2980)^0$ (see Fig. 4 (b)). Preliminary values of properties for the four observed states are collected in Table 1.

In the $\Lambda_c^+ K^- \pi^+$ final state, the SELEX collaboration reported the observation of a double charmed baryon Ξ_{cc}^+ at the mass of about $3520 \text{ MeV}/c^2$ [26], which has not been confirmed by other experiments. This result – together with the observation of new states mentioned in the previous section of this paper, and the surprisingly large cross section for double charmonium production at B-factories [27,?] – have generated renewed theoretical interest in the spectroscopy, decays and production of charmonium. It has been suggested that the the comparison with the production of double charm tetraquark $T_{cc} = cc\bar{u}\bar{d}$ [29] could shed some light on these experimental results. To search for the Ξ_{cc}^+ state, Belle extended

New State	Mass (MeV/c ²)	Width (MeV/c ²)	Yield (events)	Signif. (σ)
$\Xi_{cx}(2980)^+$	$2978.5 \pm 2.1 \pm 2.0$	$43.5 \pm 7.5 \pm 7.0$	405.3 ± 50.7	6.3
$\Xi_{cx}(3077)^+$	$3076.7 \pm 0.9 \pm 0.5$	$6.2 \pm 1.2 \pm 0.8$	326.0 ± 39.6	9.7
$\Xi_{cx}(2980)^0$	$2977.1 \pm 8.8 \pm 3.5$	43.5 (fixed)	42.3 ± 23.8	2.0
$\Xi_{cx}(3077)^0$	$3082.8 \pm 1.8 \pm 1.5$	$5.2 \pm 3.1 \pm 1.8$	67.1 ± 19.9	5.1

Table 1. Summary of the parameters of the new states in the $\Lambda_c^+ K^- \pi^+$ and $\Lambda_c^+ K_S^0 \pi^+$ final states: masses, widths, yields and statistical significance.

the range of $M(\Lambda_c^+ K^- \pi^+)$ search to include the region around 3520 MeV/c² (see Fig. 4 (c)). However, the study shows no evidence for this state, and as a result only an upper limit on the ratio of cross-sections for exclusive $\Xi_{cc}(3520)^+$ production and inclusive Λ_c^+ production is given at the 90% confidence level: $\sigma(\Xi_{cc}(3520)^+) \times \mathcal{B}(\Xi_{cc}(3520)^+ \rightarrow \Lambda_c^+ K^- \pi^+) / \sigma(\Lambda_c^+) < 1.5 \cdot 10^{-4}$.

4 Conclusion

The large data sample collected by the Belle experiment at KEKB provides an excellent opportunity for the search of new particles. During the Belle operation more than ten new states have been discovered. In this paper we report on some of the most exciting, like X(3872), Y(3940), X(3940) and Z(3930). The latter two resonances can be interpreted as charmonium states, $\eta_c(3S)$ and χ'_{c2} , respectively. None of the existing measurements contradicts the X(3872) interpretation as a $D^0 \bar{D}^{*0}$ molecule. The nature of Y(3940) remains to be addressed.

Recently, new charmed baryons, $\Xi_{cx}(2980)$ and $\Xi_{cx}(3077)$, have been observed by the Belle collaboration. These states are most naturally interpreted as the excited charmed strange baryons, Ξ_c . However, in contrast to known excited Ξ_c baryons, the observed new states decay into separate charmed (Λ_c^\pm) and strange (K) hadrons. As further studies of all new states are ongoing, more interesting results on charm spectroscopy are expected soon from the Belle experiment.

References

1. A. Abashian *et al.* (Belle Collaboration), Nucl. Instr. and Meth. A **479**, 117 (2002).
2. S. Kurokawa and E. Kikutani, Nucl. Instr. and Meth. A **499**, 1 (2003), and other papers included in this Volume.
3. B. Aubert *et al.* (BABAR Collaboration), Nucl. Instr. and Meth. A **479**, 1 (2002).
4. S.-K. Choi, S. L. Olsen *et al.* (Belle Collaboration), Phys. Rev. Lett. **91**, 262001 (2003).
5. K. Abe *et al.* (Belle Collaboration), hep-ex/0505038.
6. D. Acosta *et al.* (CDF II Collaboration), Phys. Rev. Lett. **93**, 072001 (2004).
7. V. M. Abazov *et al.* (D0 Collaboration), Phys. Rev. Lett. **93**, 162002 (2004).
8. B. Aubert *et al.* (BABAR Collaboration), Phys. Rev. D **71**, 071103 (2005).
9. W.-M. Yao *et al.* (Particle Data Group), J. Phys. G **33**, 1 (2006).

10. E. J. Eichten, K. Lane and C. Quigg, Phys. Rev. D **69**, 09401 (2004).
11. T. Barnes and S. Godfrey, Phys. Rev. D **69**, 054008 (2004).
12. E. S. Swanson, Phys. Lett. B **588**, 189 (2004).
13. L. Maiani, F. Piccinini, A. D. Polosa and V. Riquer, Phys. Rev. D **71**, 014028 (2005).
14. K. Abe *et al.* (Belle Collaboration), hep-ex/0505037.
15. G. Gokhroo, G. Majumder *et al.* (Belle collaboration), Phys. Rev. Lett. **97**, 162002 (2006).
16. A. Abulencia *et al.* (CDF Collaboration), Phys. Rev. Lett. **96**, 102002 (2006).
17. S. Uehara *et al.* (Belle Collaboration), Phys. Rev. Lett. **96**, 082003 (2006).
18. S.-K. Choi, S. L. Olsen *et al.* (Belle Collaboration), Phys. Rev. Lett. **94**, 182002 (2005).
19. D. Horn and J. Mandula, Phys. Rev. D **17**, 898 (1978).
20. F. E. Close, I. Dunietz, P. R. Page, S. Veseli, and H. Yamamoto, Phys. Rev. D **57**, 5653 (1998); G. Chiladze, A. F. Falk, and A. A. Petrov, Phys. Rev. D **58**, 034013 (1998); F. E. Close and S. Godfrey, Phys. Lett. B **574**, 210 (2003).
21. N. Isgur, R. Kokoski, and J. Patton, Phys. Rev. Lett. **54**, 869 (1985); F. E. Close and P. R. Page, Nucl. Phys. B **443**, 233 (1995) and Phys. Lett. B **366**, 323 (1996).
22. F. E. Close, Phys. Lett. B **342**, 369 (1995).
23. C. Banner *et al.*, Phys. Rev. D **56**, 7039 (1997); Z.-H. Mei and X.-Q. Luo, Int. J. Mod. Phys. A **18**, 5713 (2003); X. Liao and T. Manke, hep-lat/0210030.
24. K. Abe *et al.* (Belle Collaboration), hep-ex/0507019 (submitted to Phys. Rev. Lett.).
25. R. Chistov *et al.* (Belle Collaboration), Phys. Rev. Lett. **97**, 162001 (2006).
26. A. Mattson *et al.* (SELEX Collaboration), Phys. Rev. Lett. **89**, 112001 (2002).
27. K. Abe *et al.* (Belle Collaboration), Phys. Rev. Lett. **89**, 142001 (2002).
28. B. Aubert *et al.* (BABAR Collaboration), Phys. Rev. D **72**, 031101 (2005).
29. A. Del Fabbro, D. Janc, M. Rosina, and D. Treleani, Phys. Rev. D **71**, 014008 (2005).



Excitation of the Roper resonance^{*}

B. Golli^{a,b} and S. Širca^{b,c}

^aFaculty of Education, University of Ljubljana, 1000 Ljubljana, Slovenia

^bJožef Stefan Institute, 1000 Ljubljana, Slovenia

^cFaculty of Mathematics and Physics, University of Ljubljana, 1000 Ljubljana, Slovenia

Abstract. We study a model of the Roper resonance in which the two-pion decay proceeds via intermediate hadrons, the $\Delta(1232)$ isobar and the σ meson. We derive the coupled channel formalism for the K-matrix and show that the coupling of the σ meson to the N(1440) and N(1710) resonances is responsible for the peculiar behavior of the inelasticity in the P11 channel.

1 Introduction

Among the low-lying nucleon excitations, the Roper resonance N(1440) plays a very special role due to its relatively low energy as well as a rather peculiar behavior of the scattering and electro-excitation amplitudes. Its low energy can be explained in models in which the quarks are strongly coupled to chiral mesons, e.g. in the framework of the Constituent Quark Model [1]. Yet, the form of the scattering amplitudes which is far from the familiar Breit-Wigner shape, and in particular the unusual behavior of the inelasticity in the P11 channel, indicate that the structure of the state can not be explained by a simple excitation of the quark core (like most of the other low lying states) and that other degrees of freedom have to be included (see [2] and references therein).

In this work we shall concentrate on the decays of the Roper resonance rather than on the problem of its low energy. We shall show that the behavior of the scattering amplitude can be explained in a simple model in which the chiral partner of the pion, the σ meson, is included together with the quark and pion degrees of freedom. The model assumes that the two-pion decay proceeds only through intermediate hadrons, either the $\Delta(1232)$, the σ or the ρ meson. Since the decay into the ρ meson and the nucleon is relatively weak, we keep only the first two intermediate hadrons.

In our previous work [3,4] we have introduced an approach to calculate the K-matrix for pion scattering and electro-production in quark models with chiral mesons. We have successfully applied it to the calculation of the phase shift and electro-production amplitudes in the P33 channel. We have also presented a method how to include the simplest two pion decay, namely the decay into the intermediate Δ and the pion.

^{*} Talk delivered by B. Golli

2 K matrix in chiral quark models

Chew and Low [5] have shown that in models in which the mesons are coupled linearly to the source, it is possible to find the exact expression for the T matrix without explicitly specifying the form of asymptotic states. In [3,4] we have found that the expression for the K matrix in this case and write down an integral equation which can be used to calculate the K matrix for a particular model.

To describe the core to which the mesons are coupled we consider quark models in which the quarks emit/absorb a meson by flipping the spin and isospin, and through the excitation to a higher radial state. The part of the Hamiltonian referring to the p-wave pions can be written as

$$H_\pi = \int dk \sum_{mt} \left\{ \omega_k a_{mt}^\dagger(k) a_{mt}(k) + \left[V_{mt}(k) a_{mt}(k) + V_{mt}^\dagger(k) a_{mt}^\dagger(k) \right] \right\}, \quad (1)$$

where $a_{mt}^\dagger(k)$ is the creation operator for a pion with the third components of spin m and isospin t , and $V_{mt}(k) = -v(k) \sum_{i=1}^3 \sigma_m^i \tau_t^i$ is the general form of the pion source, with the quark operator, $v(k)$, depending on the model. It includes also the possibility that the quarks change their radial function which is specified by the reduced matrix elements $V_{BB'} = \langle B || V(k) || B' \rangle$, where B are the bare baryon states (e.g. the bare nucleon, Δ , Roper, ...)

The coupling of the σ meson to the quark core is explicitly present in the linear sigma model, however, due to the meson self-interaction potential it is no longer possible to write down the meson part of the Hamiltonian in the form (1) which would permit the use of the exact expressions for the T and the K matrix. In non-linear versions of different models with chiral mesons the σ meson represents two strongly correlated pions in a relative s-state. The σ meson has been included at purely phenomenological level in several multichannel analyzes of πN reactions (see [6] and references therein).

In our approach we consider the s-wave σ mesons as independent degrees of freedom linearly coupled to the quark core, so that we can use the same formalism as in the case of the pion. We assume the one- σ meson states are labeled by the momentum k and by the σ meson rest mass μ equivalent to the two-pion invariant mass. The effective σ Hamiltonian is taken in the form

$$H_\sigma = \int d\mu \int dk \omega_{\mu k} b_\mu^\dagger(k) b_\mu(k) + \bar{V}_\mu^\dagger(k) b_\mu^\dagger(k) + \bar{V}_\mu(k) b_\mu(k), \quad (2)$$

where

$$\omega_{\mu k}^2 = k^2 + \mu^2. \quad (3)$$

The operators b_μ and b_μ^\dagger are the annihilation and creation operators for the s-wave σ mesons with the invariant mass μ , $2m_\pi < \mu < \infty$. The quark-sigma interaction is taken in the form:

$$\bar{V}_\mu(k) = \kappa \frac{k}{\sqrt{2\omega_{\mu k}}} w_\sigma(\mu). \quad (4)$$

Here $w_\sigma(\mu)$ is a weight function centered around the experimental value of the σ meson mass (~ 600 MeV) and normalized as $\int_{2m_\pi}^\infty d\mu w_\sigma^2(\mu) = 1$. The (dimensionless) coupling parameter κ is taken as a free parameter.

In the basis with good total angular momentum J and isospin T , in which the K and T matrices are diagonal, it is possible to express the K matrix for the elastic channel in the form [4]

$$K_{NN}(k, k_0) = -\pi \sqrt{\frac{\omega_k}{k}} \langle \Psi^N(W) | V(k) | \Phi_N \rangle. \quad (5)$$

Here Φ_N is the ground state of the system, and Ψ^N the principal-value state [7] obeying

$$|\Psi^N(W)\rangle = \sqrt{\frac{\omega_0}{k_0}} \left\{ [a^\dagger(k_0) | \Phi_N \rangle]^{JT} - \frac{\mathcal{P}}{H - W} [V(k_0) | \Phi_N \rangle]^{JT} \right\}, \quad (6)$$

where $[]^{JT}$ denotes coupling to good J and T , k_0 and ω_0 are the pion momentum and energy:

$$k_0 = \sqrt{\omega_0^2 - m_\pi^2}, \quad \omega_0 = \frac{W^2 - m_N^2 + m_\pi^2}{2W}, \quad (7)$$

m_N is the nucleon rest mass and W the invariant energy of the system ($W = \sqrt{s}$). The K matrices for the inelastic processes $\pi + N \rightarrow \pi + \Delta(m)$ where m is the invariant Δ mass can be written as

$$K_{N\Delta}(k, k_0) = -\pi \sqrt{\frac{\omega_k}{k}} \langle \Psi^N(W) | V(k) | \Psi_\Delta(m) \rangle. \quad (8)$$

Here $\Psi_\Delta(m)$ is the principal value state corresponding to the πN scattering in the $P33$ channel as determined in [4] except that it is now normalized to $\delta(m - m')$ rather than to $(1 + K_\Delta(m)^2) \delta(m - m')$. For the process $\pi + N \rightarrow \sigma(\mu) + N$ we have

$$K_{N\sigma}(k_\mu, k_0) = -\pi \sqrt{\frac{\omega_{\mu k}}{k_\mu}} \langle \Psi^N(W) | \bar{V}_\mu(k_\mu) | N \rangle. \quad (9)$$

3 Coupled channels

The K matrix is related to the T matrix through the Heitler equation:

$$T = -\frac{K}{(1 - iK)} \quad \text{or} \quad T = -K + iT. \quad (10)$$

Since the elements of the K matrix corresponding to inelastic channels depend on the invariant masses m and μ , the above matrix equation becomes a set of

coupled integral equations for the T matrix, valid for each W :

$$T_{NN} = -K_{NN} + i \left[K_{NN} T_{NN} + \int_{m_N+m_\pi}^{W-m_\pi} dm K_{N\Delta}(m) T_{\Delta N}(m) + \int_{2m_\pi}^{W-m_N} d\mu K_{N\sigma}(\mu) T_{\sigma N}(\mu) \right], \quad (11)$$

$$T_{\Delta N}(m) = -K_{\Delta N}(m) + i \left[K_{\Delta N}(m) T_{NN} + \int_{m_N+m_\pi}^{W-m_\pi} dm' K_{\Delta\Delta}(m, m') T_{\Delta N}(m') + \int_{2m_\pi}^{W-m_N} d\mu K_{\Delta\sigma}(m, \mu) T_{\sigma N}(\mu) \right], \quad (12)$$

$$T_{\sigma N}(\mu) = -K_{\sigma N}(\mu) + i \left[K_{\sigma N}(\mu) T_{NN} + \int_{m_N+m_\pi}^{W-m_\pi} dm K_{\sigma\Delta}(\mu, m) T_{\Delta N}(m) + \int_{2m_\pi}^{W-m_N} d\mu' K_{\sigma\sigma}(\mu, \mu') T_{\sigma N}(\mu') \right]. \quad (13)$$

The equations involve only the on-shell K matrix elements*. Apart of the K matrix elements corresponding to the processes with the nucleon and the pion in the initial state we have to include the processes with the pion and the Δ , as well as the σ meson and the nucleon in the initial and in the final state. The pertinent on-shell matrix elements are defined as

$$\begin{aligned} K_{\Delta N}(W, m) &= -\pi \sqrt{\frac{\omega_m}{k_m}} \langle \Psi_\Delta(m) | V^\dagger(k_m) | \Psi^N(W) \rangle, \\ K_{\Delta\Delta}(W, m, m') &= -\pi \sqrt{\frac{\omega_m}{k_m}} \langle \Psi_\Delta(m') | V^\dagger(k_{m'}) | \Psi^\Delta(W, m) \rangle, \\ K_{\sigma N}(W, \mu) &= -\pi \sqrt{\frac{\omega_0}{k_0}} \langle \Phi_N | V^\dagger(k_0) | \Psi^\sigma(W, \mu) \rangle, \\ K_{\Delta\sigma}(W, m, \mu) &= -\pi \sqrt{\frac{\omega_\mu}{k_\mu}} \langle \Phi_N | \bar{V}^{\mu\dagger}(k_\mu) | \Psi^\Delta(W, m) \rangle, \\ K_{\sigma\Delta}(W, \mu, m) &= -\pi \sqrt{\frac{\omega_m}{k_m}} \langle \Psi_\Delta(m) | V^\dagger(k_m) | \Psi^\sigma(W, \mu) \rangle, \\ K_{\sigma\sigma}(W, \mu, \mu') &= -\pi \sqrt{\frac{\omega_{\mu'}}{k_{\mu'}}} \langle \Phi_N | \bar{V}^{\mu'\dagger}(k_{\mu'}) | \Psi^\sigma(W, \mu) \rangle. \end{aligned} \quad (14)$$

Here $\Psi^\Delta(W, m)$ is the principal value state corresponding to the pion scattering on the Δ state of invariant mass m in the P11 channel, and $\Psi^\sigma(W, \mu)$ the state corresponding to the scattering of the σ meson of invariant mass μ on the nucleon. These states obey similar relations as the principal value state for πN scattering (see eq. 6):

$$|\Psi^\Delta(W, m)\rangle = \sqrt{\frac{\omega_m}{k_m}} \left\{ [a^\dagger(k_m) |\Psi_\Delta(m)\rangle]^{JT} - \frac{\mathcal{P}}{H-W} [V(k_m) |\Psi_\Delta(m)\rangle]^{JT} \right\}, \quad (15)$$

* To label the on shell matrix elements we prefer to use the total invariant energy of the system, W , (which we sometimes drop) as well as the invariant masses m and μ instead of pion momenta.

where

$$\omega_m = \frac{W^2 - m^2 + m_\pi^2}{2W}, \quad k_m = \sqrt{\omega_m^2 - m_\pi^2}. \quad (16)$$

For scattering of the σ meson on the nucleon we have

$$|\Psi^\sigma(W, \mu)\rangle = \sqrt{\frac{\omega_\mu}{k_\mu}} \left\{ b_\mu^\dagger(k_\mu) |\Phi_N\rangle - \frac{\mathcal{P}}{H - W} \bar{V}^\mu(k_\mu) |\Phi_N\rangle \right\}, \quad (17)$$

where

$$\omega_\mu = \frac{W^2 - m_N^2 + \mu^2}{2W}, \quad k_\mu = \sqrt{\omega_\mu^2 - \mu^2}. \quad (18)$$

To preserve unitarity, the K matrix has to be real and symmetric, i.e.: $K_{HH'} = K_{H'H}$.

Let us mention that the set of coupled equations similar to (13) has been used in several analysis of experimental data for the pion scattering (see e.g. Ref. [8] and [9] and references therein). In these approaches the K matrix is taken at the tree level with meson-baryon form-factors as well as the masses of the hadrons considered as free parameters.

4 Integral equations for the scattering amplitudes

The equations (6), (15) and (17) are too difficult to treat in their general form and we rather use a suitable *ansatz* for the state Ψ^H , $\{H = N, \Delta \text{ or } \sigma\}$, valid in the low energy regime. Let us note that the second term in the above equations generates configurations with different recoupling of the quark spins and isospins as well as excitations to higher radial states. In addition, the quark core gets dressed by a cloud of pions and σ mesons. If we allow asymptotic states with only one pion and one σ meson, the ansatz takes the form

$$\begin{aligned} |\Psi^H\rangle = & \sqrt{\frac{\omega_H}{k_H}} \left\{ |\Psi_0^H\rangle + c_R^H |\Phi_R\rangle + \int dk \frac{\chi^{NH}(k, k_H, k_0)}{\omega_k - \omega_0} [a^\dagger(k) |\Phi_N\rangle]^{\frac{1}{2}\frac{1}{2}} \right. \\ & + \int dk \int dm' \frac{\chi^{\Delta H}(k, k_H, k_{m'})}{\omega_k - \omega_{m'}} [a^\dagger(k) |\hat{\Psi}_\Delta(m')\rangle]^{\frac{1}{2}\frac{1}{2}} \\ & \left. + \int dk \int d\mu' \frac{\chi^{\sigma H}(k, k_H, k_{\mu'})}{\omega_{\mu'/k} - \omega_{\mu'}} b_{\mu'}^\dagger(k) |\Phi_N\rangle + c_N |\Phi_N\rangle \right\} \quad (19) \end{aligned}$$

Here Ψ_0^H is the first term on the RHS of (6), (15) and (17) respectively, the state Φ_R is a resonant state with the excited quark core with the nucleon quantum numbers, (it corresponds to the Roper state as obtained in a calculation with the bound state boundary conditions). The next three terms represent one-pion states on top of the nucleon and Δ and one- σ meson state on top of the nucleon, respectively, with scattering boundary conditions (i.e. the irregular waves). The last term ensures the orthogonality of the scattering state with respect to the ground state Φ_N , and is responsible for the proper behavior of the scattering amplitudes at the nucleon pole. The states denoted by Φ may contain the meson cloud which however vanishes asymptotically; among such states, only the ground state Φ_N is the eigenstate of the Hamiltonian.

From (5), (8), and (9), we immediately obtain the relations between the matrix elements of the K matrix and the pion amplitudes, χ , in the above ansatz. For the on-shell matrix elements we have

$$\begin{aligned} K_{NH} &= \pi \sqrt{\frac{\omega_0 \omega_H}{k_0 k_H}} \chi^{NH}(k_0, k_H, k_0), \\ K_{\Delta H} &= \pi \sqrt{\frac{\omega_{m'} \omega_H}{k_{m'} k_H}} \chi^{\Delta H}(k_{m'}, k_H, k_{m'}), \\ K_{\Delta H} &= \pi \sqrt{\frac{\omega_{\mu'} \omega_H}{k_{\mu'} k_H}} \chi^{\sigma H}(k_{\mu'}, k_H, k_{\mu'}), \end{aligned} \quad (20)$$

Here $k_H = k_0$ for $H = N$, $k_H = k_m$ for $H = \Delta$ and $k_H = k_\mu$ for $H = \sigma$.

Using the ansatz (19) and the equations for the principal value state (6), (15) and (17)), we obtain a set of integral equations for the scattering amplitudes $\chi^{HH'}$ of the form

$$\begin{aligned} \chi^{HH'}(k, k_{H'}, k_H) &= -c_R^{H'} V_{RH}(k) - c_N^{H'} V_{NH}(k) + \mathcal{K}^{HH'}(k, k_{H'}, k_H) \\ &+ \sum_{H''} \int dk' \frac{\mathcal{K}^{HH''}(k, k') \chi^{H''H'}(k', k_{H''}, k_{H'})}{\omega'_k - \omega_{H''}} \end{aligned} \quad (21)$$

where the sum over H'' implies also the integration over the corresponding invariant mass m'' or μ'' in the $\pi\Delta$ and σN case, respectively, and $\omega_{H''}$ is either ω_0 , $\omega_{m''}$ or $\omega_{\mu''}$, respectively. The matrix elements V_{RH} are $V_{RN} = \langle \Phi_R | V(k) | \Phi_N \rangle$, $V_{R\Delta} = \langle \Phi_R | V(k) | \Psi_\Delta(m) \rangle$, and $V_{R\sigma} = \langle \Phi_R | \bar{V}^\mu(k_\mu) | \Phi_N \rangle$; the V_{NH} have analogous structure with Φ_R replaced by Φ_R . The coefficients c_R and c_N obey the following equations

$$(\omega_0 - \varepsilon_R^0) c_R^H = V_{RH}(k_H) + \sum_{H'} \int dk V_{RH'}(k) \frac{\chi^{H',H}(k, k_H, k_{H'})}{\omega_k - \omega_{H'}} \quad (22)$$

$$(\omega_0 - \varepsilon_N) c_N^H = V_{NH}(k_H) + \sum_{H'} \int dk V_{NH'}(k) \frac{\chi^{H',H}(k, k_H, k_{H'})}{\omega_k - \omega_{H'}} \quad (23)$$

Here $\varepsilon_R^0 = (m_R^0{}^2 - m_\pi^2)/2W$, $\varepsilon_N = m_\pi^2/2W$, and m_R^0 is the rest energy of the state Φ_R . The kernel $\mathcal{K}^{HH''}$ has in general a very complicated structure. It can be considerably simplified by making the following assumptions: (i) in the ansatz (19) the ground state Φ_N and the state corresponding to the incoming and outgoing Δ , $\Psi_\Delta(m)$, is not modified in the presence of the scattering mesons, and (ii) the integral over the invariant masses is substituted by the integrand evaluated at $m = m_B$, i.e. at the position of the resonance. The first assumption yields the usual approximation made in this type of calculation:

$$\frac{1}{\omega_k + \omega'_k - \omega} \approx \frac{\omega}{\omega_k \omega'_k}$$

which makes the kernel *separable*. The second assumption requires that the resonances are sufficiently narrow, so that the main contribution to the integral comes

from values of m close to the position of the resonance (i.e. the pole of the corresponding K matrix). This assumption is justified in the case of the Δ resonance but less valid in the case of higher resonances. In the P11 channel this approximation does not have a large effect since the contribution of the Δ resonance dominates over the contribution of higher resonances. Under these two assumptions the kernel takes the form:

$$\mathcal{K}^{\text{HH}'}(k, k') = \sum_{\text{H}''} g_{\text{HH}'\text{H}''} \frac{(\omega_{\text{H}} + \varepsilon_{\text{H}''} - \varepsilon_{\text{H}} - \varepsilon_{\text{H}'}) V_{\text{HH}''}(k) V_{\text{H}'\text{H}''}(k')}{(\omega_k + \varepsilon_{\text{H}''} - \varepsilon_{\text{H}})(\omega_{k'} + \varepsilon_{\text{H}''} - \varepsilon_{\text{H}'})}. \quad (24)$$

Here $g_{\text{HH}'\text{H}''}$ are spin-isospin recoupling coefficients; in the static approximation $\varepsilon_{\text{H}} = m_{\text{H}} - m_{\text{N}}$; taking into account the recoil, we use approximate u-channel denominators averaged over the directions of the meson momenta (see e.g. [10]).

The important point in the above derivation is that due to the separable kernels the set of integral equations reduces to a set of algebraic equations which immediately leads to the exact solution for χ and c . Furthermore, it can be explicitly shown that the approximations preserve the symmetry of the K matrix which in turn *ensures the unitarity* of the S matrix.

Neglecting the integrals in (21)–(23) the problem reduces to the tree level and is the usual starting point in analyzing the experimental data using the K matrix approach mentioned above.

The solution of the system (21)–(23) can be written in a similar form as the expression at the tree level:

$$\chi^{\text{HH}'}(k, k_{\text{H}'}, k_{\text{H}}) = -c_{\text{R}}^{\text{H}'} \mathcal{V}_{\text{RH}}(k) - c_{\text{N}}^{\text{H}'} \mathcal{V}_{\text{NH}}(k) + \mathcal{D}^{\text{HH}'}(k, k_{\text{H}'}, k_{\text{H}}), \quad (25)$$

$$c_{\text{R}}^{\text{H}} = \frac{\mathcal{V}_{\text{RH}}(k_{\text{H}}) - \mathcal{V}_{\text{NH}}(k_{\text{H}}) n_{\text{RN}}}{Z_{\text{R}}(W)(W - m_{\text{R}})}, \quad (26)$$

$$c_{\text{N}}^{\text{H}} = \frac{\mathcal{V}_{\text{NH}}(k_{\text{H}})}{Z_{\text{N}}(W)(W - m_{\text{N}})} + n_{\text{RN}} c_{\text{R}}^{\text{H}}. \quad (27)$$

Here $\mathcal{V}_{\text{HH}'}$ can be interpreted as a renormalized vertex and $Z_{\text{H}}(W)$ as the wave function renormalization of the state. In addition, the quasi bound Roper state Φ_{R} acquires an admixture of the ground state due to the requirement that the ground state is orthogonal to the full scattering state rather than to Φ_{R} itself. Furthermore, it can be easily seen that at the nucleon pole (i.e. $W = m_{\text{N}}$) the residuum involves only the pion-nucleon interaction vertex, so that the behavior of the phase shift at low energies is governed by the πNN coupling constant alone.

5 Results for the Roper in the Cloudy Bag Model

We illustrate the method by calculating scattering amplitudes in the P11 channel. Though the expressions derived in the previous sections are general and can be applied to any model in which mesons linearly couple to the quark core, we choose here the Cloudy Bag Model, primarily because of its simplicity. The pion part of the Hamiltonian of the model has the form (1) with

$$v(k) = \frac{1}{2f_{\pi}} \frac{k^2}{\sqrt{12\pi^2 \omega_k}} \frac{\omega_{\text{MIT}}^0}{\omega_{\text{MIT}}^0 - 1} \frac{j_1(kR)}{kR}, \quad (28)$$

when no radial excitation of the core takes place, while

$$v^*(k) = r_\omega v(k), \quad r_\omega = \frac{1}{\sqrt{3}} \left[\frac{\omega_{\text{MIT}}^1 (\omega_{\text{MIT}}^0 - 1)}{\omega_{\text{MIT}}^0 (\omega_{\text{MIT}}^1 - 1)} \right]^{1/2}, \quad (29)$$

when one quark is excited from the 1s state to the 2s state. Here $\omega_{\text{MIT}}^0 = 2.04$ and $\omega_{\text{MIT}}^1 = 5.40$. The free parameter is the bag radius R. Though the bare values of different 3-quark configurations are in principle calculable in the model, the model lacks a mechanism that would account for large hyperfine splitting between certain states, e.g. the nucleon and the Δ . For each R we therefore adjust the splitting between the bare states such that the experimental position of the resonance is reproduced. Furthermore, using the experimental value of f_π in (28) leads to a too small πNN coupling constant irrespectively of the bag radius; in our calculation we have therefore decreased this value by 10 %.

We include also the excited state of the Δ , the $\Delta(1600)$ isobar assuming the same radial structure as for the $N(1440)$. In order to see the effect of other higher positive-parity nucleon excitation we have included the $N(1710)$ isobar.

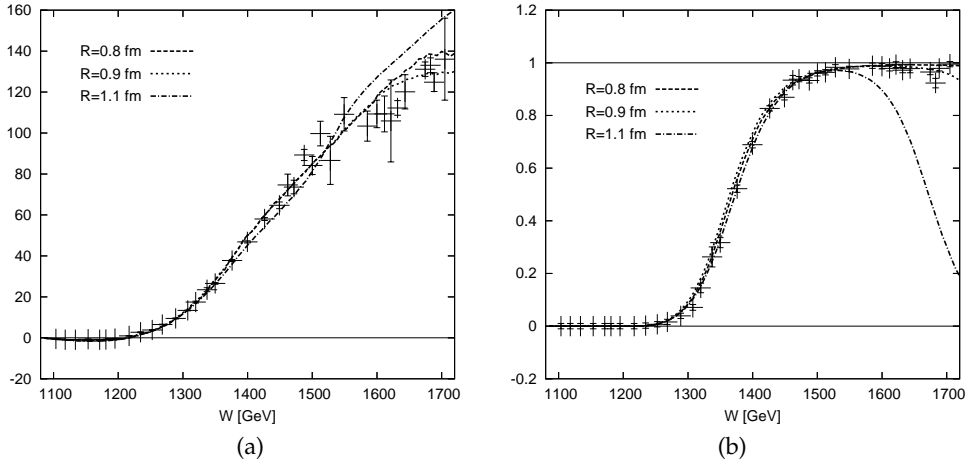


Fig. 1. The phase shift (a) and the inelasticity (b) normalized such that the unitarity limit is 1, as a function of the invariant mass for three choices of the bag radius. Beside the $\Delta(1232)$ and $N(1440)$, the $\Delta(1600) \equiv \Delta^*$ and $N(1710) \equiv R^*$ are included in the calculation. The pole in the K matrix is chosen to be at 1480 MeV for $N(1440)$, 1700 MeV for $\Delta(1600)$ and 1900 MeV for $N(1710)$. Depending on the bag radius, the strength of the $\pi\text{N}\Delta$ coupling is 45 % – 55 % larger, while that of πNR 3 % – 15 % smaller than the corresponding bare quark values. The mass of the σ meson is 550 MeV and its width 600 MeV; the effective σNR coupling parameter κ (see (4)) is between 0.7 and 0.6, depending on the bag radius. The admissible πNR^* is in the range 0 % – 20 % of the πNN coupling constant, while the couplings σNR^* and σNR are comparable. The data points are from [11].

The coupling of the σ meson to the quark core is not explicitly present in the model. It is interpreted as the coupling of two correlated pions through non-

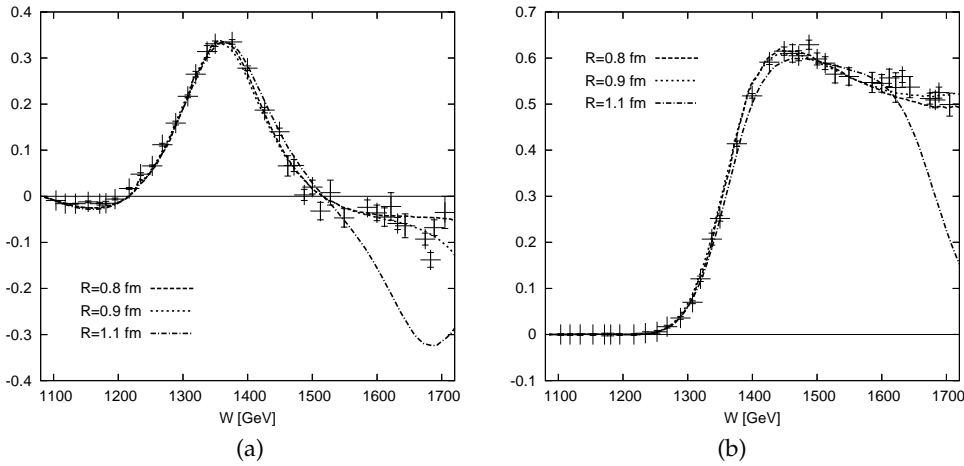


Fig. 2. The real (a) and the imaginary (b) parts of the T matrix as a function of the invariant mass for three choices of the bag radius. For the explanation of different curves see Figure 1.

linear term in the expansion of the pion field [12]. In our approach we simply include this coupling at the phenomenological level and consider its strength as an adjustable parameter.

At low energies the phase shift (Fig. 1) is dominated by the nucleon pole term, and the crossed (u-channel) term with the $\Delta(1232)$ and $\Delta(1600)$ as the intermediate states. Here the $\pi N\Delta$ coupling strength has to be increased with respect to its bare value by some 40 % to 50 % in accordance with our results in the P33 channel [4]. At higher energies around the resonance, the amplitude is governed by the πNR coupling; its strength is enhanced as compared to the bare quark value by a factor 1.4 – 1.8 through the vertex and wave function renormalization such that the bare value has to be decreased up to 15 % in order to obtain reasonable agreement with the experiment.

The presence of the σN channel is most clearly manifested in the inelasticity, $-(4\text{Im}T_{NN} + |T_{NN}|^2)$. It becomes important already at energies slightly above the two pion threshold (Fig. 1). This effect is a clear consequence of the s-wave meson coupling to the quark core and can not be obtained in the competitive process in which the two pions are produced through the intermediate Δ , since in this case the p-wave pions contribute only at relatively high energies. The results are sensitive mostly to the σNR coupling and much less to the σNN ; the latter can be even put to 0. This can be understood since in the static limit the s-channel and the u-channel contributions cancel each other in the case of the nucleon intermediate state. At higher energies ($W > 1600$ MeV) the role of the N(1710) becomes more important; we treat the corresponding meson couplings as adjustable parameters. We do not include other isobars such as the negative-parity excitations so the results in this energy range may be somewhat inconclusive. Nonetheless, there is a rather clear indication that N(1710) more strongly couples to the σN channel rather than to the elastic channel and supports our conjecture about the nature

of this excited state [2]. For the function $w_\sigma(\mu)$ we have assumed a Breit-Wigner shape; the results favor the σ meson mass in the range from 500 MeV to 600 MeV and a relatively large width of 600 MeV or even higher, though the results are rather insensitive to the width provided we readjust the strength of the parameter κ in (4). Choosing a larger width can to some extent compensate the fall-off of the inelasticity at higher energies for larger bag radii.

In conclusion, we emphasize two most important results of our calculation: (i) though the quark models – including the CBM – predict relatively weak π NR coupling which would result in a much too small width of the resonance, we have shown that through the dressing of pions and other isobars the coupling becomes considerably stronger and produces the correct behavior of the scattering amplitudes in the vicinity of the resonance (Fig. 2); (ii) by including the σ meson we have been able to explain the unusual behavior of the inelasticity as well as the scattering amplitude from the two-pion threshold up to energies well above the resonance.

References

1. L. Ya. Glozman, W. Plessas, K. Varga, and R. F. Wagenbrunn, *Phys. Rev. D* **58** (1998) 094030.
2. P. Alberto, M. Fiolhais, B. Golli, and J. Marques, *Phys. Lett. B* **523** (2001) 273.
3. B. Golli and S. Širca in: B. Golli, M. Rosina, S. Širca (eds.), *Proceedings of the Mini-Workshop "Exciting Hadrons"*, July 11–18, 2005, Bled, Slovenia, p. 56.
4. P. Alberto, L. Amoreira, M. Fiolhais, B. Golli, and S. Širca, *Eur. Phys. J. A* **26** (2005) 99.
5. G. F. Chew and F. E. Low, *Phys. Rev.* **101**, (1956) 1570.
6. D. M. Manley, E. M. Saleski, *Phys. Rev. D* **45** (1992) 4002.
7. R. G. Newton, *Scattering Theory of Waves and Particles*, Dover Publications, New York 1982.
8. R. S. Longacre and J. Dolbeau, *Nucl. Phys.* **B122** (1977) 493.
9. O. Krehl et al., *Phys. Rev. C* **62** 025207.
10. T. Ericson and W. Weise, *Pions and Nuclei*, Clarendon Press, Oxford 1988.
11. R. A. Arndt, W. J. Briscoe, R. L. Workman, I. I. Strakovsky, SAID Partial-Wave Analysis, <http://gwdac.phys.gwu.edu/>.
12. E. D. Cooper and B. K. Jennings, *Phys. Rev. D* **33** (1986) 1509.



The two-level Nambu–Jona-Lasinio model^{*}

Mitja Rosina^{a,b} and Borut Tone Oblak^c

^aFaculty of Mathematics and Physics, University of Ljubljana, Jadranska 19, P.O. Box 2964, 1001 Ljubljana, Slovenia

^bJ. Stefan Institute, 1000 Ljubljana, Slovenia

^cNational Institute of Chemistry, Hajdrihova 19, 1000 Ljubljana, Slovenia

Abstract. We show for a schematic quasispin model similar to the Nambu–Jona-Lasinio model that the Hartree-Fock and RPA approximations give accurate vacuum and pion properties in the limit of large number of quarks in the Dirac sea. This helps the understanding why the HF and RPA work so well in the full Nambu – Jona-Lasinio model, especially in the large N_c limit. We also show that the excitation spectrum in a box reveals rather accurately the pion scattering length.

1 The two-level Nambu–Jona-Lasinio model with one flavour

The Nambu–Jona-Lasinio model (NJL) has been successfully used in hadronic physics to describe the spontaneous chiral symmetry breaking, the formation of the massive constituent quark and the behaviour of pion and sigma meson as a chiral rotation and vibration. This model has not yet been solved exactly; so one does not know how accurate the approximate methods used with this model are. In order to gain some insights we simplify the NJL model from a field-theoretical model to an ordinary quantum-mechanical model with a fixed particle number N . This is achieved by

- (i) a sharp 3-momentum cutoff $0 \leq |\mathbf{p}_i| \leq \Lambda$;
- (ii) restricting the space to a box of volume \mathcal{V} with periodic boundary conditions. This gives a finite number of discrete momentum states, $\mathcal{N} = N_c N_f \mathcal{V} \Lambda^3 / 3\pi^2$ in the Dirac sea and the same number available in the “Fermi sea” (positive energy states). In the ground state (vacuum) we assume also the same number of particles, $N = \mathcal{N}$, which, due to the interactions, are distributed between the Dirac and the Fermi sea. For simplicity, we make two further approximations:
- (iii) We restrict the system to one flavour, $N_f = 1$; many qualitative and even quantitative features will remain the same, but of course not all.
- (iv) we assume all particles to have the same kinetic energy $\pm P$ instead of different individual values $\pm|\mathbf{p}_i|$: $|\mathbf{p}_i| \rightarrow P$. Furthermore, the following turns out to be a reasonable average: $P = \frac{3}{4}\Lambda$ and it is surprising how well it reproduces more detailed calculations.

^{*} Talk delivered by M. Rosina.

Then the NJL Hamiltonian can be conveniently written in the first-quantized form [1]

$$\begin{aligned}
 H'_{\text{NJL}} = & \sum_{i=1}^N \left(\gamma_5(i) h(i) \mathcal{P} + m_0 \beta(i) \right) + \\
 & - \frac{2G}{\mathcal{V}} \sum_{i=1}^N \sum_{\substack{j=1 \\ j \neq i}}^N \left(\beta(i) \beta(j) + \left(i \beta(i) \gamma_5(i) \right) \left(i \beta(j) \gamma_5(j) \right) \right) \mathcal{P}. \quad (1)
 \end{aligned}$$

Here γ_5 is the chirality operator (handedness), $h = \boldsymbol{\sigma} \cdot \mathbf{p}/|\mathbf{p}|$ is the helicity and m_0 is the small bare quark mass which explicitly breaks the chiral symmetry. The interaction has two terms in order to be chirally symmetric. The projector

$$\mathcal{P} = \sum_{\mathbf{p}_i'}^{\Lambda} \sum_{\mathbf{p}_j'}^{\Lambda} \sum_{\mathbf{p}_i}^{\Lambda} \sum_{\mathbf{p}_j}^{\Lambda} \delta_{\mathbf{p}_i' + \mathbf{p}_j', \mathbf{p}_i + \mathbf{p}_j} | \mathbf{p}_i', \mathbf{p}_j' \rangle \langle \mathbf{p}_i, \mathbf{p}_j | \quad (2)$$

restricts momenta to a sharp cutoff Λ , but it allows any two quarks to scatter into any two other momentum states provided they conserve momentum (at infinite cutoff this would correspond to a contact interaction).

2 Relation to lattice calculations

The model assumption $0 \leq |\mathbf{p}_i| \leq \Lambda$ corresponds to the cell size (resolution) $a = 6^{1/3} \pi^{2/3} / \Lambda$. Here we assumed $N_c = 3$ colours, $N_f = 1$ flavours, and two helicities. The periodic boundary condition in \mathcal{V} corresponds to the block size $L = \sqrt[3]{\frac{N}{6}} = \sqrt[3]{\mathcal{V}}/\pi^2$ with $N = \mathcal{V} \Lambda^3 / \pi^2$.

In our present calculation with $N = 144$ ($\sqrt[3]{N/6} \approx 3$) and $\Lambda = 650$ MeV this corresponds to the block size in three dimensions $L \approx 3a$ and $a \approx 1.2$ fm. It is surprising that such a poor resolution and block size yields excellent results. We shall discuss this point in the Discussion.

3 The quasispin NJL-like model

In order to get a soluble model we simplify the interaction. In the NJL model the interaction conserves the sum of momenta of both quarks, but each quark changes its momentum in any direction (in the 2-body c.m. system) with equal probability. In the simplified interaction each quark conserves its momentum. The schematic Hamiltonian can then be written as

$$\begin{aligned}
 H = & \sum_{k=1}^N \left(\gamma_5(k) h(k) \mathcal{P} + m_0 \beta(k) \right) + \\
 & - \frac{g}{2} \left(\sum_{k=1}^N \beta(k) \sum_{l=1}^N \beta(l) + \sum_{k=1}^N i \beta(k) \gamma_5(k) \sum_{l=1}^N i \beta(l) \gamma_5(l) \right) . \quad (3)
 \end{aligned}$$

Here $g = 4G/\mathcal{V}$.

The interaction part of Hamiltonian changes the chirality of each separate quark (since it does not commute with the Hamiltonian), but it conserves the helicity, color and momentum of each quark. That means that quarks have a unique label and can be treated as distinguishable.

In the interaction, the double sum has simplified into products of single sums which can be conveniently expressed with the following quasispin operators

$$j_x = \frac{1}{2} \beta, \quad j_y = \frac{1}{2} i\beta\gamma_5, \quad j_z = \frac{1}{2} \gamma_5,$$

which obey (quasi)spin commutation relations and allow us to make full use of the angular momentum algebra.

The (quasi)spin commutation relations are also obeyed by separate sums over quarks with right and left helicity ($\alpha = x, y, z$)

$$R_\alpha = \sum_{k=1}^N \frac{1+h(k)}{2} j_\alpha(k), \quad L_\alpha = \sum_{k=1}^N \frac{1-h(k)}{2} j_\alpha(k) \quad (4)$$

as well as by the total sum

$$J_\alpha = R_\alpha + L_\alpha = \sum_{k=1}^N j_\alpha(k). \quad (5)$$

The model Hamiltonian can then be written as

$$H = 2P(R_z - L_z) + 2m_0 J_x - 2g(J_x^2 + J_y^2). \quad (6)$$

It commutes with R^2 and L^2 but not with R_z and L_z . Nevertheless, it is convenient to work in the basis $|R, L, R_z, L_z\rangle$. The Hamiltonian matrix elements can be easily calculated using the angular momentum algebra. By diagonalisation we then obtain the energy spectrum of the system.

A formally similar Hamiltonian has been studied already by Moszkowski [2] in the context of nuclear rotations and vibrations; instead of the NJL interaction, it is the quadrupole-quadrupole interactions that plays a similar role and leads to the spontaneous breaking of spherical symmetry. Also Civitarese et al. [3] used a two-level quark model to describe the low-lying mesonic spectra, but their interaction is not like NJL, they couple quarks to a one-level bosonic degree of freedom (representing gluon pairs or glueballs).

4 Model parameters and basic observables

Both the full NJL model as well as the quasispin model have three model parameters, Λ , G and m_0 . We intend to adjust them to what we choose as the three basic observables $M = 335 \text{ MeV}$ (the dressed-constituent quark mass), $Q = \langle g | \bar{\psi}\psi | g \rangle = \frac{1}{\mathcal{V}} \langle g | \sum_i \beta(i) | g \rangle = \frac{2}{\mathcal{V}} \langle g | J_x | g \rangle = 250^3 \text{ MeV}^3$ (the chiral condensate) and the pion mass m_π .

We assume that the chiral condensate is related to the better defined observable, the pion decay constant, by the Gell-Mann Oakes Renner relation $f_\pi = -\sqrt{-2m_0 Q}/m_\pi = 93 \text{ MeV}$. We assume this relation also for the one-flavour case where f_π is not experimentally defined while Q has the same meaning as in the two-flavour case.

A detailed analysis of model parameters and quality of approximations for the ground state and the pionic excited state was performed by Oblak [4].

In the two-level quasispin model the exact values of the observables are determined as

$$\begin{aligned} M &= \sqrt{\left(E_g(N) - E_g(N-1)\right)^2 - p^2} \\ Q &= \frac{2}{\mathcal{V}} \langle g | J_x | g \rangle \\ m_\pi &= E_1(N) - E_g(N). \end{aligned} \quad (7)$$

As usual we have defined the constituent quark mass through the separation energy of the N -th quark and the pion mass as the energy difference between the first excited and ground state (note that pionic excitation conserves the momenta of all quarks and therefore carries no momentum).

We want to study the N -dependence of our results. Therefore it would be meaningful to adjust the model parameters for a particular N , for example for $N \rightarrow \infty$. Since we cannot calculate exactly for infinite N we rather choose as a reference the Hartree-Fock + RPA solution; anyway, also for the full NJL the model parameters have been adjusted in this way in the literature [5,6].

In the HF+RPA approximation, the relations (7) can be calculated explicitly

$$\begin{aligned} M &= \sqrt{(\alpha G \Lambda^3)^2 - p^2} \\ Q &= \frac{\Lambda^3}{\pi^2} \frac{M}{\sqrt{M^2 + p^2}} \\ m_\pi &\approx \sqrt{\sqrt{\frac{M^2 + p^2}{M^2}} G \Lambda^3 m_0}. \end{aligned} \quad (8)$$

Here $\alpha = (4/\pi^2)(1 - 1/N)(1 - m_0/M)^{-1}$. It is then easy to determine the model parameters (we choose the limit $N \rightarrow \infty$):

$$\Lambda = 648 \text{ MeV}, \quad G = 40.6 \text{ MeV fm}, \quad m_0 = 4.58 \text{ MeV}.$$

These values compare favourably with those of full Nambu-Jona Lasinio

$$\text{Coimbra [5]: } \Lambda = 631 \text{ MeV}, \quad G = 40 \text{ MeV fm}, \quad m_0 \approx 5 \text{ MeV},$$

$$\text{Buballa [6]: } \Lambda = 664 \text{ MeV}, \quad G = 37.8 \text{ MeV fm}, \quad m_0 = 5.0 \text{ MeV}.$$

The agreement is not surprising for the following reasons.

- (i) The Hartree-Fock solution in the quasispin model coincides with the Hartree-Fock solution in the two-level NJL model (apart from small Fock terms).

This can be seen from the potential energy contribution $\sum_{u \leq v} V_{uvuv}$ which is the same in both cases. Hartree-Fock ignores the off-diagonal terms $V_{uvu'v'}$ which we have anyway thrown away in the quasispin model.

- (ii) In order to make up for the contributions of the second flavour we have increased the coupling strength in (1) by a factor of two compared to the standard definition in the two-flavour NJL, $G \rightarrow 2G$
- (iii) It seems that we have chosen a good average kinetic energy $P = \frac{3}{4}\Lambda$ when we replaced the individual values by an average.

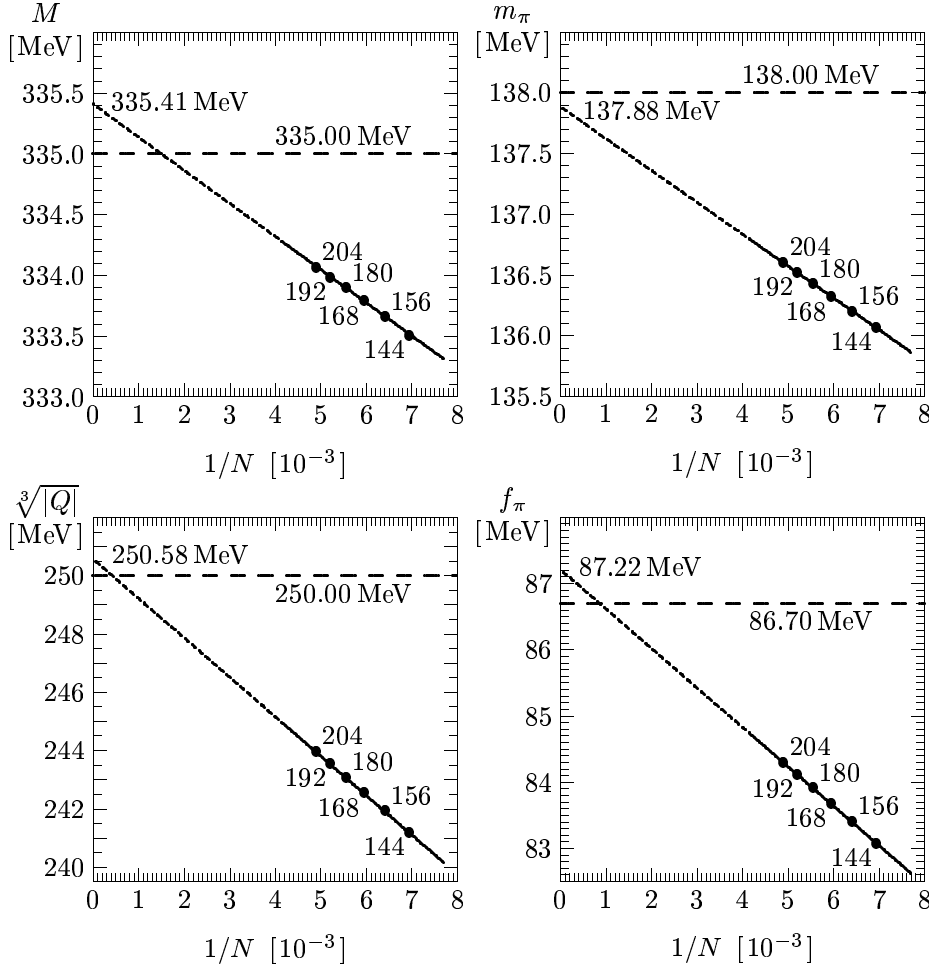


Fig. 1. Linear extrapolations of exact results of M , m_π , $\sqrt[3]{|Q|}$ and f_π for different values of N (144, 156, 168, 180, 192, 204) to the infinite N .

It is an interesting result that the exact values of the observables as a function of N approach the HF+RPA values in the limit $N \rightarrow \infty$. The linear extrapolation in Fig. 1 shows that HF+RPA is either exact or very accurate in this limit. Since full

NJL has the same HF+RPA solution, this fact gives a good credit to the HF+RPA approximation in full NJL (but does not yet prove the exactness).

5 Pion-pion scattering

An interesting application of the model is to calculate the pion-pion scattering length from the excitation spectrum in the box \mathcal{V} . Since we are working in a finite volume \mathcal{V} with periodic boundary conditions we cannot impose scattering boundary conditions. Instead of a continuous spectrum of scattering states we obtain a discrete spectrum. However, we can interpret the ground state as vacuum and excited states as multi-pion states or sigma-meson excitations or superpositions of both. For his purpose we have to choose the spectrum with ground-state quantum numbers $R = L = N/4$. In this case pionic excitations conserve the momenta of all quarks and therefore carry no momentum (nor angular momentum). Such states correspond to n pions in s -state and allow the evaluation of the average effective pion-pion potential \bar{V} and through it the pion-pion scattering length.

In Table 1 we present the spectrum for $N = 144$ and the model parameters listed in Section 4.

Table 1. The spectrum of the quasispin model with $N = 144$, quantum numbers $R+L = 36$ and model parameters listed in Section 4.

Parity	$E - E_0[\text{MeV}]$	$\bar{V}[\text{MeV}]$
+	932	-9.5
−	803	-11.7
+	771	-11.3
−	767	-8.8
+	646	-11.4
+	634	-12.2
−	580	-10.0
+	482	-10.5
−	378	-10.1
+	261	-10.3
−	136	
+	0	

For ideal n -pion states the energy should be

$$E_{n\pi} = n m_\pi + \frac{n(n-1)}{2} \bar{V}.$$

The quantity $\bar{V} = (E - E_0 - n m_\pi) / (\frac{1}{2}n(n-1))$ in Table 1 is in fact rather constant throughout the spectrum, except around 600-700 MeV where two positive parity states appear in succession and signal the presence of a sigma-excitation causing the confusion.

Another test of the concept of average effective pion-pion potential is its N-dependence. Larger N means a larger normalization volume \mathcal{V} and therefore more dilute pions leading to a proportionally smaller \bar{V} . In fact, for $N = 132$, the value $(132/144)\bar{V} = -10.6$ MeV, close to -10.3 MeV at $N = 144$. On the other hand, for $N = 108$, the value $(108/144)\bar{V} = -12.2$ MeV, rather far. This is an indication that above 132 we are already close enough to large-N limit, while 108 is still too small.

We calculate the s-state scattering length in the first-order Born approximation

$$a = \frac{m_\pi/2}{2\pi} \int V(\mathbf{r}) d^3r = \frac{m_\pi}{4\pi} \bar{V}\mathcal{V}. \quad (9)$$

This formula was first quoted by M.Lüscher[7] in 1986 and 1991 and later by many authors. It was derived in a much more sophisticated way, but in our context it is just the first-order Born approximation.

In our example for $N = 144$ we have $\bar{V} = -10.3$ MeV and $\mathcal{V} = \pi^2 N / \Lambda^3 = 40 \text{ fm}^3$. This gives

$$a m_\pi = \frac{m_\pi^2}{4\pi} \bar{V}\mathcal{V} = -0.0836. \quad (10)$$

Of course, there are no experiments with one-flavour pions. It is, however, interesting to compare with the two-flavour value ($I = 2$). The chiral perturbation theory (soft pions) suggests in leading order $a_0^{I=2} m_\pi = -m_\pi^2 / 16\pi f_\pi^2 = -0.0445$. The old analysis of Gasser and Leutwyler gave -0.019 and the more recent analysis by Lesniak gave -0.034 (“non-uniform fit”) or -0.044 (“uniform fit”). It is not yet clear to us why we get about twice larger value in our one-flavour model. Possibly this is due to the artifact that we made up for the second flavour by replacing $G \rightarrow 2G$ which might give too strong attraction between pions. We are still exploring this point.

6 Conclusion

From the quasispin model of the Nambu–Jona-Lasinio type one can learn several lessons:

- (i) The Hartree-Fock solution is (almost) exact for a truncated Nambu–Jona-Lasinio model in which the off-diagonal interaction matrix elements (corresponding to scattering of two quarks into different final momenta) are neglected. Since the full NJL model has the same HF solution as the truncated one it is well approximated by HF provided the effect of the off-diagonal terms is suppressed.
- (ii) The off-diagonal terms are important for pairing since scattering in all possible directions provides a large phase space for long range pairing correlations to develop. On the other hand, the interaction matrix elements which

conserve each momentum and scatter the two quarks between the lower and the upper level (between the Dirac and Fermi sea) are responsible for the chiral deformation of the system (spontaneous chiral symmetry breaking). There is a competition between pairing and deformation. Here we draw a pictorial analogy with nuclear physics where it is also a competition between pairing and quadrupole deformation. The pairing energy is proportional to the number of valence nucleons and the deformation energy to the square of their number. Therefore near closed shells pairing prevails and nuclei are spherical, while far from closed shells (at large number of valence nucleons) the deformation prevails and nuclei are deformed. Similarly, due to a large number N of quarks and large chiral symmetry breaking we expect the pairing to be suppressed by order $1/N$. We have still to test this idea by studying the Hartree-Fock-Bogoliubov approximation of two-level NJL and verifying that the solution does not support pairing; if this is the case it would strongly support the idea that HF is an accurate approximation of NJL.

- (iii) The picture that we have a chiral deformation of the mean field and of quark wavefunctions can be mapped into a picture in which we have quark-antiquark pairing. The interaction terms of the truncated NJL (and our quasispin model) scatter two quarks between the Dirac and Fermi sea but conserve their individual momenta; this leads to chiral deformation. We can, however, also call quark holes antiquarks, antiquarks carry opposite momenta as the missing quarks. Two quarks having whichever different momenta scatter back in the same momenta; in the other picture, quark and antiquark have opposite momenta and scatter in whichever pair of different opposite momenta. This is then just the condition stimulating pairing. The formal relation between the chiral deformation of Hartree-Fock quarks and the quark-antiquark pairing will be described elsewhere.
- (iv) In the quasispin model it is very instructive that the number of colours N_c and the number of spatial states $\mathcal{V}\Lambda^3/6\pi^2$ appear on equal footing in the product $N = 2N_c \mathcal{V}\Lambda^3/6\pi^2$. The colour and the momentum quantum number together are just the house number of the particle since the interaction does not depend on them. Therefore it is the same limit $N \rightarrow \infty$ whether we take the large N_c limit or a large block \mathcal{V} . This explains why even with 3 colours the quasispin model behaves similarly as the theorems regarding large N_c limit suggest (good HF approximation, suppression of off-diagonal terms and their effects, etc.).
- (v) The presented quasispin model is reminiscent of the schematic model of Lipkin, Agassi, Glick and Meshkov [8], popular in nuclear many-body problems. The purpose of the Lipkin model was to show essential features of approximations such as HF, perturbation theory, Projected HF, Time-dependent HF, RPA, Peierls-Yoccoz, Peierls-Thouless, Generator Coordinate Method, as well as to test their accuracy. Our schematic NJL-like model could be designed as “the Lipkin model of chiral symmetry”.

References

1. J. da Providência, M. C. Ruivo and C. A. de Sousa, *Phys. Rev. D* **36**, 1882 (1987).
2. S. A. Moszkowski, *Phys. Rev.* **110**, 403 (1958).
3. S. Lerma H., S. Jesgarz, P. O. Hess, O. Civitarese, and M. Reboiro, *Phys. Rev. C* **67**, 055209 (2003).
4. B. T. Oblak, *Bled Workshops in Physics* **4**, No. 1, 95 (2003), also available at <http://www-f1.ijs.si/Bled2003>.
5. M. Fiolhais, J. da Providência, M. Rosina and C. A. de Sousa, *Phys. Rev. C* **56**, 3311 (1997).
6. M. Buballa, *Phys. Reports* **407**, 205 (2005).
7. M. Lüscher, *Commun. Math. Phys.* **104**, 177 (1986); **105**, 153 (1986); *Nucl. Phys.* **B354**, 531 (1991).
8. H. J. Lipkin, N. Meshkov, A. J. Glick, *Nucl. Phys.* **62**, 188 (1965).
N. Meshkov, A. J. Glick, H. J. Lipkin, *Nucl. Phys.* **62**, 199 (1965).
A. J. Glick, H. J. Lipkin, N. Meshkov, *Nucl. Phys.* **62**, 211 (1965).
D. Agassi, H. J. Lipkin, N. Meshkov, *Nucl. Phys.* **86**, 321 (1966).



Recent measurements of nucleon electro-magnetic and spin structure at MIT-Bates, MAMI, and JLab

S. Širca^{a,b}

^aFaculty of Mathematics and Physics, University of Ljubljana, 1000 Ljubljana, Slovenia

^bJozef Stefan Institute, 1000 Ljubljana, Slovenia

Abstract. Recent measurements of nucleon (elastic) electro-magnetic form-factors, of nucleon resonance electro-excitation amplitudes, generalized polarizabilities from real and virtual Compton scattering, of parity-violating contributions to electron scattering, and of neutron spin structure functions are described. The main emphasis is on the results from the OOPS Collaboration at MIT-Bates, the A1 Collaboration at MAMI (Mainz), and the Hall A Collaboration at Jefferson Lab.

1 Nucleon electro-magnetic form-factors

The experimental effort on the elastic form-factor front has recently been mostly focused on the electric form-factor of the neutron (G_E^n) and the ratio of the electric and magnetic form-factors of the proton (G_E^p/G_M^p). With respect to existing data, the measurements of G_E^n in Hall A at Jefferson Lab [1] have been extended to significantly larger values of Q^2 where no usable older data exist (see Fig. 1). The new data were taken in early 2006.

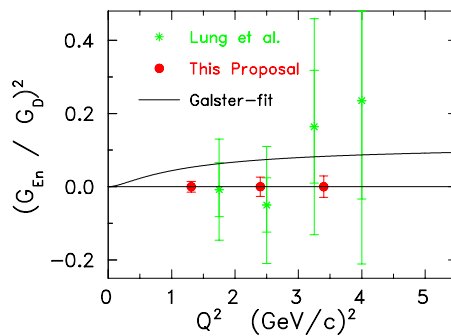


Fig. 1. Expected uncertainties of the high- Q^2 measurement of G_E^n in Hall A at Jefferson Lab (symbols on the axis). The existing experimental points below $Q^2 = 1 \text{ (GeV/c)}^2$ are not shown. The continuous line shows the traditional Galster parameterization.

The proton form-factor ratio case has stirred a lively discussion due to the rather surprising result of the double-polarized measurement [2] which exhib-

ited a rapid Q^2 -fall-off of the G_E^p/G_M^p ratio. Accuracy of older Rosenbluth-type measurements has been questioned, but a recent precise Rosenbluth-separation determination of the form-factors [3] indicates that both experimental approaches are correct and that two-photon corrections to the polarized result, previously considered to be negligible, may be responsible for the majority, if not all of the discrepancy. This is an ongoing investigation.

A high-precision unpolarized (Rosenbluth) measurement of G_E^p and G_M^p at low Q^2 is presently also being pursued at MAMI, while extensions of the double-polarization to momentum transfers beyond $Q^2 \sim 6$ (GeV/c)² are planned for the 12-GeV upgrade of CEBAF. The high- Q^2 experiment will require the construction of a new focal-plane polarimeter and is likely to be performed in Hall C.

2 Nucleon resonances

Conventionally, the EMR and CMR ratios

$$\text{EMR} = \text{Re} \left(E_{1+}^{(3/2)} / M_{1+}^{(3/2)} \right), \quad \text{CMR} = \text{Re} \left(S_{1+}^{(3/2)} / M_{1+}^{(3/2)} \right)$$

are used to quantify what strength the electric and Coulomb quadrupole amplitudes E_{1+} (or E2) and S_{1+} (or C2) contribute to the $N \rightarrow \Delta$ transition in the isospin-3/2 channel with respect to the dominant spin-isospin-flip transition amplitude M_{1+} (or M1). The E2 and EMR are more difficult to isolate in pion electroproduction than C2 and CMR because the transverse parts of the cross-section are dominated by the $|M_{1+}|^2$ term which is absent in the longitudinal parts.

New precise data from the process $H(e, e'p)\pi^0$ in the region of the $\Delta(1232)$ resonance have been published by the OOPS Collaboration at the MIT-Bates facility [4]. The measurements were performed at $Q^2 = 0.127$ (GeV/c)². The measurements at MIT-Bates were particularly sensitive to the E2 amplitude through the partial cross-section

$$\begin{aligned} \sigma_{E2}(\theta) = & 2 \text{Re} \left[E_{0+}^* (3E_{1+} + M_{1+} - M_{1-}) \right] (1 - \cos \theta) \\ & - 12 \text{Re} \left[E_{1+}^* (M_{1+} - M_{1-}) \right] \sin^2 \theta. \end{aligned}$$

The advantage of this approach is that the $E_{1+}^* M_{1+}$ interference term in σ_{E2} is amplified by a factor of 12 (which can be fully exploited at $\theta = 90^\circ$), while the σ_0 and σ_{TT} parts of the cross-section are dominated by $|M_{1+}|^2$ (see Fig. 2).

An experiment at the same value of Q^2 was performed by the A1 Collaboration at the MAMI facility at Mainz. With measurements at three values of the pion center-of-mass azimuthal angle ϕ at a fixed polar angle θ , and using polarized electron beam, the cross-sections σ_0 , σ_{TT} , σ_{LT} , and σ'_{LT} were extracted from the azimuthal and the beam-helicity dependence of the cross-section. The preliminary result [5] for the magnetic dipole amplitude at $W = 1232$ MeV is

$$M_{1+}^{(3/2)} = (40.33 \pm 0.63_{\text{stat+syst}} \pm 0.61_{\text{model}}) \cdot 10^{-3} / m_{\pi^+},$$

while the EMR and CMR ratios are

$$\begin{aligned} \text{EMR} &= (-2.28 \pm 0.29_{\text{stat+syst}} \pm 0.20_{\text{model}}) \% , \\ \text{CMR} &= (-4.81 \pm 0.27_{\text{stat+syst}} \pm 0.26_{\text{model}}) \% . \end{aligned}$$

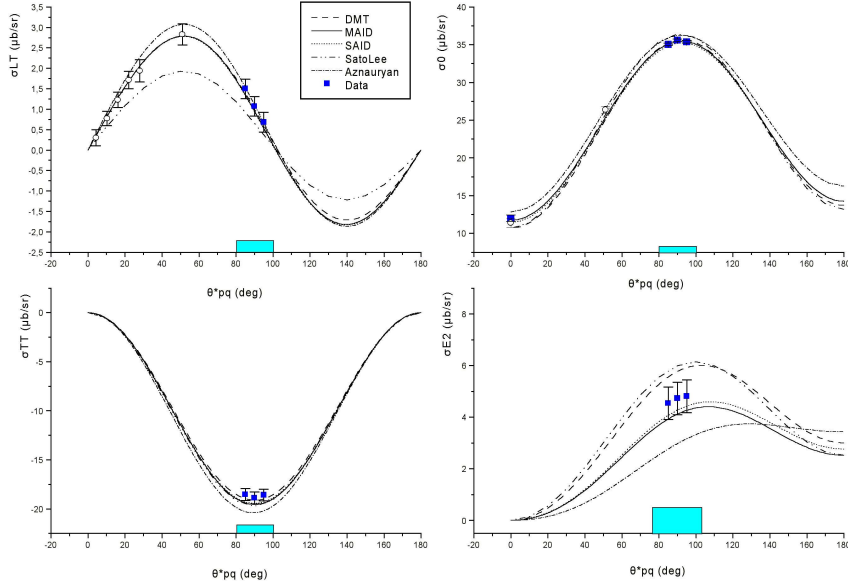


Fig. 2. Partial cross-sections in the MIT-Bates measurement of the $N \rightarrow \Delta$ transition in neutral-pion electro-production at $Q^2 = 0.127 \text{ (GeV/c)}^2$. The σ_{E2} partial cross-section is particularly sensitive to the E2 multipole transition strength.

Looking at the experimental efforts at higher Q^2 , the Hall A measurement at $Q^2 = 1 \text{ (GeV/c)}^2$ [6] still stands as a benchmark experiment of unprecedented physics insight and unparalleled accuracy. This double-polarization experiment utilized the technique of focal-plane polarimetry to determine the polarization of protons recoiled from the $H(e, e'p)\pi^0$ reaction. Thanks to the extended coverage in azimuthal and polar angles at the single Q^2 -point, a nearly model-independent multipole analysis could be performed. We obtained very precise values of

$$\begin{aligned} \text{EMR} &= (-2.91 \pm 0.19) \% , \\ \text{CMR} &= (-6.84 \pm 0.15) \% \end{aligned}$$

that are distinctly different from those from the traditional Legendre analyses based upon the dominance of the M_{1+} amplitude and the truncation of the partial-wave series at $l \leq 1$.

3 Real and virtual Compton scattering

Polarization transfer in real-photon Compton scattering (RCS) off the proton at high momentum transfer was measured by the Hall A Collaboration at Jefferson Lab (experiment E99-114, [7]). The measurements were performed at $s = 6.9 \text{ GeV}^2$ and $t = -4.0 \text{ GeV}^2$ via polarization transfer from circularly polarized

incident photons. The longitudinal and sideways polarization transfer parameters

$$K_{LL} = \frac{d\sigma(\uparrow\uparrow) - d\sigma(\uparrow\downarrow)}{d\sigma(\uparrow\uparrow) + d\sigma(\uparrow\downarrow)}, \quad K_{LS} = \frac{d\sigma(\uparrow\leftarrow) - d\sigma(\uparrow\rightarrow)}{d\sigma(\uparrow\leftarrow) + d\sigma(\uparrow\rightarrow)}$$

were extracted from the measurement of the proton recoil polarization. The results are in disagreement with the prediction of perturbative QCD based on a two-gluon exchange mechanism, indicating that the perturbative regime has not been reached yet in the kinematics of this experiment. On the other hand, the results agree well with the prediction based on a reaction mechanism in which the photon interacts with a single quark carrying the spin of the proton (the handbag reaction mechanism). For details, see [7].

Experiments in virtual Compton scattering (VCS) off the proton are a prime example of how the leading electron-scattering laboratories exploit the complementarity of their experimental equipment in order to achieve a common goal. The Jefferson Lab Hall A Collaboration has recently completed an extensive VCS program at $Q^2 = 0.92 \text{ (GeV/c)}^2$ [8], complemented by the work of the A1 Collaboration at MAMI at $Q^2 = 0.33 \text{ (GeV/c)}^2$ [9]. The results of the measurements by the OOPS Collaboration at MIT-Bates at very small $Q^2 = 0.06 \text{ (GeV/c)}^2$ are at a preliminary stage and are being published shortly [10]. The purpose of this joint effort is to determine the Q^2 -evolution of the electric and magnetic polarizabilities of the proton α_p and β_p . The measurements at low Q^2 from MIT-Bates are of particular relevance since both α and β appear to have strong Q^2 -dependencies. In particular, the prediction of chiral perturbation theory that $\beta(Q^2)$ has a positive slope at origin (indicating a negative magnetic polarizability mean-square radius) will be tested. Taken together, the experiments will also shed light on the theory that the proton possesses a distinct paramagnetic core and a diamagnetic tail [11].

Most recently, the A1 Collaboration has initiated a study of the single-spin and double-polarization asymmetries in the VCS process [12]. In these time-consuming and experimentally demanding experiments, an attempt is being made to extract six generalized polarizabilities of the proton: P_{LL} (corresponding to electric polarizability α in RCS), P_{LT} (magnetic polarizability β in RCS), P_{TT} (spin polarizability γ in polarized RCS), as well as three new ones, P_{LT}^z , $P_{LT}'^z$, and $P_{LT}'^\perp$. This experimental effort (close to 2000 hours beam-time) is ongoing, and data acquisition is nearing completion. Figure 3 shows the anticipated error budget for three different linear combinations of generalized polarizabilities contained in the Ψ_0 , $\Delta\Psi_{x0}$, and $\Delta\Psi_{z0}$ structure functions.

4 Parity violation

Parity-violating (PV) experiments exploit the interference of neutral weak (Z^0 exchange) and electro-magnetic (photon exchange) currents in scattering of polarized electrons off light nuclei, with typical PV asymmetries on the order of 10^{-4} to 10^{-7} . Most experiments to-date have been performed at momentum transfers below $\sim 1 \text{ (GeV/c)}^2$. The SAMPLE Collaboration at MIT-Bates, the A4 Collaboration at MAMI, and the HAPPEX Collaboration at Jefferson Lab are involved

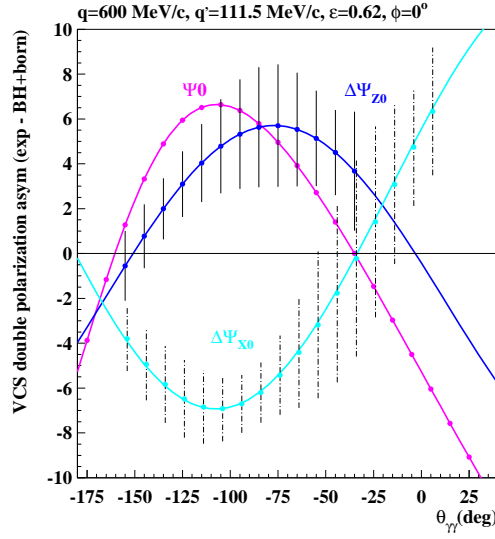


Fig. 3. Anticipated uncertainties in three different linear combinations of generalized polarizabilities contained in the Ψ_0 , $\Delta\Psi_{x0}$, and $\Delta\Psi_{z0}$ structure functions, for the double-polarized VCS measurement at Mainz.

in a comprehensive program to determine the strange-quark contributions to the distributions of charge (G_E^s) and magnetization (G_M^s) within the proton. The PV asymmetry on hydrogen is proportional to a linear combination of G_E^s and G_M^s , while it is proportional to G_E^s only in the case of the spin-less ${}^4\text{He}$ nucleus. It is therefore important that both targets are used in experiments under different kinematical conditions in order to achieve a good lever-arm for an intercept in the G_E^s - G_M^s plane.

Most recent results, taken in 2006, come from the HAPPEX II Collaboration who measured elastic scattering of 3 GeV electrons off hydrogen and ${}^4\text{He}$ targets, and provide the most precise data so far on the PV asymmetries. Strange electric and magnetic form-factors

$$\begin{aligned} G_E^s &= 0.002 \pm 0.014 \pm 0.007 & \text{at } Q^2 = 0.077 \text{ (GeV/c)}^2, \\ G_E^s + 0.09G_M^s &= 0.007 \pm 0.011 \pm 0.006 & \text{at } Q^2 = 0.109 \text{ (GeV/c)}^2 \end{aligned}$$

were extracted, providing new limits on the role of strange quarks in the nucleon charge and magnetization distributions [13].

5 Neutron spin structure

Most exciting new results on the neutron spin structure functions g_1^n (or the corresponding asymmetry A_1^n) and g_2^n come from experiments with the high-pressure polarized ${}^3\text{He}$ target in Hall A at Jefferson Lab. The measurements of these structure functions are motivated by several open questions.

Relativistic constituent quark models (RCQM) incorporating orbital angular momentum (OAM) of the quarks and leading-order perturbative QCD (pQCD) predictions assuming hadron helicity conservation (no OAM) make dramatically different predictions polarized quark distributions in the valence region. The A_1^n asymmetry and the corresponding polarized spin structure function g_1^n are sensitive tools to improve upon our knowledge of the neutron spin structure.

The naive quark-parton model predicts $g_2^n = 0$, while non-zero values occur in more realistic models of the nucleon which include quark-gluon correlations, finite quark masses, or quark orbital angular momentum. If the electron is considered to scatter from a non-interacting quark, the g_2^n structure function can also be obtained from NLO fits of g_1^n to world data. Deviations from this connection provide an opportunity to examine the dynamics of QCD in nucleon structure.

A precision measurement of A_1^n and a spin-flavour decomposition in the valence-quark region has been performed in Hall A at Jefferson Lab [14]. The results show a zero-crossing of A_1^n at $x \sim 0.47$, and A_1^n becoming significantly positive at $x \sim 0.60$. In general, the results agree with RCQM and pQCD analyses based on earlier data. However, they deviate from pQCD predictions based on hadron helicity conservation. Within the 12-GeV upgrade of CEBAF, there is an ambitious program to continue the A_1^n to Bjorken $x \sim 0.7$ at $W > 2$ GeV or even beyond $x \sim 0.9$ at $W > 1.2$ GeV.

The first measurement of the Q^2 -dependence of g_2^n has also been performed at Hall A [15]. The kinematics spanned five points in the range of $0.57 \leq Q^2 \leq 1.34$ (GeV/c)² at Bjorken $x = 0.2$. The results indicate a departure from the g_2^n - g_1^n connection at lower Q^2 , indicating that contributions such as quark-gluon interactions may be important.

References

1. G. Cates, K. McCormick, B. Reitz, B. Wojtsekhowski (co-spokespersons), Jefferson Lab Experiment E02-013.
2. O. Gayou et al. (Hall A Collaboration), Phys. Rev. Lett. **88** (2002) 092301.
3. I. A. Qattan et al. (Hall A Collaboration), Phys. Rev. Lett. **94** (2005) 142301.
4. N. Sparveris et al. (OOPS Collaboration), Phys. Rev. Lett. **94** (2005) 022003.
5. S. Stave et al. (A1 Collaboration), submitted to Eur. Phys. J. A (2006).
6. J. J. Kelly et al. (Hall A Collaboration), Phys. Rev. Lett. **95** (2005) 102001.
7. D. Hamilton et al. (Hall A Collaboration), Phys. Rev. Lett. **94** (2005) 242001.
8. G. Laveissiere et al. (Hall A Collaboration), Phys. Rev. Lett. **93** (2001) 122001.
9. J. Roche et al. (A1 Collaboration), Phys. Rev. Lett. **85** (2000) 798.
10. P. Bourgeois et al. (OOPS Collaboration), submitted to Phys. Rev. Lett. (2006).
11. A. I. L'vov, S. Scherer, B. Pasquini, C. Unkmeir, D. Drechsel, Phys. Rev. C **64** (2001) 015203.
12. N. d'Hose (contact person), MAMI Experiment A1/01-00.
13. A. Acha et al. (HAPPEX Collaboration), preprint nuc1-ex/0609002, submitted to Phys. Rev. Lett.
14. X. Zheng et al. (Hall A Collaboration), Phys. Rev. Lett. **92** (2004) 012004.
15. K. Kramer et al. (Hall A Collaboration), Phys. Rev. Lett. **95** (2005) 142002.

BLEJSKE DELAVNICE IZ FIZIKE, LETNIK 7, ŠT. 1, ISSN 1580–4992

BLED WORKSHOPS IN PHYSICS, VOL. 7, NO. 1

Zbornik delavnice 'Progress in Quark Models', Bled, 10. – 17. julij 2006

Proceedings of the Mini-Workshop 'Progress in Quark Models', Bled, July 10–17, 2006

Uredili in oblikovali Bojan Golli, Mitja Rosina, Simon Širca

Publikacijo sofinancira Javna agencija za raziskovalno dejavnost Republike Slovenije

Tehnični urednik Vladimir Bensa

Založilo: DMFA – založništvo, Jadranska 19, 1000 Ljubljana, Slovenija

Natisnila Tiskarna ??? v nakladi 100 izvodov

Publikacija DMFA številka 1651

Brezplačni izvod za udeležence delavnice
